NVD Rit

SERRITGERÐ
Thesis

TØKNIFRÁGREIÐING
Technical Report

UNDIRVÍSINGARTILFAR
Teaching Material

UPPRIT
Notes

MSc Thesis

Performance analysis of the Weather Research and Forecast (WRF) Model – A case study of the storm Urd on the Faroe Islands

Andrias Klein Gregoriussen

NVD*Rit* 2020:11

NÁTTÚRUVÍSINDADEILDIN
Faculty of Science and Technology
FRÓÐSKAPARSETUR FØROYA
University of the Faroe Islands

Heiti / Title	***Performance analysis of the Weather Research and Forecast (WRF) Model – A case study of the storm Urd on the Faroe Islands*** Góðskumeting av Weather Research and Forecast (WRF) modellinum – Ein nágreinilig stakkanning av ódnini Urd í Føroyum
Høvundar / Authors	**Andrias Klein Gregoriussen**
Vegleiðari / Supervisor	Bárður Niclasen, Fróðskaparsetur Føroya Ólafur Rögnvaldsson, Belgingur
Ábyrgdarvegleiðari / Responsible Supervisor	Bárður Niclasen, Fróðskaparsetur Føroya
Ritslag / Report Type	MSc ritgerð í náttúruvísindum við serligum atliti at Veðurfrøði *MSc Thesis in Natural Sciences – with emphasis on Meteorology*
Latið inn / Submitted	3. juli 2020

NVD*Rit*	2020:11
©	Náttúruvísindadeildin og høvundarnir 2020
ISSN	1601-9741
Útgevari / Publisher	Náttúruvísindadeildin, Fróðskaparsetur Føroya
Bústaður / Address	Vesara Bryggja 15, FO 100 Tórshavn, Føroyar (Faroe Islands)
✆ • 🖷 • @	+298 352 550 • +298 352 551 • nvd@setur.fo

Samandráttur

Føroyar eru staðsettar mitt í Norðuratlantshavinum, har lágtrýst og ódnir javnan koma framvið og hava nógvan vind við sær. Neyvar veðurforsøgnir hava tí sera stóran týdning fyri bæði fólk og vinnulív í Føroyum. Vegna bratta fjallalendinum í Føroyum er neyðugt at gera veðursimuleringar við høgari upploysn, fyri at fáa neyvar veðurforsagnir. Eitt av endamálunum við hesari ritgerðini er at fáa úrslit, ið kunnu brúkast aftur, tá ið farið verður undir at gera operationellar veðurforsagnir við høgari upploysn fyri Føroyar í framtíðini.

Endamálið við hesari ritgerðini er at kanna í hvønn mun Weather Research and Forecast (WRF) modellið megnar at spáa um veðurviðurskiftini, tá ið ódnin Urd rakti Føroyar 25. desember 2016. Simuleringar við WRF modellinum eru gjørdar fyri tíðarskeiðið 25. og 26. desember 2016 við horisontalari upploysn á 1km og 400m.

Fyri at meta um, hvussu neyvt báðar simuleringarnar megna at spáa um vindferð, trýst og hitastig, eru simuleringarnar samanbornar við mátingar frá 23 veðurstøðum í Føroyum, sum Landsverk umsitur.

Harafturat er 400m simuleringin samanborin við 1km simuleringina viðvíkjandi vindviðurskiftum á útvaldum veðurstøðum, tá ið stormurin var í hæddini.

Úrslitini frá kanningini vísa , at bæði 1km simuleringin og 400m simuleringin megna at spáa um, nær hitabrúgvin rakar Føroyar. Simuleringarnar undirmeta tó broytingarnar í hitastigum og trýsti og hava sostatt møguliga undirmett, hvussu hørð ódnin var.

Nakrar avbjóðingar hava verið í sambandi við greiningina av modeldátunum, av tí at tað vísti seg, at føroyska lendið var skeivt staðsett í báðum WRF simuleringunum. Orsaka av hesum vóru veðurstøðirnar fluttar til økir, ið betri umboða veruliga lendi, har veðurstøðirnar eru staðsettar. Henda greiningin inniheldur munandi færri modeldátur.

Eftir at hava flutt tær 23 veðurstøðirnar megnaðu WRF simuleringarnar betri at spáa um vindstyrkina samanborið við mátingarnar frá veðurstøðunum.

400m simuleringin vísti tó í størri mun lokal vindviðurskiftir í fjallalendi í mun til 1km simuleringina, sum vísti eina meira javna vindstyrki, eisini í fjallalendi.

Abstract

Due to frequent passage of cyclones in the North Atlantic causing extreme weather conditions on the Faroe Islands, accuracy of weather predictions is of high importance to the people and industry on the Faroe Islands. Due to the complex terrain in the Faroe Islands, one of the key points in providing accurate weather forecasts, especially on a local scale, is to provide high resolution operational forecasts for the islands. One goal of this study was to obtain results that can be applied in the work of setting up and running operational high resolution forecasts for the Faroe Islands in the future.

The aim of this thesis is to study the performance of the Weather Research and Forecast (WRF) model during the passage of the storm Urd that hit the Faroe Islands on December 25th 2016. The WRF model simulated weather conditions for the period between December 25th and December 26th 2016 with horizontal resolutions of 1km and 400m.

The accuracy of the two simulations in predicting wind speed, pressure levels and temperatures during this storm is examined by comparing them with on-ground measurements from 23 weather stations operated by Landsverk. In addition, the two simulations are compared to each other in terms of wind conditions at selected measurement sites during the peak of the storm.

The results of the study show that both the 1km and the 400m run predicted when the warm front hit the Faroe Islands. However, they did not capture the severity of the front as the changes in temperature and pressure levels over time were underestimated during the passage of the warm front.

Some complications arose when analysing the model data as it appeared as if the Faroese terrain was misplaced southwards in both WRF simulations. Therefore most of the measurement sites were relocated to more representative locations, but consequently, the model data for this analysis was reduced significantly.

Relocating the 23 measurement sites showed a great improvement in the prediction of wind speeds by the 400m run, but not by the 1km run during the passage of Urd.

The 400m run showed localized wind speeds attributed by the surrounding complex terrain in contrast to the 1km run, which predicted more uniform wind speeds.

Acknowledgement

In fall 2013, I had a short introductory course in meteorology by Hjálmar Hátún, where I discovered my first interest in the subject. The interest in meteorology was decisive for the courses in atmospheric science and geophysical fluid dynamics that I had chosen during my exchange semester in Denmark during fall 2015.

As I graduated my Bachelor Degree during summer 2016, Bárður Niclasen presented me the opportunity to study a Master's degree with emphasis in meteorology at the University of the Faroe Islands. This study was possible with great help from the University of Bergen, which allowed me to take 45 ECTS in courses at the Geophysical Institute.

Following the events of December 25th 2016 when a low pressure system struck the Faroe Islands with extreme wind magnitudes, the Minister of Fisheries and Maritime Affairs had set up a working group whose task is to plan for an updated weather service center in the Faroe Islands. This sparked the idea of studying the passage of the low pressure system that hit the Faroe Islands on December 25th 2016 in my thesis.

I have worked on this thesis with emphasis on making operational forecasts for the Faroe Islands in the future.

I would like to thank the staff at the University of the Faroe Islands and the people affiliated with the working group set up by the Ministry of Fisheries that have sparked my interest in meteorology. I would also like to thank the Geophysical Institute for a lovely exchange semester in Bergen. I would like to thank the administration at the University of the Faroe Islands for making this education possible. I would also like to thank Ólafur Rögnvaldsson for supervising throughout this thesis. At last, I would like to thank Bárður Niclasen for all the support during my study in meteorology, for interesting discussions and for all the advices.

Contents

1. Introduction

On December 25th and 26th 2016, a low pressure system struck Northern Europe. The system was named Urd by the Norwegian Meteorological Institute. The system hit the Faroe Islands with gusts reaching as high as 78.7m/s and later hit the Norwegian coast with wind speeds measured above hurricane magnitudes. Along with two other storms during Christmas, the hurricane caused severe damage on the Faroe Islands causing up to 75 million in insurance coverages[1].

Due to the frequent passage of cyclones in the North Atlantic causing extreme weather conditions on the Faroe Islands, the quality of weather prediction is of high importance to the islands, their people and industry.

The Faroe Islands are a fishing nation and the activities of industries as for example the fishing industry, salmon breeding, green energy and airline industry are very much linked to weather forecasts. There seems to be a broad consensus among Faroese organizations and companies that there is a great need for more accurate and reliable weather forecasts (Rasmussen et al., 2019).

After the passage of Urd, discussions about the formation of a local meteorological service emerged in the media (Rasmussen et al., 2019). In May 2018, the Minister of Fisheries and Maritime Affairs set up a working group whose task is to plan for an updated meteorological service in the Faroe Islands, which can provide more accurate and reliable weather forecasts. Due to the complex terrain of the Faroe Islands, one of the key points in providing accurate weather forecasts, especially on a local scale, is to provide high resolution operational forecasts for the islands.

This study focuses on the application of simulating weather during a storm. One goal of this study is to obtain results that can be applied in the work of setting up and running operational high resolution forecasts for the Faroe Islands in the future. Hopefully the

[1] Article: “Skaðar fyri 75 miliónir” by Bjarni Mohr, 16/01-2017 (in Faroese)
source: http://kvf.fo/greinar/2017/01/16/skadar-fyri-75-millionir

results of this study will help improve the short- to medium-range weather forecasts for the Faroe Islands in the near future.

The aim of this thesis is to study the accuracy of the Weather Research and Forecast (WRF) model when simulating the passage of the storm Urd in high resolution. The passage of Urd has been simulated several times with different model configurations during this study. However due to time limitations, this thesis focuses on analysing two model implementations: one with 40 vertical layers and a horizontal resolution of 1km, and one with 60 vertical layers and a horizontal resolution of 400m. More specifically, this thesis aims to answer the following questions:

1. What is the accuracy of the two WRF simulations of the storm Urd in terms of wind magnitudes, temperature and pressure levels?
2. To what extent are these simulations able to predict some of the local wind magnitudes that may be highly influenced by its surrounding complex terrain?
3. What is the benefit of simulating wind during the passage of Urd with a 400m horizontal resolution compared to a 1km horizontal resolution?

The WRF model was used to simulate the period of December 25th and 26th 2016 during the passage of Urd, and the model data are compared to measured data from 23 local weather stations operated by Landsverk. The background data used for these simulations are NOAA's operational analysis data from the GFS model. The measurement sites operated by Landsverk are mostly located in a highly complex terrain such as mountain passes, mountainsides and fjords surrounded by steep mountains, which may have influenced the weather conditions at these sites during the passage of Urd.

This study focuses on analysing surface weather parameters from model data and measurement stations. However, measured radiosonde data has to some extent been compared to model data from the 1km run and is shown in Appendix A.

An analysis of various different configurations of the WRF model is beyond the time limitations and scope of this thesis. However, several WRF simulations of the passage of Urd were made during the writing of this thesis. Verification metrics of these simulations are shown in Appendix E.

1.1 The Hurricane Urd

On December 25th 00:00 UTC a low pressure system at 968 hPa (Figure 1 A) was situated just south of Iceland and headed north-east. The cyclone deepened to 952 hPa at noon (Figure 1 B) as it passed the Faroe Islands with extreme wind speeds from the west- to southwest exceeding hurricane magnitudes. Severe damage was caused by the strong winds and the local police received 350 reports of storm damages. The NATO radio-communication station in Sornfelli was blown off the mountain, an entire warehouse was blown off by a gust in Kambsdalur while one person was swept by a gust and broke his leg.

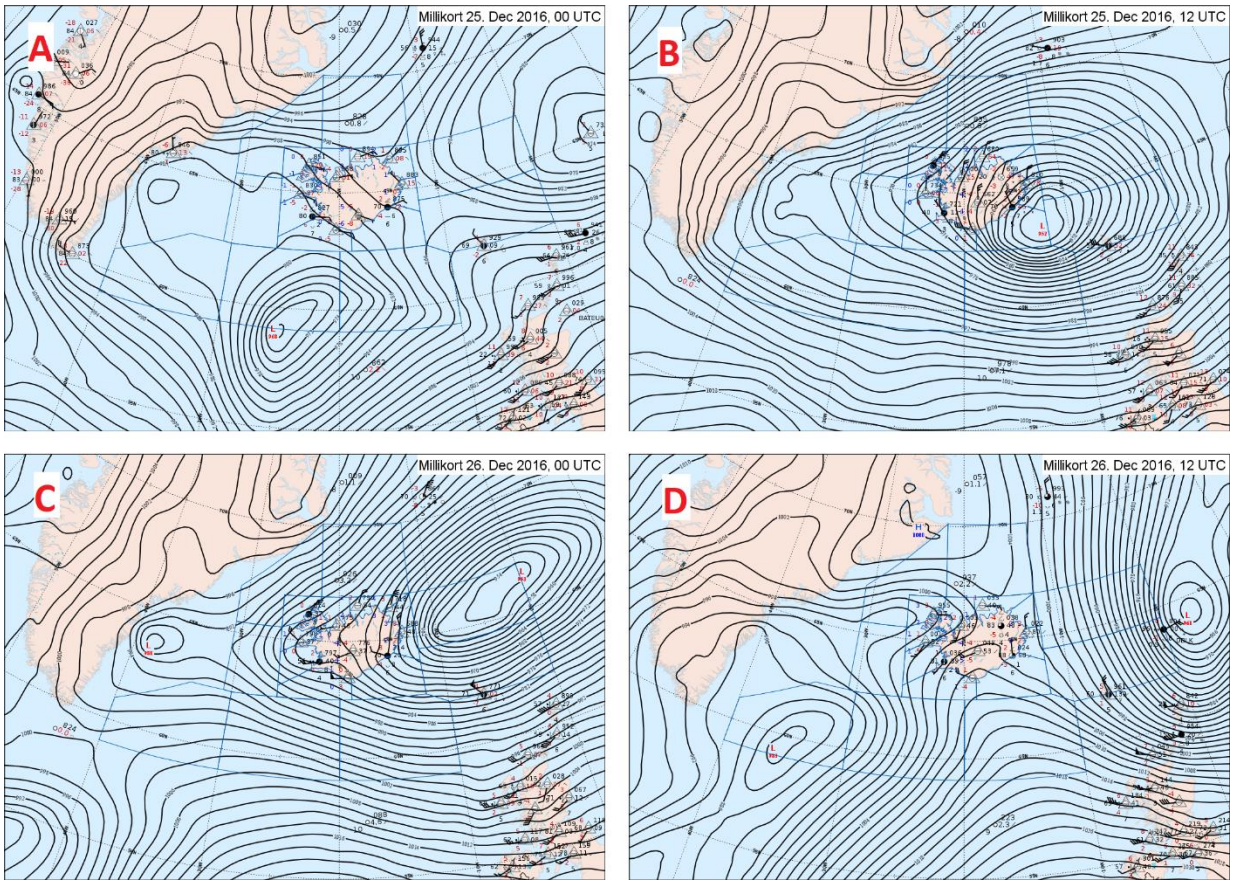

Figure 1 Synoptic overview of Urd (Source: Icelandic Met Office)

The strong winds continued until noon on December 26th (Figure 1 D) as the low pressure moved eastwards striking Norway with average wind magnitudes reaching 42 m/s and

gusts reaching 53 m/s (Olsen and Granerød, 2017) and Denmark with average wind magnitudes reaching 29.4 m/s and gusts reaching 37.8 m/s.[2]

1.2 The Faroe Islands

The Faroe Islands are an archipelago of 18 islands situated between Scotland and Iceland. The Faroese terrain is characterised by grasslands with tundra in the mountains and a highly complex topography. A large part of the sites investigated in this study experience strong local effects possibly related to gap winds, corner winds and other channelling effects due to the complexity of the surrounding terrain. The islands extend 113 km from north to south and 75 km from east to west with its highest elevation being Slættaratindur at 880 meters.

The climate in the Faroe Islands is highly influenced by the warmth of the Gulf Stream. This influence along with the high frequency of cyclones arriving mostly from the south and west cause a humid, unsettled and windy climate with mild winters and cool summers.

The topographical and meteorological conditions affect the precipitation patterns on the islands, as nearly all coastal areas receive around 1000 mm precipitation yearly, while the central parts receive more than 3000 mm of precipitation and more than 4000 mm of precipitation in some places (Cappelen and Laursen 1998).

[2] Article: "I kort og tal: Urd passerede Danmark", by Niels Hansen, 27/12-2016 (in Danish)
Source: https://www.dmi.dk/nyheder/2016/i-kort-og-tal-urd-passerede-danmark/

2. Theory

This chapter covers the theoretical background used in this study with emphasis on the complex terrain on the Faroe Islands.

2.1 Cyclonic movement in the North Atlantic

Extratropical cyclones such as the hurricane Urd form in a baroclinic atmosphere where density can be a function of both pressure and temperature such that temperature gradients are misaligned in comparison to the isobars. This is common in the mid-latitudes where the surface is being heated unevenly, as land to the south receives more solar radiation than land to the north. The southern part of the mid-latitudes thus receives more energy than the northern part. As temperature increases along the horizontal lines of constant pressure in this area, density also decreases, which creates a vertical wind shear in the upper atmosphere also called the thermal wind. Disturbances in this region may form frontal wave which develops to a mid-latitudinal cyclone (Holton, 2013).

The stages of an extratropical cyclone are also described in Figure 2. After a baroclinic wave is formed (Figure 2 I), air from all directions moves towards the centre of the low pressure in order to "fill the gap". However, the converging air moves cyclonically due to the Coriolis force causing warm air from the south to propagate eastwards, while cold air from the north propagates westward forming the warm and cold front respectively (Figure 2 II & III). As the cyclone matures, the cold front catches up and mixes with the warm front, which forms an occluded front of mixed precipitation clouds (Figure 2 IV). Once the warm front is caught up, the cyclone is surrounded by cold air and will slowly start to

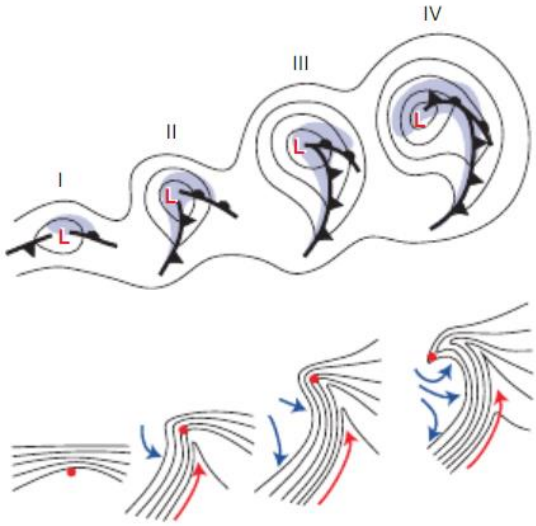

Figure 2 The lifecycle of a cyclone divided into four stages (Source: Wallace & Hobbs, 2006)

dissipate as there is no more energy left to support the cyclone. (Wallace and Hobbs, 2006, p. 336).

For a low pressure moving eastwards, an observer at the surface would first experience a drop in pressure levels followed by increasing temperature and wind speeds as the warm front passes. The largest wind magnitudes are observed closest to the centre of the low pressure between the warm and cold front. As the cold front passes, temperatures will drop and pressure levels rise, and gusts may increase in magnitude.

As the Faroe Islands are situated close to the common cyclone tracks in the North Atlantic region, they frequently experience cyclones passing by causing rainfall and strong winds (Cappelen and Laursen, 1998). This is particularly prominent in the winter with the semi-permanent Icelandic Low situating between Iceland and Greenland as shown to the left in Figure 3. During summer, the North Atlantic region goes from being dominated by the Icelandic Low to be more affected by the Azores High as shown to the right in Figure 3. The Azores High is sometimes displaced towards the Faroe Islands such that summer weather with fairly high temperatures can prevail for weeks (Cappelen and Laursen, 1998).

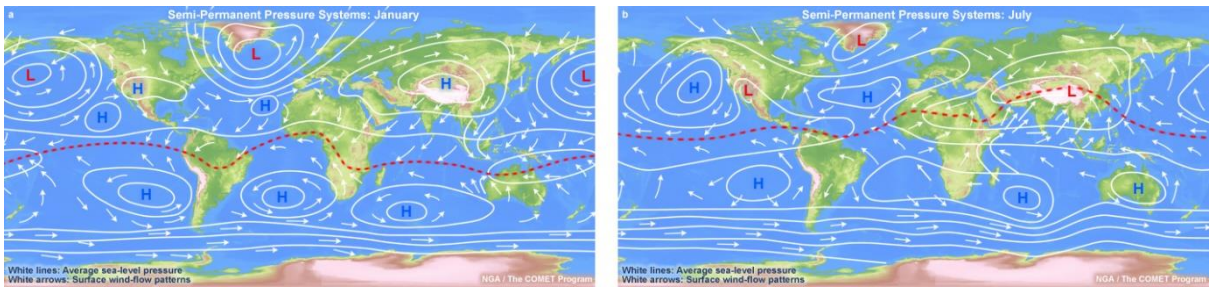

Figure 3 Semi-permanent pressure systems in January (left) and July (right) (Source: Introduction to Tropical Meteorology, 2nd ed., 2016)

2.2 Effects of rotation and the Rossby number

If the only forces acting on the wind are the horizontal pressure gradient force and the Coriolis force, horizontal wind is in geostrophic balance. Taking this into account and neglecting friction, the horizontal momentum equation on a rotating frame can be written as (Holton, eq. 2.24, 2.25):

$$\frac{Du}{Dt} = f(v - v_g) = f v_a$$

$$\frac{Dv}{Dt} = f(u - u_g) = f u_a$$

Here, f is the Coriolis parameter and u_a and v_a are ageostrophic winds. This expression shows that acceleration of the wind is just the difference between the geostrophic wind and the actual wind. Whether the Coriolis force has a significance to the flow can be determined by the Rossby number, which on a scale analysis compares acceleration (which has dimensions of $\frac{D\boldsymbol{U}}{Dt} \sim \frac{U^2}{L}$)to the Coriolis force (which has dimensions of $\boldsymbol{U} \times 2\Omega \sin\phi \sim f_0 U$) (Holton, 2013). The non-dimensional Rossby number is given by:

$$Ro = \frac{U}{f_0 L}$$

Here U is the horizontal wind speed, f_0 is the Coriolis parameter and L is the horizontal scale length. If $Ro \gg 1$ such as in tornadoes, it is because the Coriolis force is much weaker than the inertial force and therefore has no significant impact on the phenomenon. If $Ro \ll 1$ like seen in low-pressure systems, the Coriolis force plays a significant role to the behaviour of the flow. Considering the Faroe Islands as a whole during the passage of Urd, a realistic number for U could be 25 m/s, $f_0 = 10^{-4}$, $L = 50\ km$, such that $Ro = 5$ and the Coriolis force would not make a significant impact for strong wind speeds. For regular winds where $U = 10\ m/s$, the Rossby number would be 2, such that the Corilois force still wouldn't make a significant impact on the flow.

2.3 Complex Terrain meteorology and local effects

The complexity of a terrain can make a large impact on the wind conditions at a measurement site, as various topographic shapes can alter the flow. When approaching a mountain or a barrier, the flow can either be carried over the barrier, carried around the barrier, be forced through gaps in the barrier or be blocked by the barrier it is approaching.

Three factors determine the behaviour of an approaching flow in response to a mountain barrier (Whiteman, 2000, p. 141):

- The stability of the air approaching the mountains
- The speed of the air flow approaching the mountains and
- The topographic characteristics of the underlying terrain

In addition to stability, flow over a mountain barrier also depends on the characteristics of the barrier. If it is long, the flow will tend to go above the mountain barrier and the flow can generate mountain waves on the lee side.

A deeper understanding of a flow approaching a mountain is explained by Smith (1989). His work shows that for a steady, Boussinesq, hydrostatic, nonrotating flow, unbound above, both flow going around a mountain barrier (flow splitting) and above a mountain (wave breaking) depend on the formation of a stagnation point of the flow. Only the non-dimensional mountain height $\hat{\mathrm{h}}$ and the horizontal aspect ratio is required to describe the fate of this flow. The non-dimensional mountain height is defined as:

$$\hat{\mathrm{h}} = \frac{Nh}{U}$$

where N is the Brunt-Väisälä frequency[3], h is the height of the mountain and U is the up-slope wind speed. The horizontal aspect ratio is defined as:

$$r = \frac{a_y}{a_x}$$

Here, a_y is the length of the mountain barrier and $a_x$is the width of the mountain barrier. Note that as mentioned earlier, the behaviour of the approaching flow depends on the

[3] The Brunt-Väisälä frequency is a measure of static stability of the environment. If $N^2 > 0$, the air is stable and a vertical displacement will cause an air parcel to oscillate around its initial point. If $N^2 = 0$, there is no restoring force and the parcel will remain at the vertical position its moved to if displaced. If $N^2 < 0$, the air is unstable and a vertical displacement up – or downwards will cause the parcel to accelerate in that direction. (Rogers & Yau, 1989, p. 32)

stability of the flow (Brunt-Väisälä frequency), the speed of the air approaching the mountain and the topographic characteristics (dimensions of the mountain). Figure 4 summarises the onset of stagnation in an unstructured atmosphere as a function of the horizontal aspect ratio and the non-dimensional mountain height.

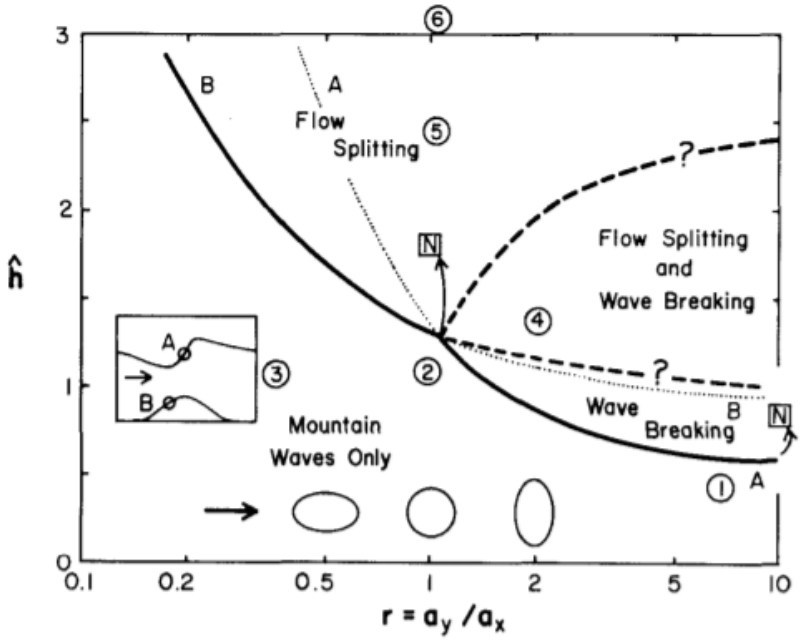

Figure 4 Regime diagram for hydrostatic flow over a mountain. The diagram shows the horizontal aspect ratio on the x-axis and the non-dimensional mountain height on the y-axis. The solid curves A and B are linear theory estimates of wave breaking (A) and flow splitting (B). Made by Smith (1989).

When analysing flow over complex topography, wind at the sites being investigated in this study can be sped up or slowed down. The orientation and shape of a ridgeline affect the speed and direction of a flow crossing a mountain barrier. Figure 5 shows different possible scenarios of the orientation of a ridgeline compared to the flow. The highest speedups can occur over ridgelines that are perpendicular to the flow or have a concavity oriented into the flow (Whiteman, 2000, p. 145).

The Faroe Islands have a complex topography with steep mountain ranges, and a large portion of the sites investigated in this study experience strong local effects due to the surrounding terrain. For this reason, we are expecting the local terrain to produce different wind conditions with change in intensity and direction on some of the measurement sites as some of these sites are placed in a fjord, while others are placed in a mountain pass or along a mountain with steep terrain. Depending on the type of complex terrain a site is placed in, it can be exposed to many of the different types of winds briefly explained above. When simulating winds in complex terrain, other studies do find deviations between the

simulated and measured wind speeds in terms of means and gusts. Ágústsson and Ólafsson (2009) for instance found both overestimations of upstream gusts and underestimations of downslope maximum gusts in their study of simulating winds in a complex terrain.

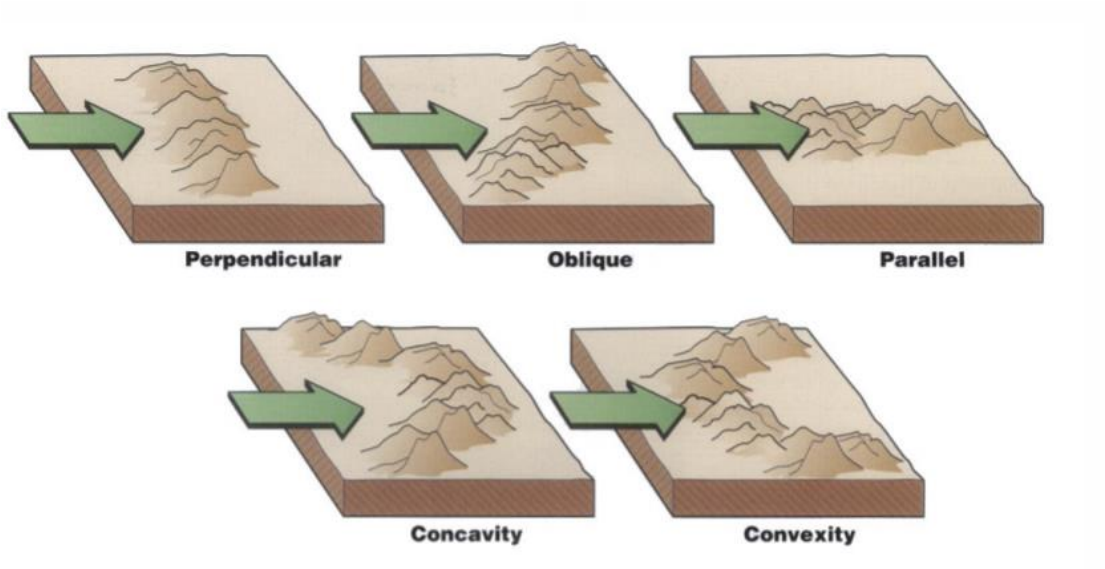

Figure 5 Different possible scenarios of orientation of a ridgeline with respect to the wind direction (Whiteman, 2000, p. 145)

2.3.1 Downslope winds

Downslope winds are enhanced downstream winds formed on the lee side of a mountain in association with gravity waves and stability of the air as flow goes over a barrier. Strong stability and gravity waves may lead to large wind magnitudes downstream on the lee side of a mountain, and these winds may be present a few kilometres from the mountain of origin, but can with the right conditions extend much further (Águstsson and Ólafsson, 2010). Various studies have investigated the relation between downslope winds and other phenomena such as hydraulic jumps (Long, 1953) and large-amplitude vertically propagating waves (Eliassen and Palm, 1960). Durran (1990) advises two conditions to be present for downslope winds in a deep cross-mountain flow and no mean-state critical layer:

I. The flow is directed across the mountain at an angle within 30° of being perpendicular to the ridgeline
II. The upstream temperature profile exhibits an inversion or a layer of strong stability near the mountaintop level

2.3.2 Gap winds

Some measurement sites such as Norðadalsskarð analysed in this study are located in mountain passes and are often exposed to strong prevailing winds where measurements of high wind speeds may be frequent. Most winds through gaps and passes are driven by the difference in pressure from one side of the gap to the other. These winds blow across the pressure contours from the area of high pressure (where air is being "forced" through) to the area of low pressure (where air is being "let out"). Gaberšek and Durran, (2004, 2006) investigated the behaviour of a gap flow as a function of the mountain height. They found out that the gap flow enhanced at different mountain heights. For a small mountain height of $\hat{\mathrm{h}} = 0.25$, no significant increase in the gap wind occurred, but for $\hat{\mathrm{h}} = 1.4$, the flow experienced acceleration from the gap outlet and wave breaking which caused strong downstream winds.

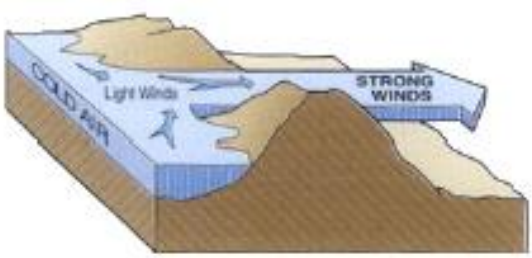

Figure 6 Accelerated flow through a mountain pass

3. Method

This chapter describes the equipment used to measure the weather data that is used in this study as well as the method of which it has been set up. Likewise, the modelling procedure as well as the statistical methods used in this study are described.

3.1 Instrumentation

Weather data used in this study was observed from the surface by weather stations operated by Landsverk, which is the Faroese public provider of road infrastructure. Most of these stations function as part of a Road Surface and Analyzer (ROSA). These weather stations have anemometers, barometers, thermometers, hygrometers and rain detectors installed for weather monitoring. Figure 7 shows the location of each weather station here mapped in QGIS[4] on a Faroese map provided by Umhvørvisstovan[5]. Table 1 shows a basic description of each weather station operated by Landsverk in 2016.

Figure 7 Weather stations operated by Landsverk displayed on a Faroese map (Source: Umhvørvisstovan)

[4] QGIS is an open source Geographic Information System. For more information, see http://www.qgis.com
[5] The GIS-map of the Faroe Islands is downloadable at https://www.foroyakort.fo/tak-datur-nidur/tak-nidur-fjarmyndir/

3.1.1 The Weather Station

Most of the weather stations operated by Landsverk are a part of a road surface analyser (ROSA) on the Faroe Islands. The objective of Landsverk as the Faroese provider of road infrastructure is to have information about the road conditions as well as the meteorological conditions near the public roads.

The weather instruments used at the weather stations operated by Landsverk are manufactured by Vaisala, a Finnish manufacturer of products for environmental and industrial measurements to meteorological and hydrological service. All weather instruments are compatible with the ROSA system operated by Landsverk. More information on the weather stations operated by Landsverk can be read by Gregoriussen (2019).

Figure 8 Image of the ROSA station near Tjørnuvík

Table 1 Overview of the weather stations operated by Landsverk used in this study

Station ID	Station Name	Altitude (m)	Wind sensor	Temperature / Humidity probe	Barometer	Rain detector	Longtitude	Lattitude
F-10	Kambsdalur	110	Vaisala WS 425	Vaisala HMP 155D	Vaisala PMB 100	Vaisala DRD 11A	-6.80463	62.21873
F-12	Høgareyn	280.5	Vaisala WMT 703	Vaisala HMP 155D	Vaisala PMB 100	Vaisala DRD 11A	-7.15005	62.12655
F-21	Sund	51.5	Vaisala WMT 703	Vaisala HMP 155D	Vaisala PMB 100	Vaisala DRD 11A	-6.83880	62.04660
F-22	Runavík	9.8	Vaisala WS 425	Vaisala HMP 45D	Vaisala PMB 100	Vaisala DRD 11A	-6.72860	62.10930
F-23	Vatnsoyrar	40	Vaisala WS 425	Vaisala HMP 155D	Vaisala PMB 100	Vaisala DRD 11A	-7.24630	62.06960
F-24	Klaksvík	22	Vaisala WS 425	Vaisala HMP 155D	Vaisala PMB 100	Vaisala DRD 11A	-6.56973	62.22632
F-25	Sandoy	120.5	Vaisala WMT 703	Vaisala HMP 155D	Vaisala PMB 100	Vaisala DRD 11A	-6.75910	61.82900
F-26	Syðradalur	2.5	Vaisala WS 425	Vaisala HMP 155D	Vaisala PMB 100	Vaisala DRD 11A	-6.66380	62.24642
F-27	Porkeri	160	Vaisala WMT 703	Vaisala HMP 155D	Vaisala PMB 100	Vaisala DRD 11A	-6.75160	61.48860
F-28	Krambatangi	2.5	Vaisala WS 425	Vaisala HMP 155D	Vaisala PMB 100	Vaisala DRD 11A	-6.81690	61.54800
F-29	Skopun	2.5	Vaisala WS 425	Vaisala HMP 155D	Vaisala PMB 100	Vaisala DRD 11A	-6.87884	61.90308
F-33	Norðadalsskarð	273	Vaisala WMT 703	Vaisala HMP 155D	Vaisala PMB 100	Vaisala DRD 11A	-6.91893	62.05478
F-34	Glyvursnes 2	115	Viasala waa/waw 151	Vaisala HMP 155D	Vaisala PTB 220	Vaisala DRD 11A	-6.74980	61.97733
F-35	Tjørnuvík	66	Vaisala WS 425	Vaisala HMP 155D	Vaisala PMB 100	Vaisala DRD 11A	-7.12778	62.29497
F-36	Kollafjørður	72	Vaisala WS 425	Vaisala HMP 155D	Vaisala PMB 100	Vaisala DRD 11A	-6.89310	62.14013
F-37	Norðskálatunnilin	133.5	Vaisala WMT 703	Vaisala HMP 45D	Vaisala PMB 100	Vaisala DRD 11A	-6.92955	62.22318
F-40	Viðareiði	37.5	Vaisala WS 425	Vaisala HMP 155D	Vaisala PMB 100	Vaisala DRD 11A	-6.54496	62.33215
F-41	Sandavágur	225	Vaisala WMT 703	Vaisala HMP 155D	Vaisala PMB 100	Vaisala DRD 11A	-7.15380	62.08567
F-42	Gjáarskarð	310	Vaisala WMT 703	Vaisala HMP 155D	Vaisala PMB 100	Vaisala DRD 11A	-6.97005	62.29843
F-43	Oyndarfjørður	245	Vaisala WMT 703	Vaisala HMP 155D	Vaisala PMB 100	Vaisala DRD 11A	-6.87689	62.24513
F-44	Hvalba	170	Vaisala WS 425	Vaisala HMP 155D	Vaisala PTB 110	Vaisala DRD 11A	-6.93730	61.57558
F-45	Streymnes	32	Vaisala WS 425	Vaisala HMP 155D	Vaisala PTB 110	Vaisala DRD 11A	-7.02022	62.19278
F-48	við Velbastaðháls	185	Vaisala WMT 703	Vaisala HMP 155D	Vaisala PTB 110	Vaisala DRD 11A	-6.84718	61.98625

3.2 The Weather Research and Forecast model (WRF)

Weather Research and Forecasting (WRF) is a numerical weather prediction system for operational weather forecasting and atmospheric research. WRF was developed in a collaboration between NCAR's Mesoscale and Microscale Meteorology Division, the National Oceanic and Atmospheric Administration's (NOAA) National Centres for Environmental Prediction (NCEP) and Earth System Research Laboratory (ESRL), the Department of Defense's Air Force Weather Agency (AFWA) and Naval Research Laboratory (NRL), the Centre for Analysis and Prediction of Storms (CAPS) and the University of Oklahoma, and the Federal Aviation Administration (FAA) with the participation of university scientists (Skamarock et al., 2008). The following description of the WRF model is mostly taken from Skamarock et al. (2008):

The WRF model is featuring two cores, the Advanced Research WRF (ARW) solver and the WRF-NMM (Nonhydrostatic Mesoscale Model). The WRF model also features a data assimilation system and allows for parallel computation. Figure 9 shows a schematic of the components contained in the WRF software.

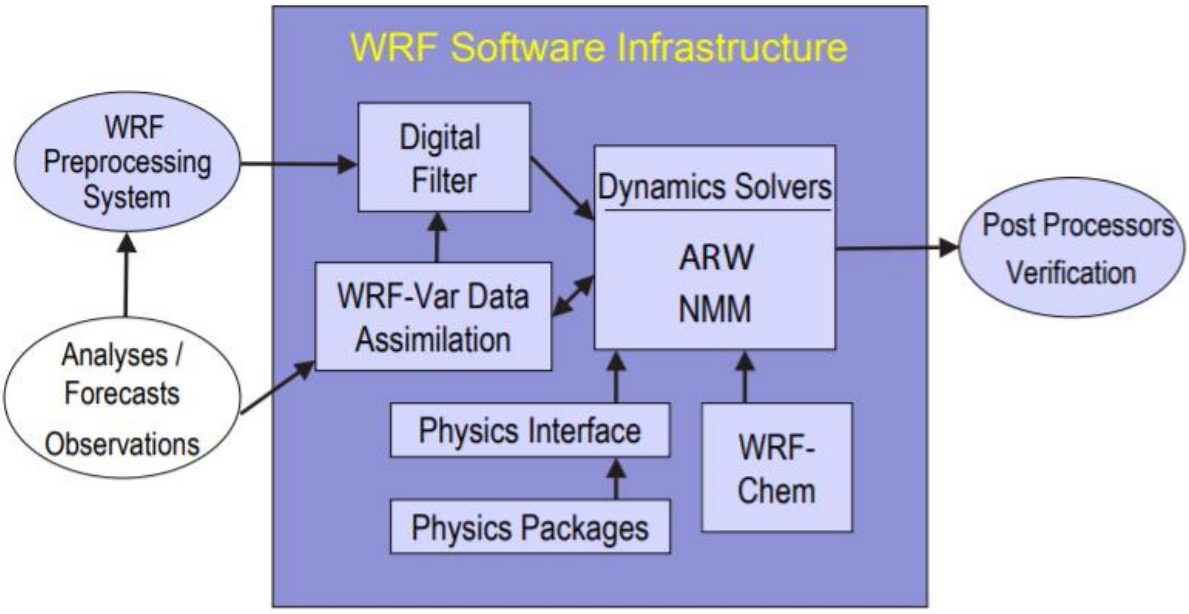

Figure 9 WRF's system components (Source: Skamarock et al. (2008))

For this study, the ARW dynamics solver from WRF version 3.8 and 4.0 has been used to simulate the storm Urd. The ARW dynamics solver integrates the compressible nonhydrostatic Euler equations, which are formulated using the sigma (σ) terrain-following mass vertical coordinate (Laprise, 1992). The vertical coordinate is denoted by η and defined as:

$$\eta = \frac{p_h - p_{ht}}{\mu} \text{ , where } \mu = p_{hs} - p_{ht} \qquad (2.4.1)$$

Here, p_h is the hydrostatic component of the pressure, while $p_{hs}$and p_{ht} are the values along the surface and top boundaries.

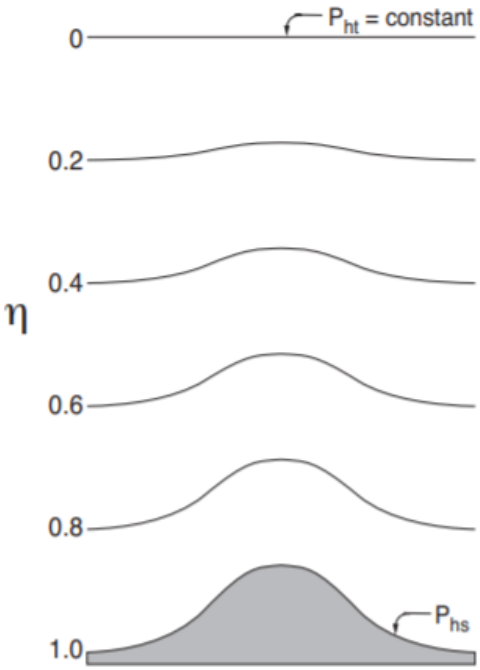

Figure 10 The η coordinate used by ARW (Source: Skamarock et al. (2008))

Considering Figure 10 $\mu(x, y)$ represents the mass per unit area within the column in the model domain at (x, y). The related flux form variables are defined as:

$$\mathbf{V} = \mu\mathbf{v} = (U, V, W), \quad \Omega = \mu\acute{\eta}\,, \Theta = \mu\theta. \qquad (2.4.2)$$

Here, $\mathbf{v} = (u, v, w)$ represents the covariant velocities in the two horizontal and vertical directions, respectively. $\omega = \acute{\eta}$ is the vertical covariant velocity, while θ is the potential temperature. Non-conserved variables such as the geopotential $(\phi = gz)$, pressure (p) and specific volume $\left(\alpha = \frac{1}{\rho}\right)$.

Using the defined variables above, the Euler equations can be written in flux form as:

$$\partial_t U + (\nabla \cdot \mathbf{V}u) - \partial_x\left(p\phi_\eta\right) + \partial_\eta(p\phi_x) = F_U \tag{2.4.3}$$

$$\partial_t V + (\nabla \cdot \mathbf{V}v) - \partial_x\left(p\phi_\eta\right) + \partial_\eta\left(p\phi_y\right) = F_V \tag{2.4.4}$$

$$\partial_t W + (\nabla \cdot \mathbf{V}w) - g\left(\partial_\eta p - \mu\right) = F_W \tag{2.4.5}$$

$$\partial_t \Theta + (\nabla \cdot \mathbf{V}\theta) = F_\Theta \tag{2.4.6}$$

$$\partial_t \mu + (\nabla \cdot \mathbf{V}) = 0 \tag{2.4.7}$$

$$\partial_t \phi + \mu^{-1}[(\mathbf{V} \cdot \nabla\phi) - gW] = 0 \tag{2.4.8}$$

The diagnostic relation for the specific volume α is:

$$\partial_\eta \phi = -\alpha\mu, \tag{2.4.9}$$

Meanwhile, the equation of state is:

$$p = p_0 \left(\frac{R_d\theta}{p_0\alpha}\right)^\gamma. \tag{2.4.10}$$

In equations $2.4.3 - 2.4.10$, the subscripts x, y and η denote the differentiations:

$$\nabla \cdot \mathbf{V}_a = \partial_x(Ua) + \partial_y(Va) + \partial_\eta(\Omega a), \quad \text{and} \quad \mathbf{V} \cdot \nabla a = U\partial_x a + V\partial_y a + \Omega\partial_\eta a$$

When discretizing, the ARW solver uses a time-split integration scheme in order to handle different wavelengths and frequencies in the atmosphere. Low frequency modes are integrated by using a third-order Runge-Kutta (RK3) time integration scheme, while high frequency modes are integrated over a smaller time step than the low frequency modes. As shown in Figure 11, a staggered C grid is used for numerically solving the variables. Normal velocities are staggered one-half grid length from the thermodynamic variables.

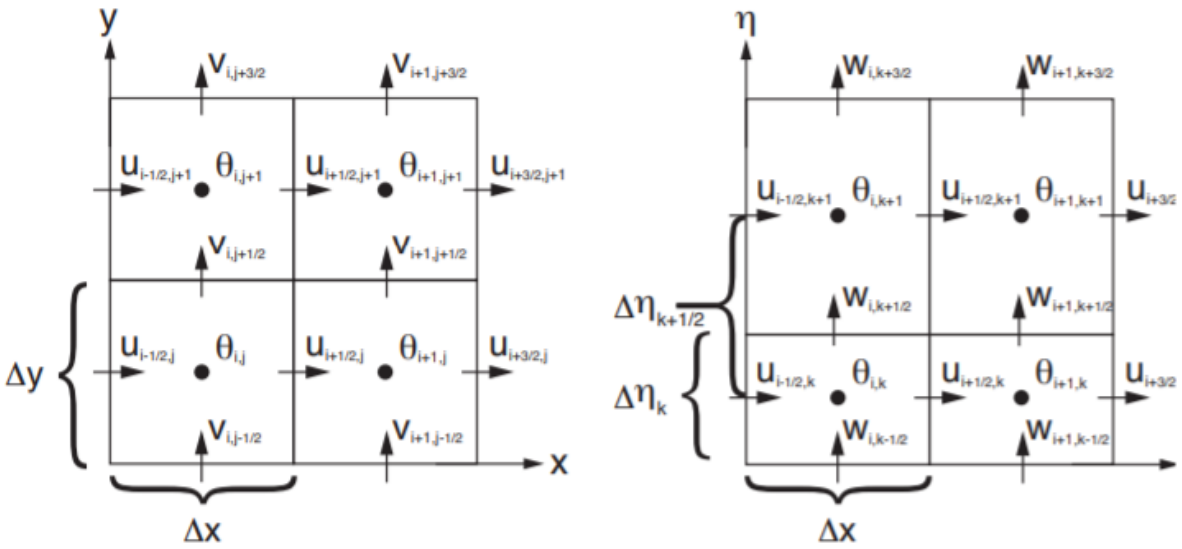

Figure 11 The C grid staggering method used for when discretizing in the ARW solver (Source: Skamarock et al. (2008))

3.2.1 Nesting

Horizontal nesting is possible with the ARW solver such that one can focus on a region of interest and increase the horizontal resolution in that area. This is done by simulating an outer domain with coarse resolution and at least one inner domain with finer resolution receiving information from the outer domain. There are two different methods used for horizontal nesting, namely one-way nesting and two-way nesting. Figure 12 sums up the difference between two-way nesting and the two methods used for one-way nesting.

In a two-way nested run, there is communication between both domains such that information is both transferred from the outer domain to the inner domain and fed back from the inner domain to the outer domain during a simulation. The inner domain receives boundary information from the outer domain, iterates a few time steps (depending on the time-step ratio between the two domains), feeds back the information to the outer domain which iterates one time step before the process is repeated.

In a one-way nested run, communication only goes from the outer domain to the inner domain during. This technique can be done by using offline or online nesting. Offline nesting (Figure 12, left box) is done by first running a full simulation of the parent domain, whose output data is then used as boundary conditions for the inner domain in another simulation. Online nesting (Figure 12, middle box) is done by running the parent domain and inner domain in the same simulation, where the parent domain iterates a time step

and the inner domain uses the new information at that time step as boundary conditions for iterating the next time steps. The major difference between these two techniques is that the inner domain receives updated boundary conditions from the parent domain much more frequently.

In this study, both one-way offline and inline nested runs as well as two-way nested runs have been made. However, the only simulations in focus of this study is a 1km one-way offline nested run and a 400m one-way inline nested run. Model verification tables from the two-way nested runs are shown in Appendix E.

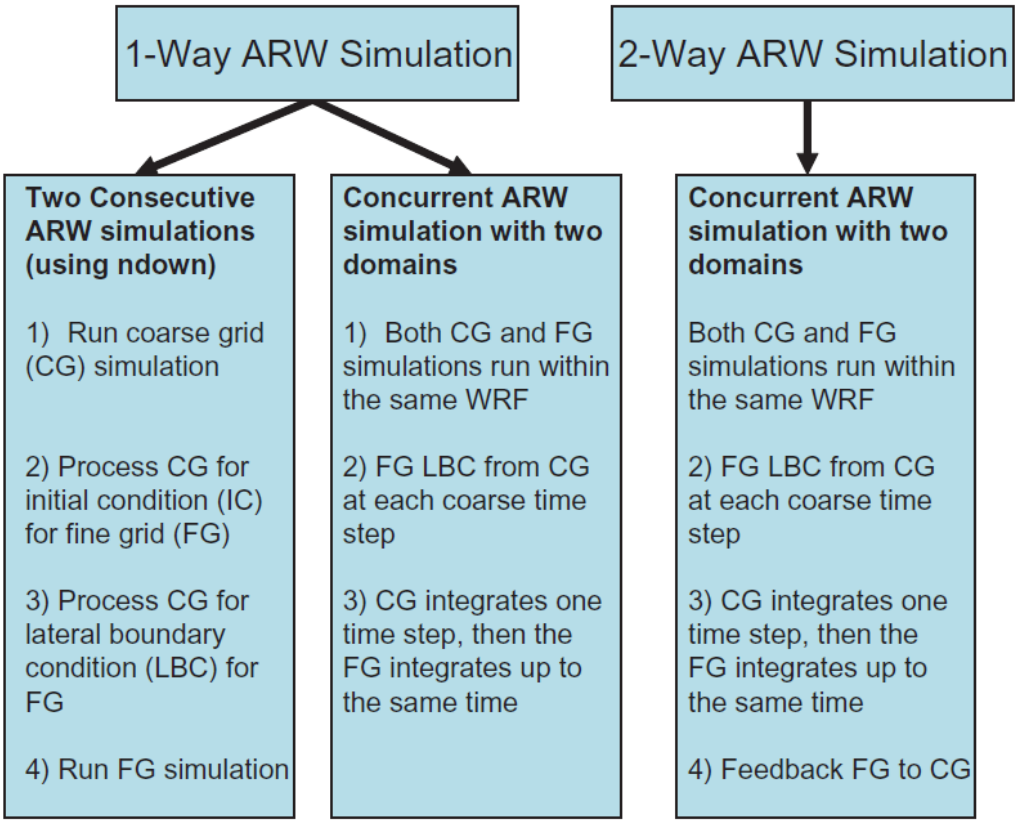

Figure 12 The process of runnning a one-way offline nested run (left box), a one-way online nested run (middle box) and a two-way nested run (right box) (Source: Skamarock et al. (2008))

3.3 Model Setup and Boundaries

In this study, WRF simulations of the storm Urd with horizontal resolutions of 1km using one-way offline nesting and 400m using one-way inline nesting are compared with measurements. The namelists that were used for both simulations can be found in Appendix B.

Two different domain boundaries were defined in this study for when simulating the different horizontal scales – one for the 1km run and one for the 400m run. The initial conditions used in this study are 6-hourly GFS analysis data produced by the National Oceanic and Atmospheric Administration (NOAA) with a 0.5 degrees resolution. The topography used in this study is the integrated WRF Gtopo 30 topography with a resolution of 30 arc-seconds. This topographic data was interpolated to a 1km and 400m resolution with WRF when simulating the 1km and 400m run respectively. The coarse domains received boundary information from the GFS-data every 6th hour, while the offline nests received boundary information every 3rd hour.

Figure 13 shows the domains used for the 1km simulation. The outer domains had horizontal resolutions of 27km, 9km and 3km respectively. As can be seen in the figure, the outermost domain covers most of the North Atlantic as well as most of Greenland and Europe. The 2nd domain covers Iceland, a part of Scotland, the Faroe Islands and some of the sea surrounding. The 3rd domain covers the Faroe Islands along with some of the surrounding sea, while domain 4 covers the Islands themselves.

The coarse simulation runs the largest domain with a horizontal resolution of 27km. The domain is 150x150 grid points in size while the other three nested domains are 160x160 grid points in size. All three domains have 40 Vertical layers and use the Lambert conformal map projection.

Figure 13 The 4 domains used for the 1km simulation. The horizontal resolution is 27km, 9km, 3km and 1 km respectively

Figure 14 shows the domains used for the 400m run. The coarse domain had a horizontal resolution of 10km, while the two nests had horizontal resolutions of 2km and 400m. The outermost domain covers Iceland, part of the British Isles, the Faroe Islands and some of the North Atlantic Sea. Domain 2 covers most of the Faroese sea territory, while the 3rd domain covers the islands themselves. The parent domain is centred around 61° N, -10° W. The coarse domain is 151x151 grid points in size while the 2km domain is 201x201 grid points in size. The 3rd domain is 289x289 grid points in size for the 400m run. The 1km simulation has 40 vertical layers, while the 400m simulation has 60 vertical layers. Both simulations use the Lambert conformal map projection.

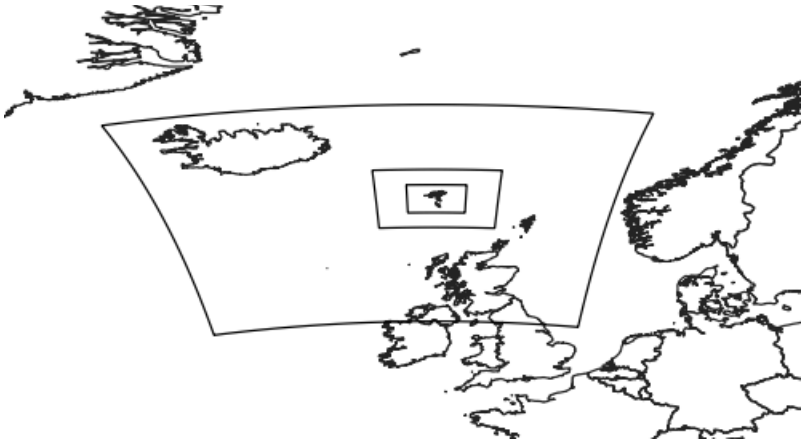

Figure 14 Domain of the 10km simulation with 2 nests. The horizontal resolution is 10km, 2km and 400m respectively

3.3.1 Physics and parametrization

WRF contains different sets of model physics to use for weather simulations. For the sake of convenience in this study when comparing between 2 different model resolutions, both simulations used the same parametrization schemes, and a short description of each scheme is written in this subsection. Table 2 shows a list of the parametrization schemes that have been used in this study.

Microphysics scheme

In order to take account for all the processes that occur on the scale of cloud droplets, microphysics schemes are used to parametrize these processes. Microphysics processes can play an important role in the formation of downslope windstorms and accurate simulations of the moisture distribution are important for predicting their magnitudes (Rögnvaldsson et al., 2011). The Morrison 2-Moment microphysics scheme has been used

for both WRF runs. This scheme is a two-moment bulk microphysics scheme which includes vapor, cloud droplets, cloud ice, rain, snow and graupel/hail (Skamarock et al., 2008).

Parametrization of radiation

For parametrizing radiation, the Rapid Radiative Transfer Model (RRTMG) scheme has been used for both shortwave and longwave radiation. The scheme uses pre-set tables to represent longwave processes due to water vapour, ozone, CO2 and trace gasses as well as accounting for cloud optical depth (Skamarock et al., 2008).

Planetary boundary layer (PBL) scheme

The planetary boundary layer is the lowest part of the atmosphere that separates Earth's surface from the free atmosphere and has a varying height between a few hundred meters and 1-2 kilometres. This part of the atmosphere experiences a lot of turbulent heat and moisture transport due to ground heating and friction, which realistically cannot be solved with the equations of motion due to the small-scale eddies present. Instead, these processes are parametrized by using planetary boundary layer schemes, which essentially try to make a closure to the turbulent terms that become present when one takes fluctuations into account in the equations of motion. The Mellor-Yamada-Janjic (MYJ) pbl scheme is a level 2.5 turbulence closure model and is used for both simulations.

Surface Layer and Land surface

The Eta surface layer scheme is based on similarity theory (Monin and Obukhov, 1954) and is used for both simulations.

Table 2 List of the physics schemes used in this study

Type of parametrization	Number and name
Microphysics	10 Morrison 2-moment scheme
Longwave radiation (LW)	4 RRTMG scheme
Shortwave radiation (SW)	4 RRTMG shortwave scheme
Surface layer	2 Eta similarity. Used in the Eta model (Janjic, 1996, 2002)
Land surface	2 Noah Land Surface Model
Planetary boundary layer (PBL-scheme)	2 Mellor-Yamada-Janjic scheme (Eta)

3.4 Verification Metrics

It is possible to calculate the values of verification metrics such as the Mean Absolute Error, the Mean Squared Error as well as the Bias by comparing the model data with measurements as a continuous variable.

In order to evaluate the performance of a weather simulation, the 1km run and the 400m run is compared with each other in terms of their verification metrics. This has been done in order to determine the improvement in weather prediction obtained by the 400m run compared to the 1km run.

3.4.1 Mean Absolute Error (MAE)

The mean absolute error is the average absolute difference between observed and simulated quantities over a timeline and is defined as:

$$MAE = \frac{1}{n}\sum_{k=1}^{n}|x_k - o_k|$$

Where (x_k, o_k) is the k-th of n pairs of simulations and observations. A lower MAE means a generally better prediction of the model (Warner, 2011, p. 295).

3.4.2 Mean Squared Error (MSE)

The mean squared error is the squared absolute difference between observed and simulated quantities over a timeline, and is for the same reason more sensitive to large errors. defined as:

$$MSE = \frac{1}{n}\sum_{k=1}^{n}(x_k - o_k)^2$$

3.4.3 Bias

The bias is a way of measuring a systematic error in the model prediction when compared to observations. The bias is calculated as:

$$Bias = \frac{1}{n}\sum_{k=1}^{n}(x_k - o_k)$$

Or simply the average of the simulated quantities minus the average of the observed quantities.

3.4.4 Skill Scores

Skill scores for continuous variables can be written as (Warner, 2011)

$$SS = \frac{MSE - MSE_{ref}}{0 - MSE_{ref}} = 1 - \frac{MSE}{MSE_{ref}}$$

Here SS denotes the skill score of a forecast compared to a reference forecast, where MSE is the squared error of the forecast, while MSE_{ref} is the squared error of a reference forecast.

3.5 Model Topographies

When simulating at different horizontal resolutions, the simulations also have different resolutions of topography to simulate with. This is one of the reasons why simulations with a coarse resolution are expected to yield a different result compared to simulations of higher resolution, as these include a more detailed topography. Higher resolution of a model is therefore also expected to be able to capture more topographic effects compared to the coarser runs. Figure 15 shows the Faroese topography as interpreted by each simulation at their respective resolutions.

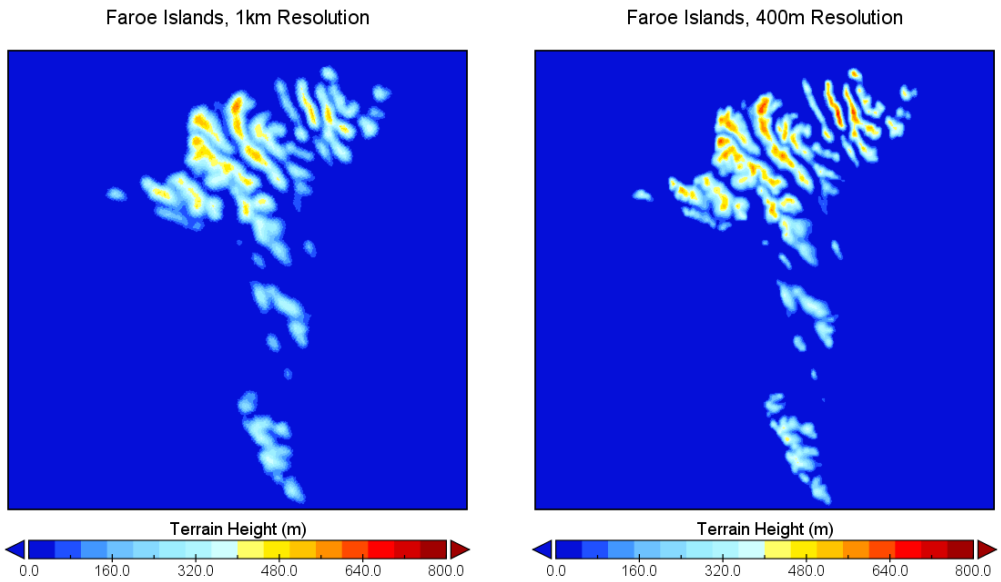

Figure 15 The model topography of the Faroe Islands viewed in Panoply with 1km resolution (left) and 400m resolution (right) These figures display interpolated height values from the model grid boxes

3.6 Challenges with the model topography

While working on the data analysis, some of the time series retrieved from the WRF simulations seemed to display severely different wind magnitudes than expected. The reason for this appeared to be that the Faroese topography as a whole in the output file was misplaced southwards compared to where the Faroese topography really is. The result of this was, that most of the locations that were determined to store time-series during the WRF simulation were misplaced compared to what is physically realistic. As an example, one measurement station located in Klaksvík near the sea was placed northwards on top of a mountain. Figure 16 shows an example of a comparison between the Global 30 arc-second elevation used in the WRF simulations for the 1km and 400m run compared to a Digital Surface Model (DSM) of the Faroe Islands provided by the Faroese Environment Agency. When looking at the southern tip of Streymoy and the surrounding islands in Figure 16, the 30 arc-second topography used in the WRF model appears to be misplaced southwards compared to the actual Faroese terrain.

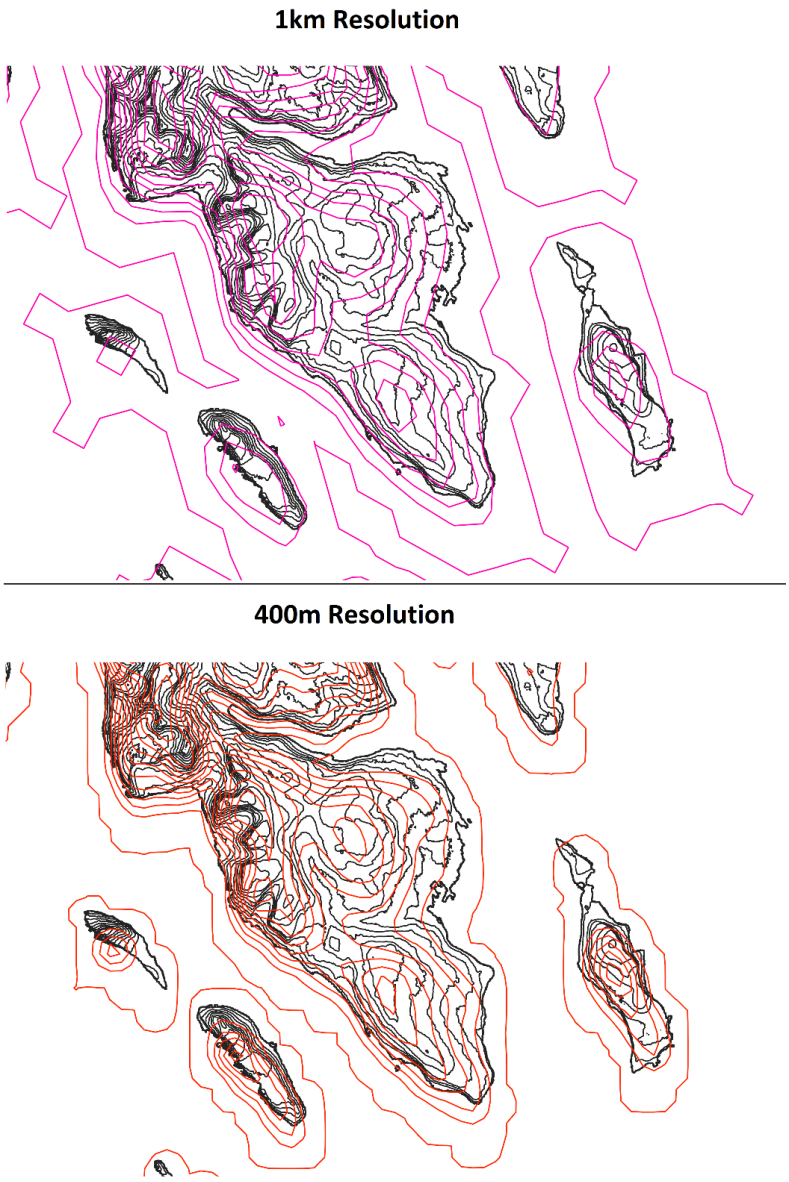

Figure 16 Comparison of the Faroese topography with the Global 30 Arc-Second Elevation used in the WRF simulations for the 1km resolution run (upper figure) and 400m resolution run (lower figure)

In order to retrieve meaningful weather data from points that physically corresponded well with the location of each weather station, a thorough analysis has been done for all 23 measurement sites. Table 3 shows that most measurement sites were moved 1-3 grid-boxes southwards, while some sites were moved 1 or two grid-boxes west or east.

Table 3 Overview of how far each measurement site was relocated in the WRF model topography

Station ID	Station Name	Altitude (m)	Longtitude	Lattitude	Gridboxes placed southwards (1km run)	Gridboxes places westwards (1km run)	Gridboxes placed southwards (400m run)	Gridboxes placed westwards (400m run)
F-10	Kambsdalur	110	-6.80463	62.21873	1	1	1	-1
F-12	Høgareyn	280.5	-7.15005	62.12655	1	-2	2	-2
F-21	Sund	51.5	-6.83880	62.04660	0	0	1	0
F-22	Runavík	9.8	-6.72860	62.10930	1	0	3	-1
F-23	Vatnsoyrar	40	-7.24630	62.06960	1	1	1	0
F-24	Klaksvík	22	-6.56973	62.22632	2	0	3	-1
F-25	Sandoy	120.5	-6.75910	61.82900	1	0	1	0
F-26	Syðradalur	2.5	-6.66380	62.24642	0	0	1	0
F-27	Porkeri	160	-6.75160	61.48860	2	1	3	-1
F-28	Krambatangi	2.5	-6.81690	61.54800	0	1	0	0
F-29	Skopun	2.5	-6.87884	61.90308	0	0	1	0
F-33	Norðadalsskarð	273	-6.91893	62.05478	1	1	3	1
F-34	Glyvursnes 2	115	-6.74980	61.97733	2	1	3	1
F-35	Tjørnuvík	66	-7.12778	62.29497	0	0	1	0
F-36	Kollafjørður	72	-6.89310	62.14013	0	1	2	0
F-37	Norðskálatunnilin	133.5	-6.92955	62.22318	0	0	2	0
F-40	Viðareiði	37.5	-6.54496	62.33215	1	0	2	0
F-41	Sandavágur	225	-7.15380	62.08567	1	1	1	0
F-42	Gjáarskarð	310	-6.97005	62.29843	0	0	1	0
F-43	Oyndarfjørður	245	-6.87689	62.24513	1	1	3	0
F-44	Hvalba	170	-6.93730	61.57558	0	0	2	-1
F-45	Streymnes	32	-7.02022	62.19278	0	0	1	0
F-48	við Velbastaðháls	185	-6.84718	61.98625	2	-1	2	-1

In order to determine, how far each measurement site had to be moved, Matlab was used to read the raw WRF output files and plot the model terrain at all 23 sites in order to get a clear picture of the terrain surrounding the site. Section 4.4 shows four examples of this.

It should be noted that the result of moving measurement sites to other locations in the WRF model is, that one can only work with hourly instantaneous model data during the simulation. The reason being that this is the only data in the output file saved at a location that is not included in the time series list. Meanwhile, the measured weather data in this study is 10-minute averages. As a result, one will have to take into account the uncertainty when comparing instantaneous values to 10-minute averages.

Prior, the study had time series sampled for each time step at the measurement location. These time series were interpolated to 10-minute averages which could be compared to the measured 10-minute average data throughout the passage of Urd. Thus, the amount of data available to compare with measurements has been reduced six times, as only one instance of a 10-minute average measurement is compared to the hourly instantaneous model data.

4. Results

This chapter presents the model data obtained from the WRF simulations and an analysis comparing the model data with observations as well as comparing the two runs with each other. Firstly, a synoptic overview of the passage of Urd is shown and analysed from the coarse domain run. Secondly, a closer look is taken at the Faroe Islands and time series of temperature, pressure and wind speeds measured during the passage of the storm. Furthermore, the challenges that were faced with the model topography of the Faroe Islands are studied closer at relevant measurement sites. This analysis is followed by an analysis of the model data results obtained at these selected measurement sites. Lastly, verification metrics were used to determine the performance of the 400m run in comparison to the 1km run.

4.1 The synoptic situation in the North Atlantic during the passage of Urd

4.1.1 Temperature

Figure 17 shows the two-meter surface temperature on a synoptic scale simulated by the 1km simulation's outermost domain with a horizontal resolution of 27km as Urd passes the Faroe Islands. The Faroe Islands seem to be situated in a cold spot shortly before the warm front passes the islands at 06:00 from south. Considering Figure 17 as well as the wind speeds in Figure 18, it appears as if an occluded front forms just as the cold front hits the Faroe Islands at 12:00.

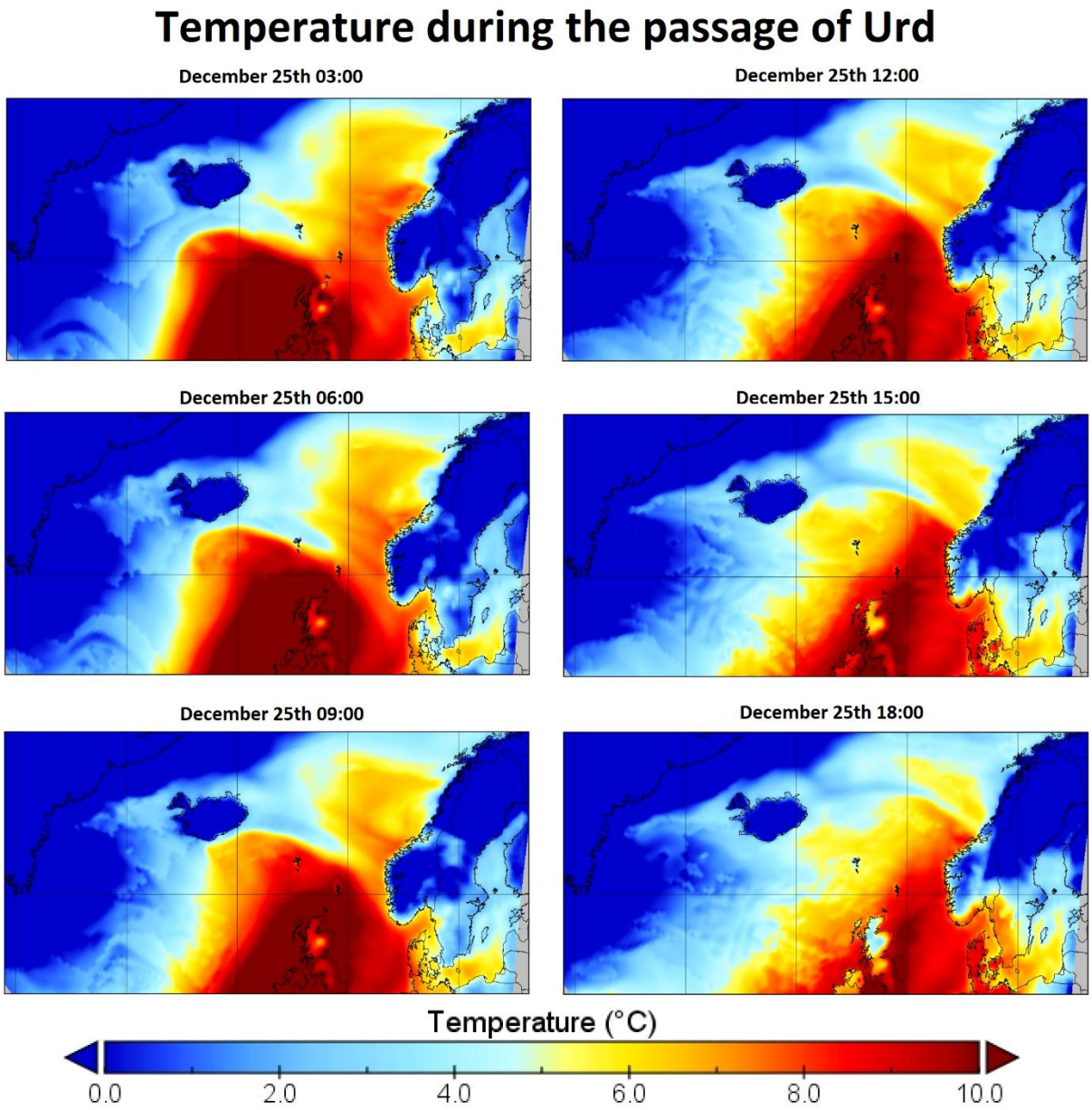

Figure 17 The frontal passage of Urd between 03:00 A.M. and 12:00 P.M. on December 25th 2016 viewed by the 1km run's outermost domain with a horizontal resolution of 27km

4.1.2 Wind speed

Figure 18 shows the modelled wind speeds during the frontal passage. The simulation shows increasing wind magnitudes hitting the Faroe Islands between 06:00 and 09:00 as the warm front passes. The wind magnitudes increase to above 30 m/s continuing as the cold front passes the Faroe Islands peaking at around 15:00.

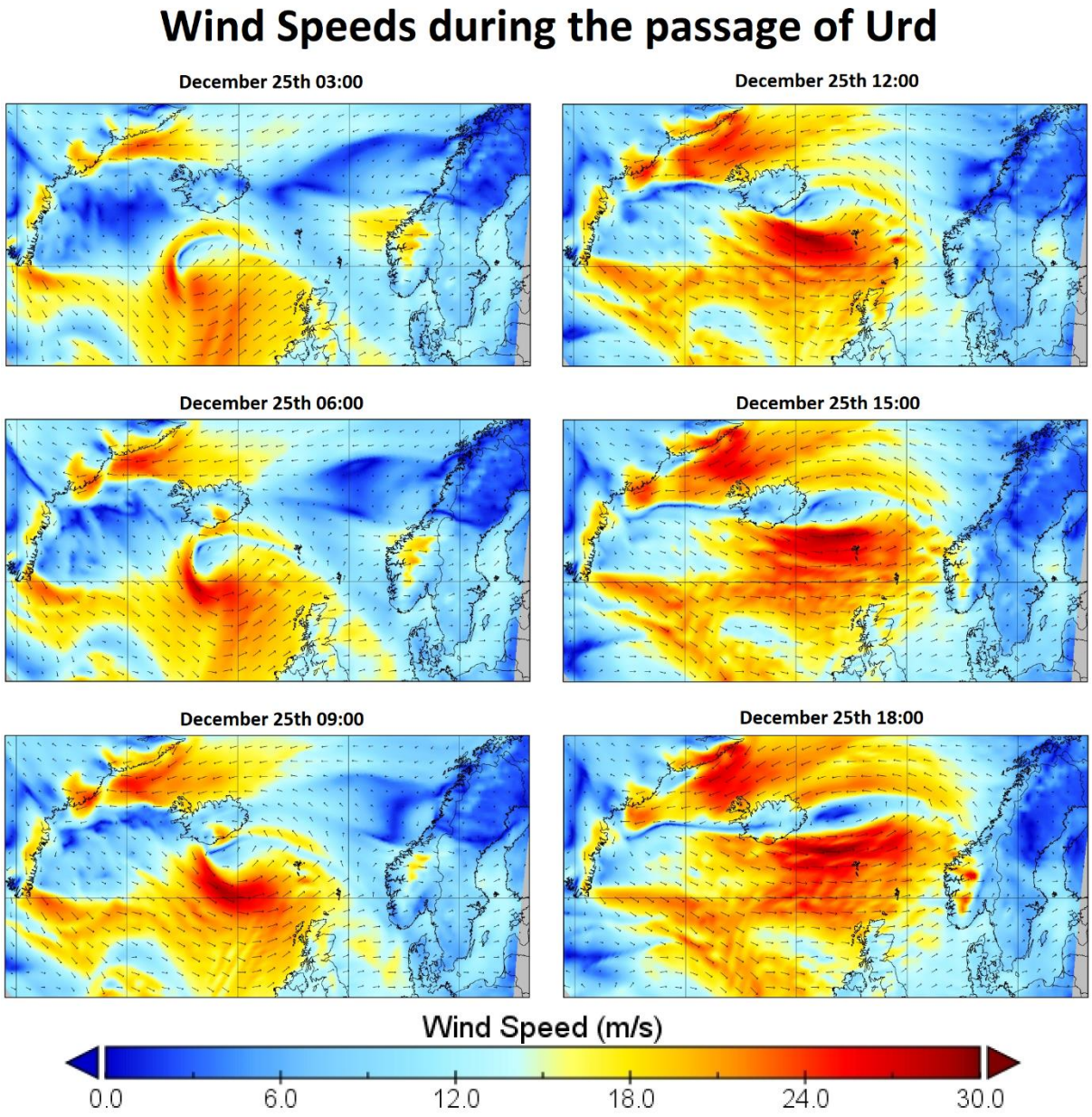

Figure 18 Wind magnitudes during the frontal passage between 03:00 A.M. and 18:00 P.M. on December 25th 2016 viewed by the 1km run's outermost domain with a horizontal resolution of 27km

4.2 The Faroe Islands

4.2.1 The Frontal Passage

Figure 19 shows the potential temperature at 06:00 simulated by the 1 km run and the 400m run during the frontal passage. Both simulations predict the warm front to hit the Faroe Islands at 06:00. One may also observe, that the 400m run shows more complex patterns of potential temperature than the 1 km run. Considering the figure, one may expect the weather stations in Suðuroy to measure the rise in temperatures before the rest of the Faroe Islands for these two simulations to be representative.

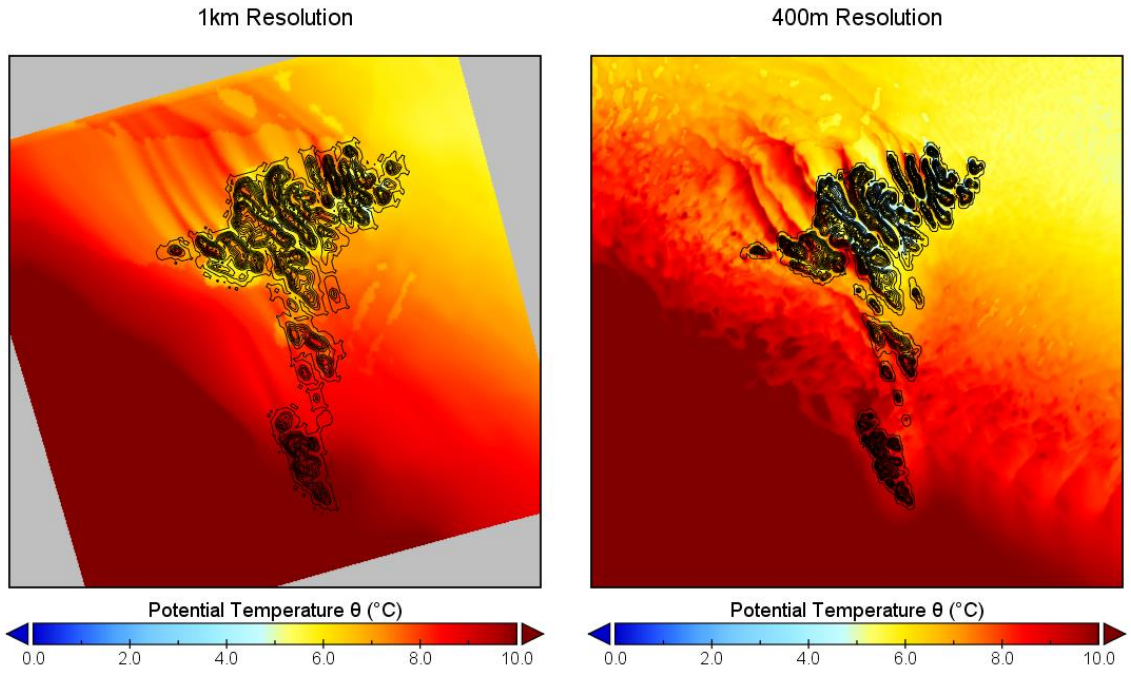

Figure 19 Potential temperature θ on the Faroe Islands simulated on a 1km grid (left) and a 400m grid (right), 6:00 A.M. on December 25th 2016.

4.2.2 Wind Magnitudes during the passage of Urd

Figure 20 shows the surface wind magnitudes simulated at 1km and 400m run during the frontal passage, while Figure 21 shows the wind magnitudes simulated during the measured peak in wind speeds, which was at 15:00. Considering the situation at 06:00, winds generally blow from the south and both the 1km run and 400m run show turbulence on the lee side of the Faroe Islands and increased surface wind speeds north of the islands.

Considering the situation at 15:00, the 1km run shows the wind to come from the west compared to the 400m run, which predicts the wind direction to be more south-west. In

contrast to the events during the frontal passage, turbulence on the lee side of the islands appears to decrease the surface wind magnitudes. This is especially prominent for the 400m run.

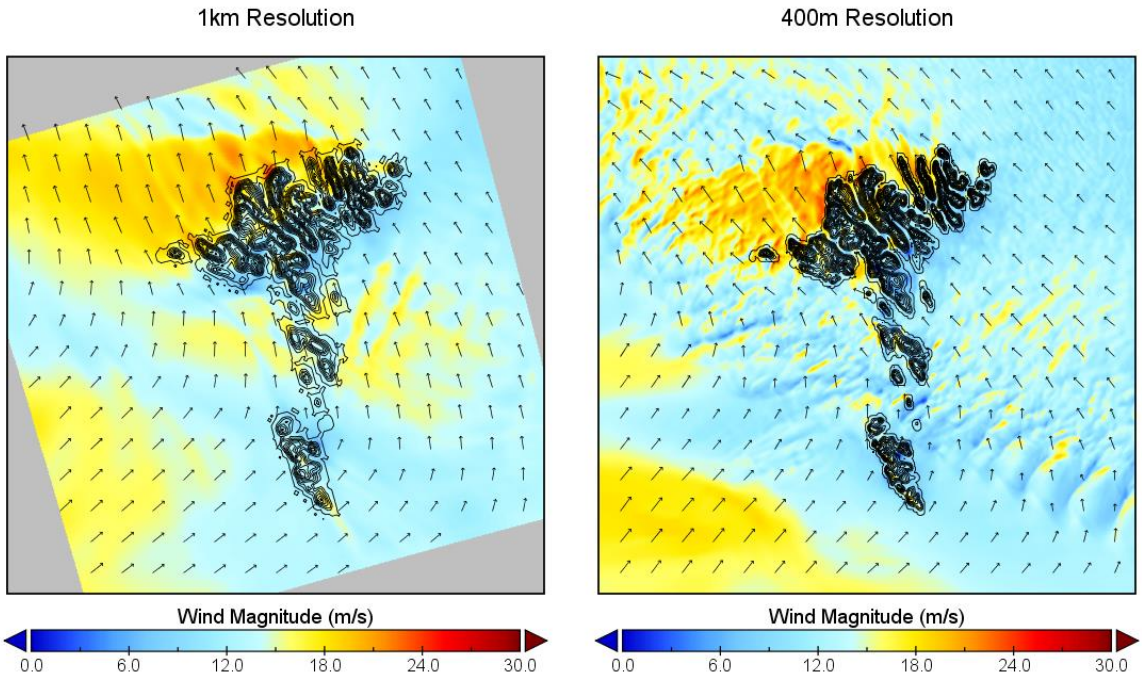

Figure 20 Simulated wind magnitudes on the Faroe Islands during the frontal passage by the 1km (left) and 400m (right) simulation, 6:00 A.M. on December 25th 2016.

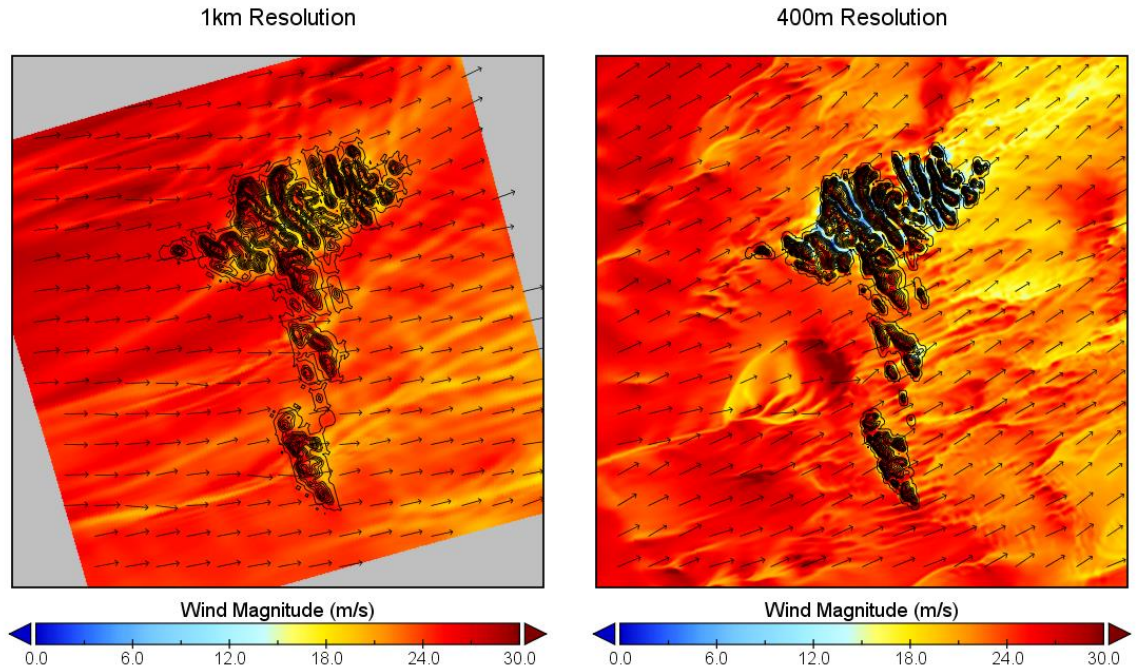

Figure 21 Simulated wind magnitudes on the Faroe Islands at the peak of the storm by the 1km (left) and 400m (right) simulation, 15:00 P.M. on December 25th 2016.

4.3 Comparison between model data and measurements

Temperature

Figure 22 shows a time series of the temperature measured between December 25th and December 26th. The weather stations operated by Landsverk measure a decrease in temperature. The average measured temperature dips to below 1°C before a sharp rise at 06:00 in the morning of December 25th during the frontal passage. The temperatures peak at 10:00 with average measured temperatures of 10°C followed by a decline in temperature after noon as the cold front passes.

While there is a general deviation in temperature measured of about 2-3 degrees between individual sites, none of the time series included deviate heavily from the rest. The differences in temperature measured may be factors such as the different altitudes at which the measurement stations are placed, but is also due to the spatial variability resulting in some of the stations experiencing the frontal passages earlier than the others. For instance, the stations placed in Suðuroy are also the first stations to measure the increase in temperature.

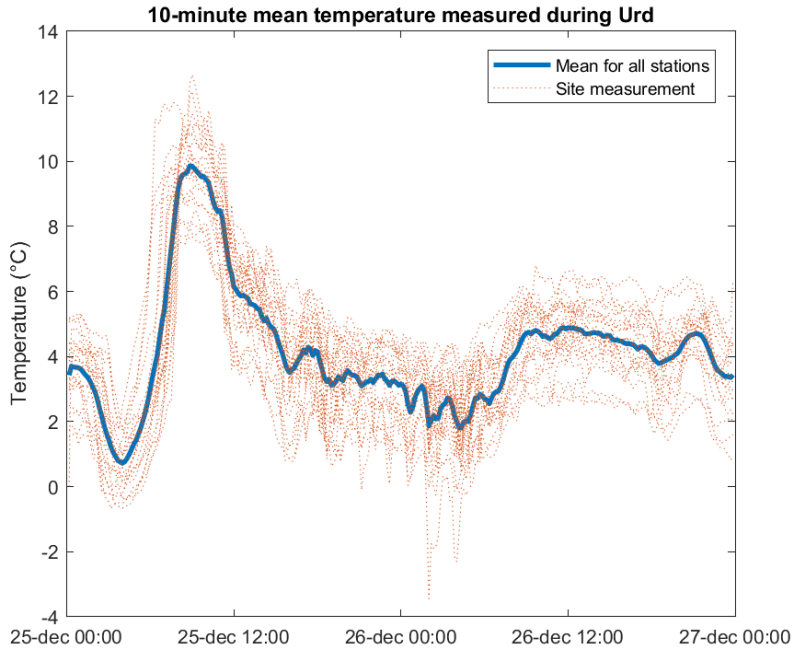

Figure 22 Time series of the hourly averaged temperature measured at each station (dashed red lines) and the average of all weather stations (blue line)

The comparison between the mean temperatures measured and modelled in Figure 23 shows that the WRF model predicted the warm front to hit the Faroe Islands on time. It was however not able to capture the sharp gradient in temperatures measured during the warm front passage. This may indicate that the WRF model underpredicted the severity of this storm.

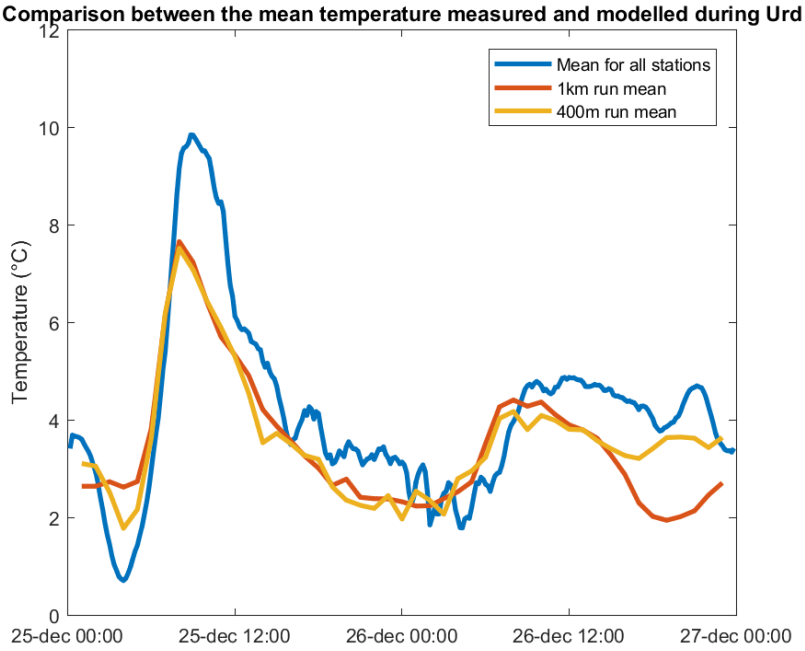

Figure 23 Comparison between the mean temperature measured and modelled during Urd

Figure 24 shows two scatter plots comparing the measured and modelled temperatures at the 23 measurement sites during the passage of Urd, after the adjustments of the placement of each measurement site was made. The red line indicates points of perfect forecasts (x=y), where points above the red line show underestimated values and points below the red line show overestimated values. Considering both the 400m run and the 1km run, the high temperatures appear to be underestimated. This is also attributed to the underestimation of the warm front passing the Faroe Islands during the storm, and is shown in the time series in Figure 23. In addition, the 400m run succeeds in predicting some of the lowest measured temperatures, which the 1km run doesn't succeed to.

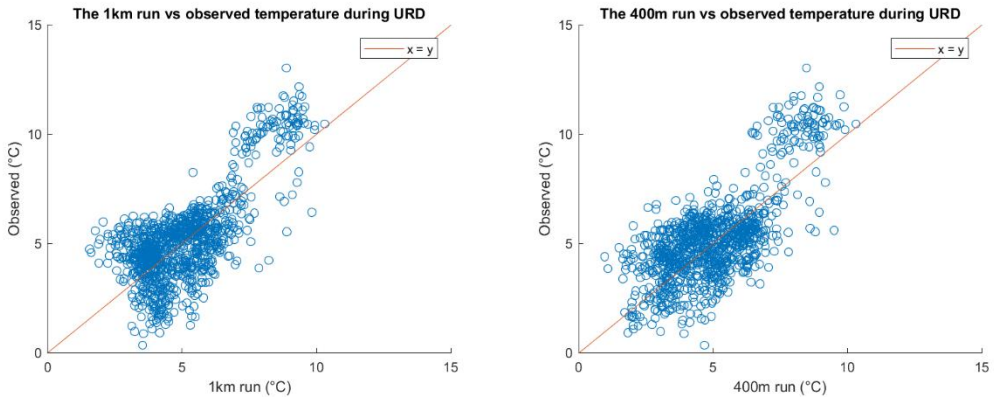

Figure 24 Scatter plots of simulated and measured temperatures adiabatically adjusted to 0m elevation during Urd, after the relocation of each measurement site

Figure 25 shows two density plots of the scatter plots in Figure 24. One may observe that the 1km run generally tends to underestimate the temperatures by a small fraction with two hotspot surrounding 4°C modelled over 4°C measured and 5.5°C modelled over 5.5°C measured. The 400m run has a similar hotspot as well as an additional hotspot at 6°C modelled over 5.5°C measured.

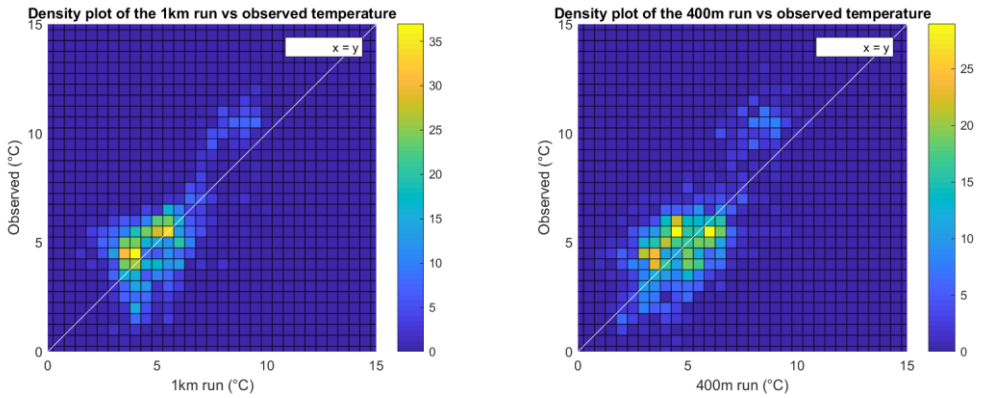

Figure 25 Scatter density plots of simulated and measured temperatures adiabatically adjusted to 0m elevation during Urd, after the relocation of each measurement site

Pressure

Figure 26 shows the evolution of pressure measured during the passage of Urd. The figure shows that the low pressure is closest to the Faroe Islands just after mid-day on December 25th, as the pressure levels reach their lowest point before the storm slowly departs eastwards.

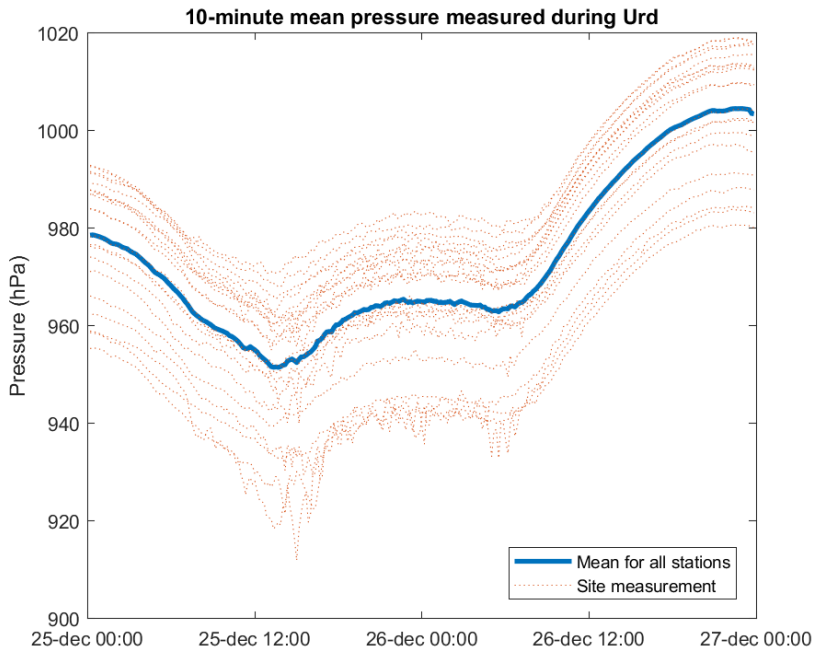

Figure 26 Time series of the hourly averaged pressure levels measured at each station (dashed red lines) and the average of all weather stations (blue line)

As one would expect since none of the weather stations are more than 100 kilometers apart, similar pressure tendencies were measured between December 25th and December 26th at all locations. It is however worth noting the rapid fluctuations in pressure levels that were measured between December 25th 09:00 and December 26th 09:00, which was also the time window with the strongest winds.

It is well known that gusts can affect the measured atmospheric pressure in buildings. If a building has an opening, the internal pressure of the building is affected by the outdoor wind speeds to an extent that depends on the wind direction compared to where the opening is. If an opening exists on the windward side, internal pressure should be higher than the ambient pressure levels. If an opening exists on any of the other sides, the internal pressure should be lower than its ambient levels (Liu and Grant, 1989).

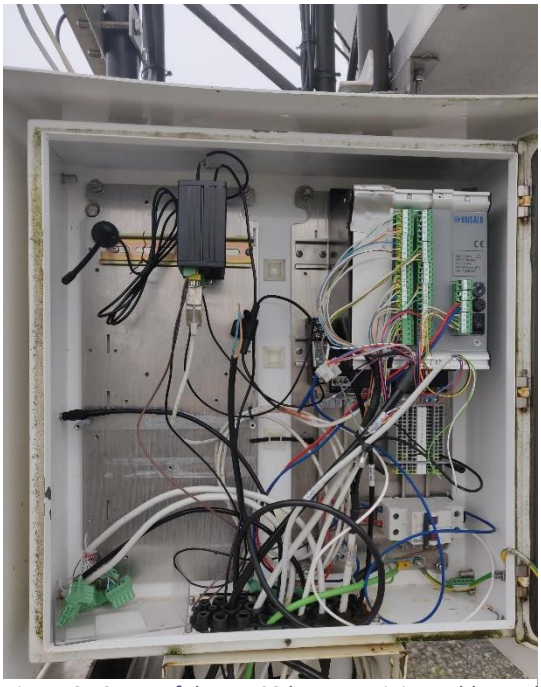

Figure 27 Setup of the DM32 box containing cables and instruments such as the barometer at Norðadalsskarð

The barometers used at the weather stations in this study were stored in boxes as shown in Figure 27. However, there is clear air passage in the bottom of these boxes (Gregoriussen, 2019, p. 6) and consequently, measured pressure levels could drop during strong wind speeds. Given that the measured pressure is instantaneous, this might cause the fluctuations that were observed during the passage of Urd as gusts may change the internal pressure of the box. Since the error in internal pressure increases with the square of wind speed (Liu and Grant, 1989), this could also explain why the fluctuations are so prominent during the peak of this storm.

Figure 28 shows a comparison between the average measured and modelled pressure as a deviation from the pressure level at 00:00 on December 25th 2016. Similar to what was found when comparing the temperature gradients in Figure 23, it is evident from this figure that the WRF model was not able to simulate the steepness of the pressure gradient over time that was measured during the peak of this storm. This may have resulted in an underestimation of the severity of Urd by the simulations, as the low pressure was measured to be deeper than what was simulated. When comparing with model data, it should however be noted that a change in internal pressure due to wind speeds could also to some degree have affected the measured pressure levels.

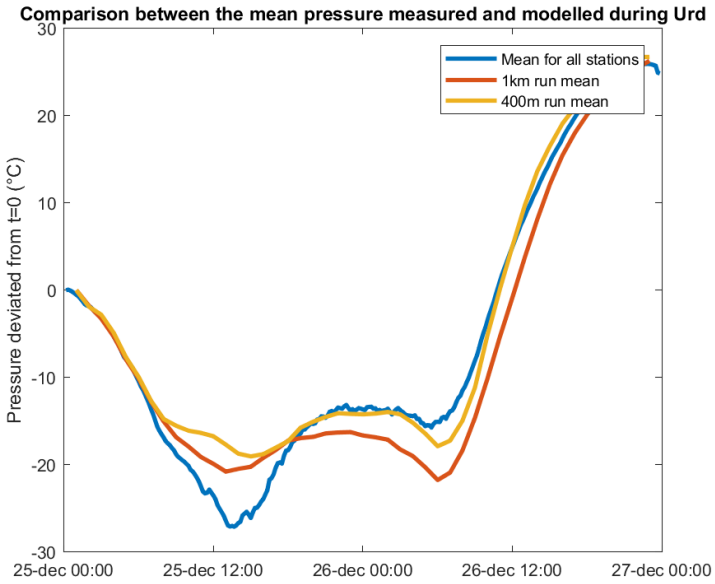

Figure 28 Comparison between the average pressure levels measured and modelled during the passage of Urd as a deviation of a reference pressure. The reference pressure level is set at t=0 for each individual dataset

Figure 29 shows a scatterplot of the simulated pressure levels by the two simulations in comparison to measurements during the passage of Urd. The difference between the modelled terrain altitude and the actual altitude may play a significant role in the general under and overestimations of pressure levels in this figure. In order to compensate for the issue, pressure levels have been adiabatically adjusted to the 0m elevation in Figure 30.

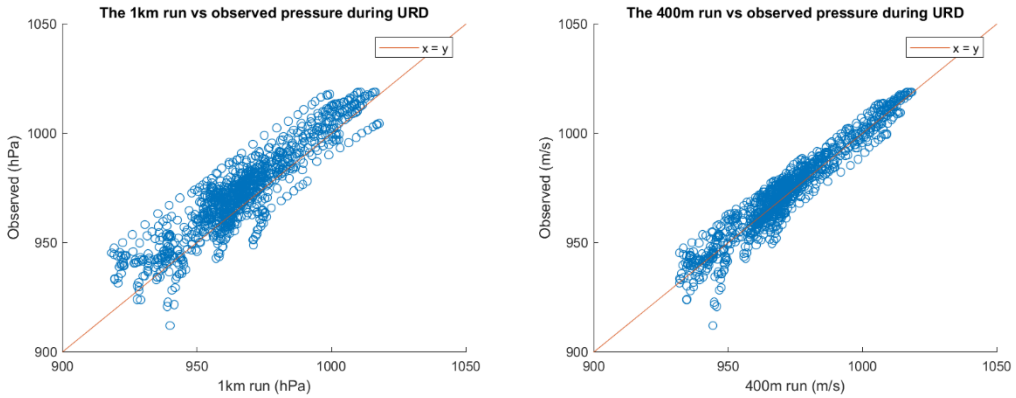

Figure 29 Scatter plots of simulated and measured pressure during Urd, after the relocation of each measurement site

Considering the scatterplots in Figure 30, it seems that the 1km run marginally overestimated most of the measured pressure, while the 400m run was able to capture the pressure more accurately. Both simulations seem to have overestimated the lowest pressure values, which was also evident from the time series in Figure 28.

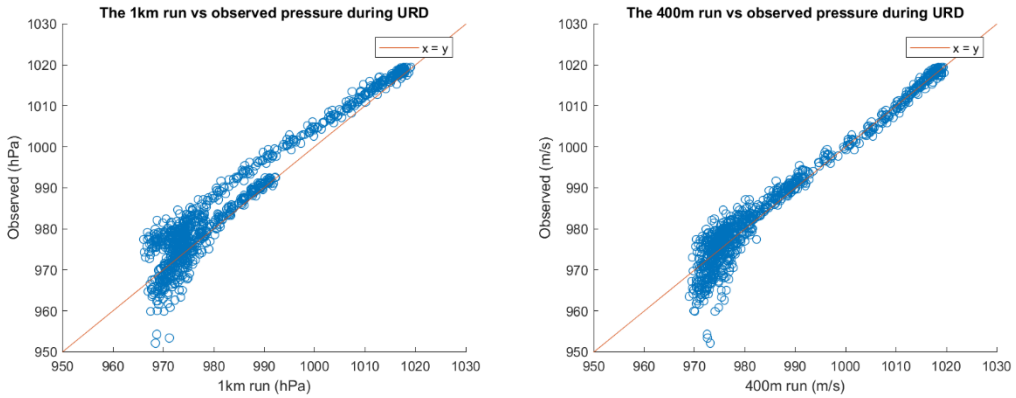

Figure 30 Scatter plots of simulated and measured pressure adiabatically adjusted to 0m elevation during Urd, after the relocation of each measurement site

Both density plots in Figure 31 show two hotspots, one at 1020 hPa modelled over 1020 hPa measured, and one at 975 hPa modelled over 975 hPa measured. The overestimation of pressure by the 1km run seen in Figure 30 also becomes apparent in this figure.

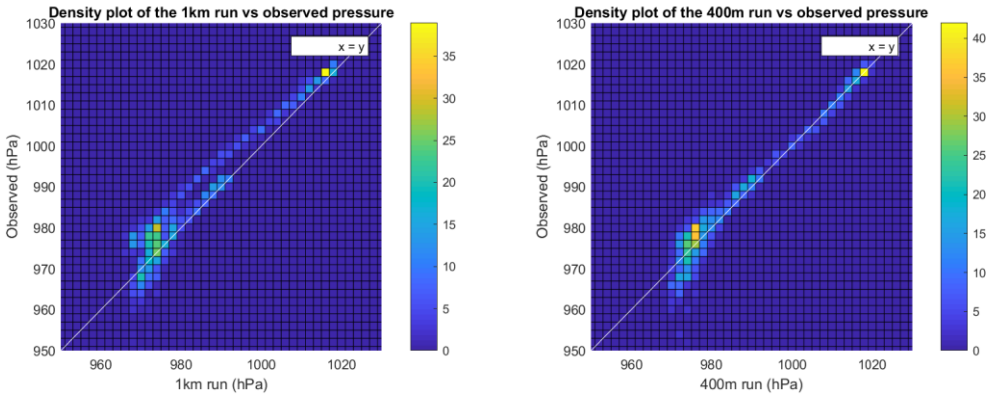

Figure 31 Scatter density plots of simulated and measured pressure adiabatically adjusted to 0m elevation during Urd, after the relocation of each measurement site

Wind Speed

Figure 32 shows that the 10-minute average wind speeds measured on the Faroe Islands during the passage of Urd had a broad spectrum in magnitudes depending on each measurement site. While some weather stations only measured 10-minute average wind speeds of maximum 10 m/s during the entire storm, other weather stations measured 10-minute average wind speeds above 50 m/s. The average of all wind measurements steadily increase peaking at 15:00 after the cold front has passed.

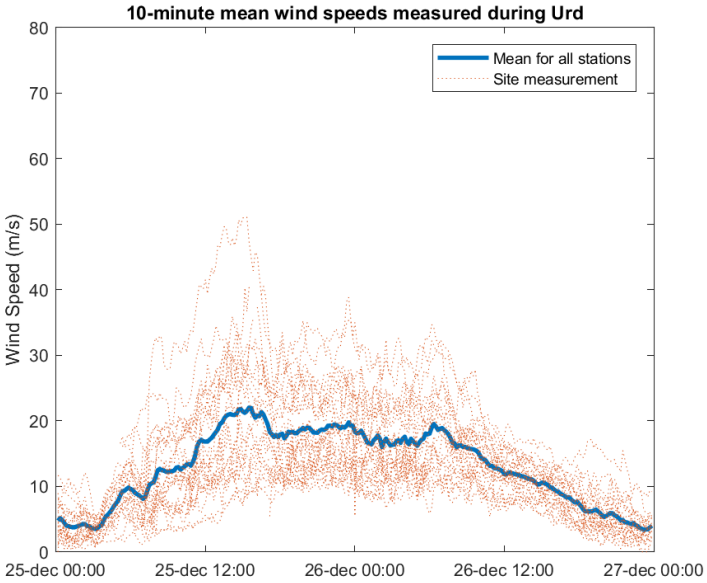

Figure 32 Time series of the 10-minute averaged wind magnitudes measured at each station (dashed red lines) and the average of all weather stations (blue line) during the passage of Urd.

Meanwhile, Figure 33 shows all measurement sites to measure gusts above 20 m/s during the passage of Urd, while some stations measured gusts above 70 m/s. The overall larger magnitudes of gusts measured compared to the 10-minute average wind speeds also gives evidence for the turbulent nature caused by the complex terrain surrounding each site. The large variability between each measurement site may also be largely attributed to the local terrain and weather effects caused by the surrounding terrain of these sites.

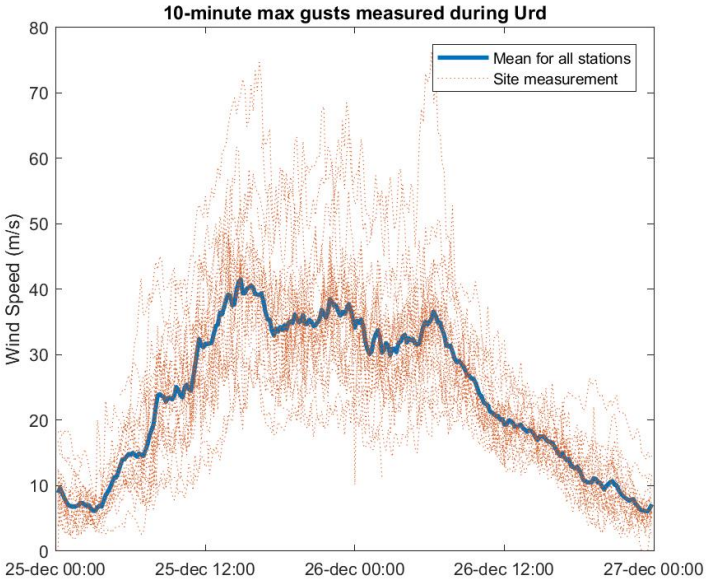

Figure 33 Time series of the 10-minute max gusts measured at each station (dashed red lines) and the average of all weather stations (blue line) during the passage of Urd.

Figure 34 shows a scatter plot comparing the measured and modelled wind magnitudes at the 23 measurement sites during the passage or Urd, before the adjustments of the placement of each measurement site was made. Considering the 400m run, some of the simulated wind speeds have been vastly underestimated throughout the spectrum. The same can be said for the 1km run, however only for wind magnitudes measured to be above 30 m/s. The 1km run also has some vast overestimations at wind speeds that were measured to be around 10 m/s.

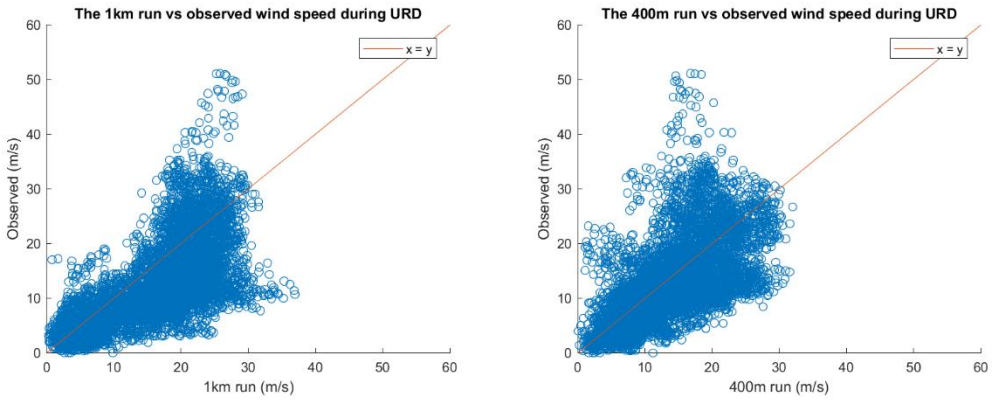

Figure 34 Scatter plots of simulated and measured wind magnitudes during Urd, before the relocation of each measurement site

Figure 35 shows density plots of the scatter plots in Figure 34. One may observe that the 1km run generally tends to overestimate the wind speeds measured with a hotspot surrounding 20 m/s simulated over 12 m/s measured. The 400m run has a similar but smaller hotspot closer to the perfect-forecast line, near 17 m/s simulated over 12 m/s measured. Overall, the 400m run appears to simulate wind magnitudes closer to what was measured between December 25th and 26th.

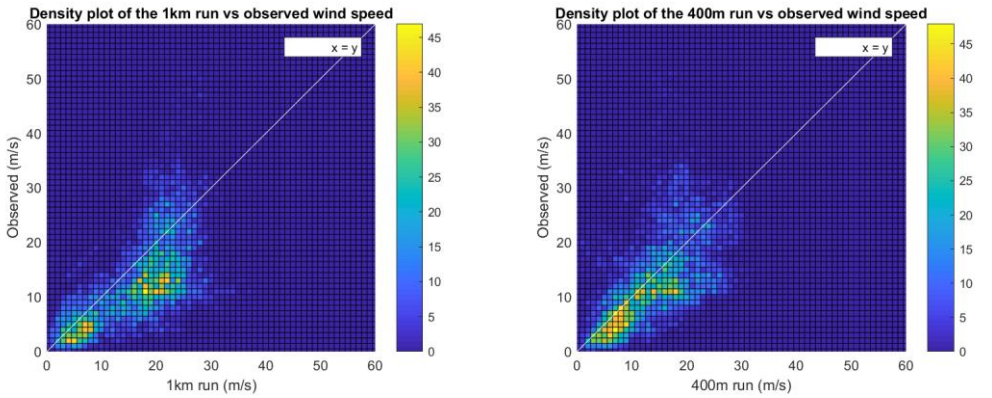

Figure 35 Scatter density plots of simulated and measured wind magnitudes during Urd, before the relocation of each measurement site

Figure 36 shows a scatterplot comparing the measured and modelled wind magnitudes at the 23 measurement sites during the passage or Urd, after the adjustments of the placement of each measurement site was made. Compared to Figure 34, the 400m run now shows much less cases of wind magnitudes that previously were vastly underestimated, while the 1km run still shows a similar pattern of the overestimations and

underestimations that were present earlier. The density scatterplot of Figure 37 show similar patterns to the density scatterplot in Figure 35 before the measurement sites were moved.

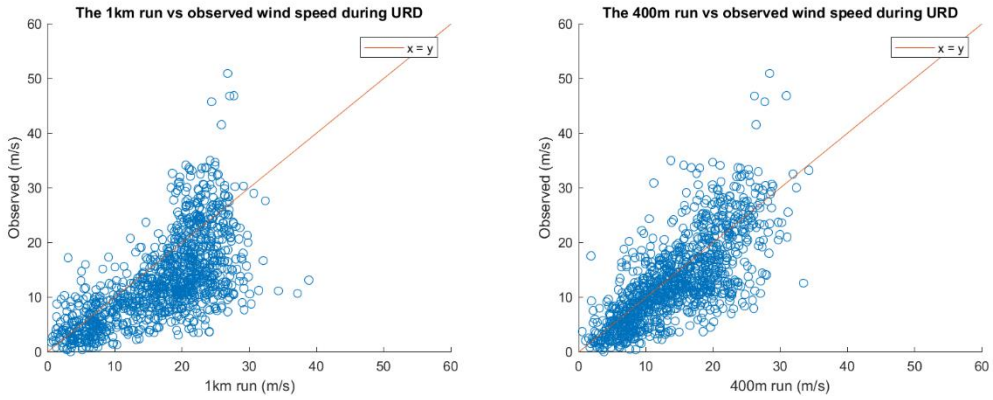

Figure 36 Scatter plots of simulated and measured wind magnitudes during Urd, after the relocation of each measurement site

When comparing Figure 34 and Figure 35 with Figure 36 and Figure 37, one has to take into account that there are almost 6 times less measurements present after the adjustments of the placement of each measurement site as explained in section 3.6. This may also change the general picture of these scatterplots. In order to get a deeper understanding of the impact that moving the measurement sites has, one needs to make a deeper analysis at each individual site with time series analysis and statistics. This is done for three selected measurement sites in section 3.6.

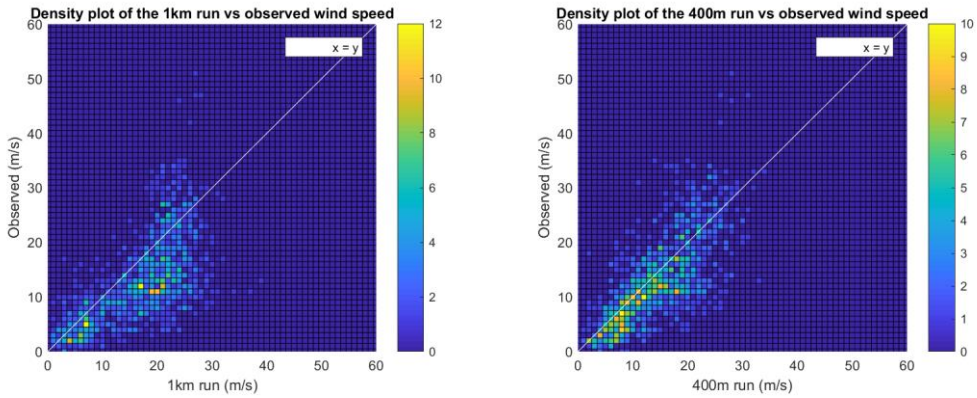

Figure 37 Scatter density plots of simulated and measured wind magnitudes during Urd, after the relocation of each measurement site

4.4 Topographic analysis of the Faroese terrain at selected measurement sites

The following figures in this section show the WRF topography as interpreted by the two simulations in comparison to Google Earth. The black dots in these figures represent the grid point where the time series were originally collecting model data from. The red dots in the figures represent the new points that have been selected for this analysis. This is in order to represent a more physically realistic location with respect to the actual site location due to the apparent misalignment of the WRF-topography used in this study compared to the actual topography.

4.4.1 Norðadalsskarð

Figure 38 shows Norðadalsskarð as shown by Google Earth in a north-east to south-west perspective with the measurement site placed on the mountain pass. The village of Norðadalur is placed on the other side of the mountain pass, while Kaldbaksfjørður is seen in the bottom of this figure.

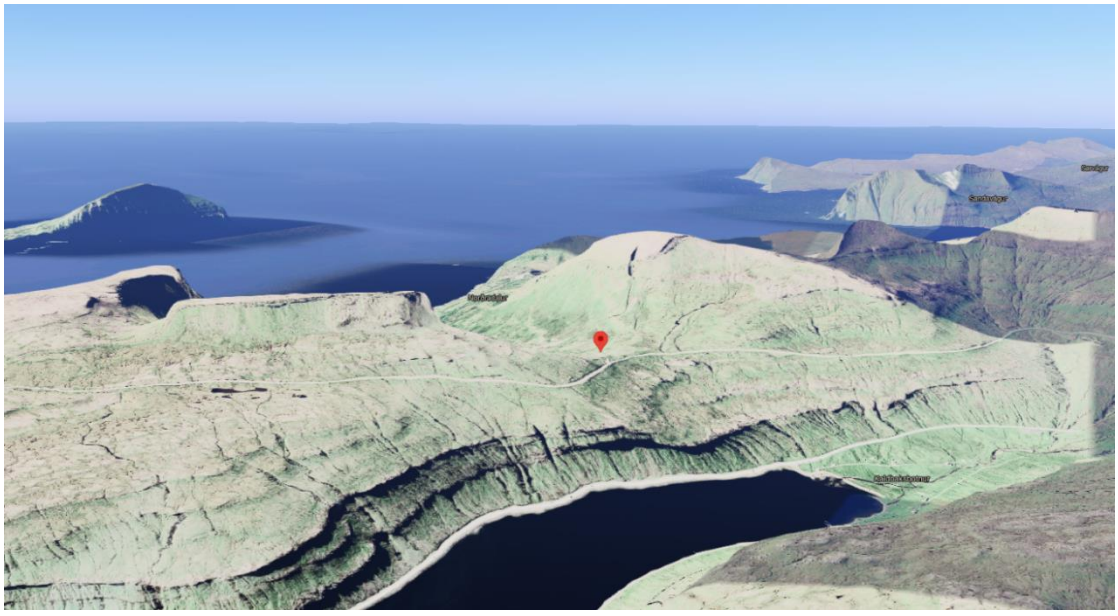

Figure 38 Norðadalsskarð as shown by Google Earth. The red dot denotes the coordinate of the measurement station

Figure 39 and Figure 40 show the WRF topography of the mountain pass of Norðadalsskarð as interpreted by the 1km simulation and 400m simulation respectively. For both the 1km

and 400m simulation, the grid box that WRF had selected with respect to the coordinates of the measurement site appears to be placed in the adjacent fjord of Kaldbaksfjørður instead of the mountain pass. In order to compensate for this, the gridcell chosen to represent the simulated values has been moved southwards to a location that physically resembles more that of the mountain pass.

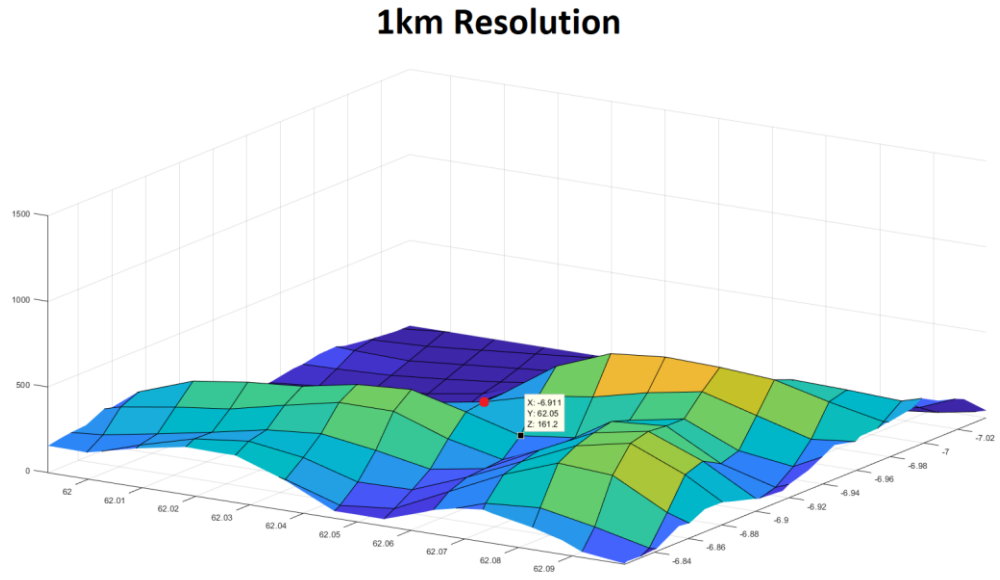

Figure 39 Norðadalsskarð as interpreted by the 1km grid. The black dot denotes the gridcell chosen to represent the simulated values, while the red dot denotes the relocation of the measurement site for this study

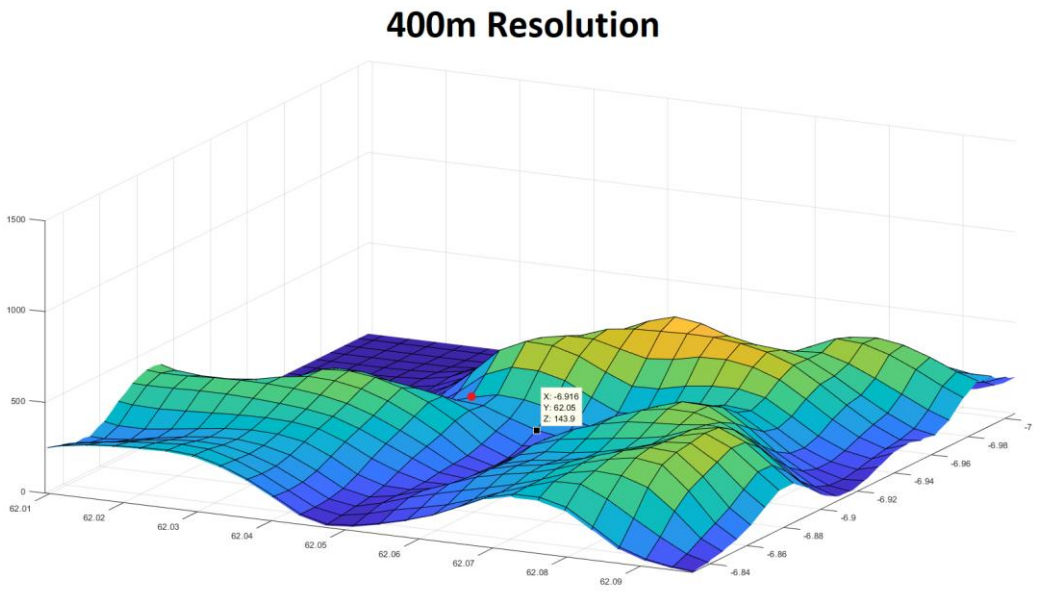

Figure 40 Norðadalsskarð as interpreted on the 400m grid. The black dot denotes the gridcell chosen to represent the simulated values, while the red dot denotes the relocation of the measurement site for this study

Despite these issues, the mountain pass appears to be well defined in both the 1km and 400m simulation with the two adjacent mountains present as well as the fjord just north of the pass. It is however interesting to note that the fjord has a relatively high elevation and never reaches 0m in these figures. The reason for this could be that the topographic dataset with a 1km resolution is too coarse to define the fjords when interpolating down to a 400m resolution.

4.4.2 Høgareyn

Figure 41 shows Høgareyn as shown by Google Earth in a south to north perspective with the measurement site placed on the mountainside. The village of Vestmanna lies just north-west of Høgareyn and the surrounding water seen in this figure is the channel of Vestmannasund.

Figure 41 Høgareyn as shown by Google Earth. The red dot denotes the coordinate of the measurement station

Figure 42 and Figure 43 show the WRF topography of the 1km simulation and 400m simulation respectively. The topography displayed by these simulations seems to scale well with what is seen in Google Earth. It is however interesting to point out that the channel of Vestmannasund does not have 0m elevation at any point in the model data for both simulations. The reason could again be that the topographic dataset with a 1km resolution is too coarse to define the channel when interpolating down to 400m.

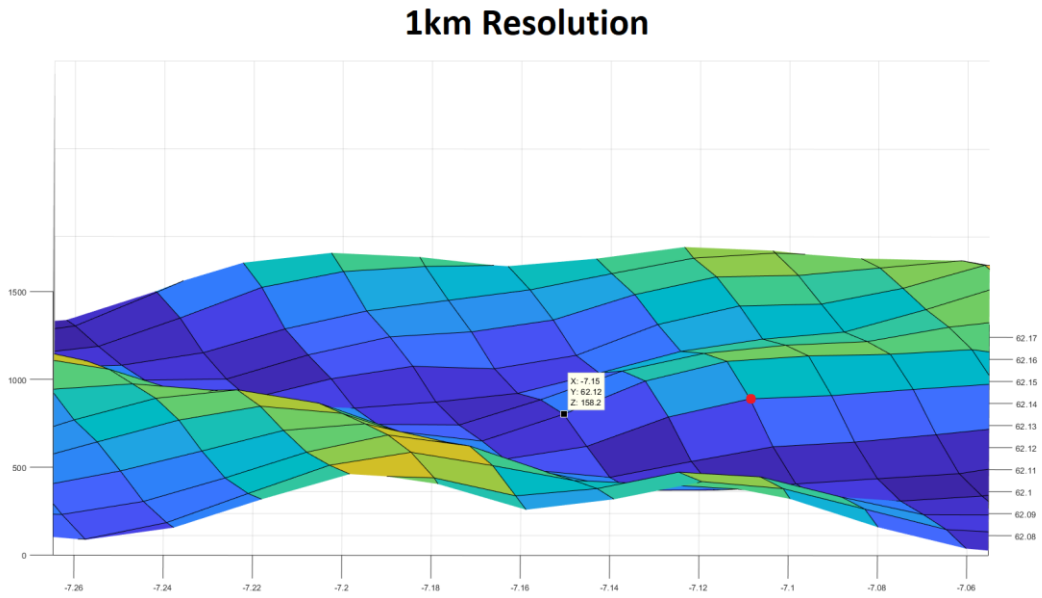

Figure 42 Høgareyn as interpreted on the 1km grid. The black dot denotes the gridcell chosen to represent the simulated values, while the red dot denotes the relocation of the measurement site for this study

The grid box selected by WRF to store time series in both the 1km and 400m simulation appears to be misplaced northwards compared to what is physically representative. For this reason the site has been moved southwards to a grid point that physically resembles more the location of the measurement site.

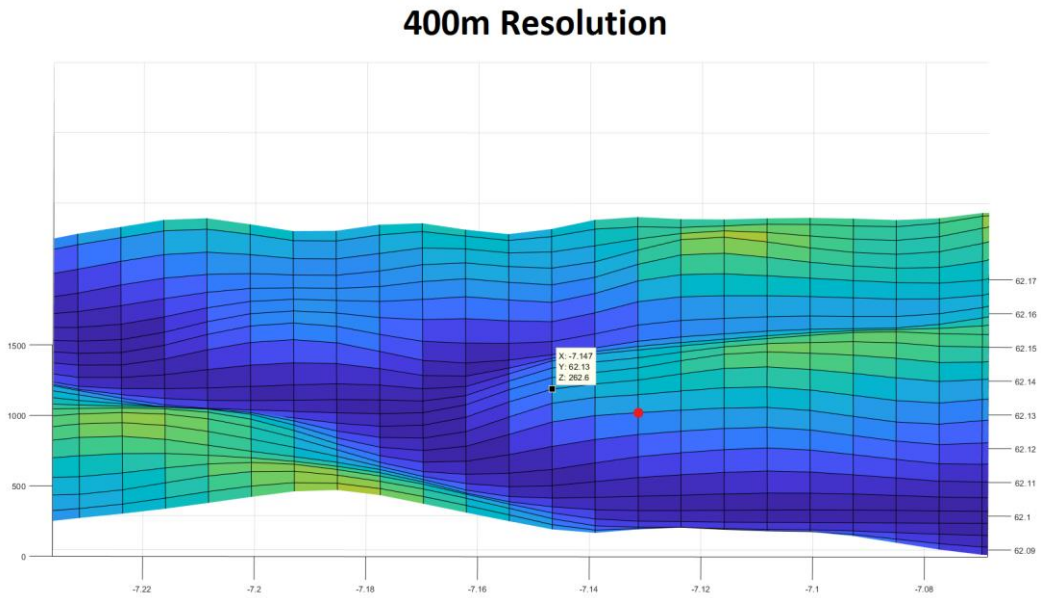

Figure 43 Høgareyn as interpreted on the 400m grid. The black dot denotes the gridcell chosen to represent the simulated values, while the red dot denotes the relocation of the measurement site for this study

4.4.3 Klaksvík

Compared to many other sites used in this study, this site is surrounded with an even more complex topography with steeper mountains. Figure 44 shows Klaksvík as shown by Google Earth in a south-east to north-west perspective. The measurement site is located by the edge of Klaksvík close to the shore and a steep mountain incline. The two mountain barriers surrounding Klaksvík to the south-west and north-east are seen to the left and right of this figure respectively.

Figure 44 Klaksvík as shown by Google Earth. The red dot denotes the coordinate of the measurement station

Figure 45 shows the WRF topography as interpreted by the 1km run, while Figure 46 shows the WRF topography as interpreted by the 400m run. The topography displayed by the 1km run seems to somewhat resemble most features of the topography compared to what is seen in Google Earth. However, the topography displayed on the 400m grid resembles these features to a much greater detail. Most of the water surrounding Klaksvík and the northern islands as a whole in Figure 44 has elevations above 0m in the 1km model topography, while only parts of the water is actually at 0m elevation in the 400m model topography.

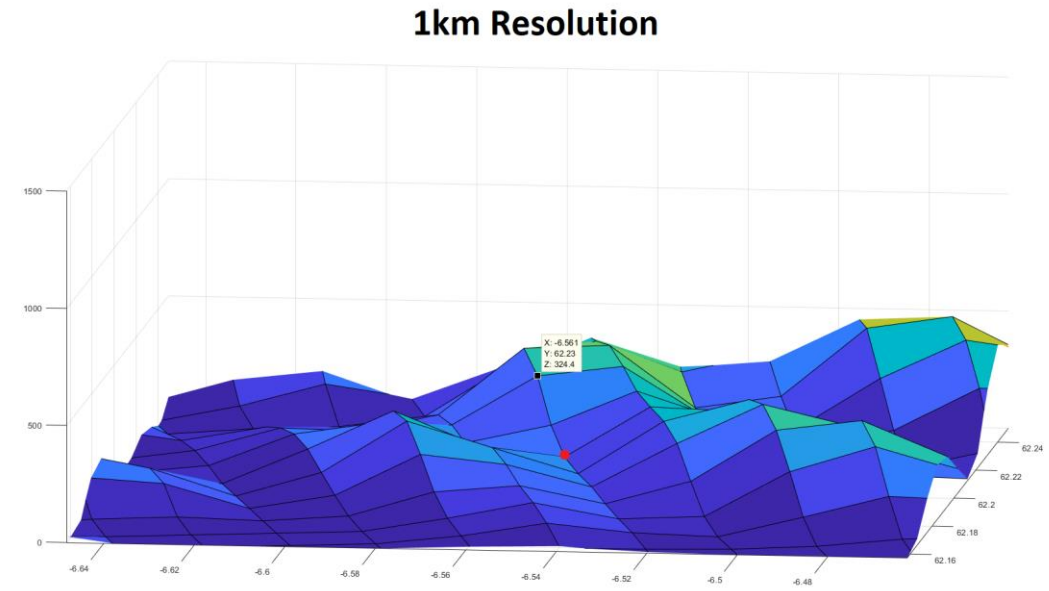

Figure 45 Klaksvík as interpreted on the 1km grid. The black dot denotes the gridcell chosen to represent the simulated values, while the red dot denotes the relocation of the measurement site for this study

The grid box selected by WRF to store time series in the 1km run appears to be placed atop of the mountain adjacent to Klaksvík and along the mountainside in the 400m grid, while the actual site is placed further south relatively close to the shoreline. For this reason the site has been moved southwards to a grid point that physically resembles more the location of the measurement site.

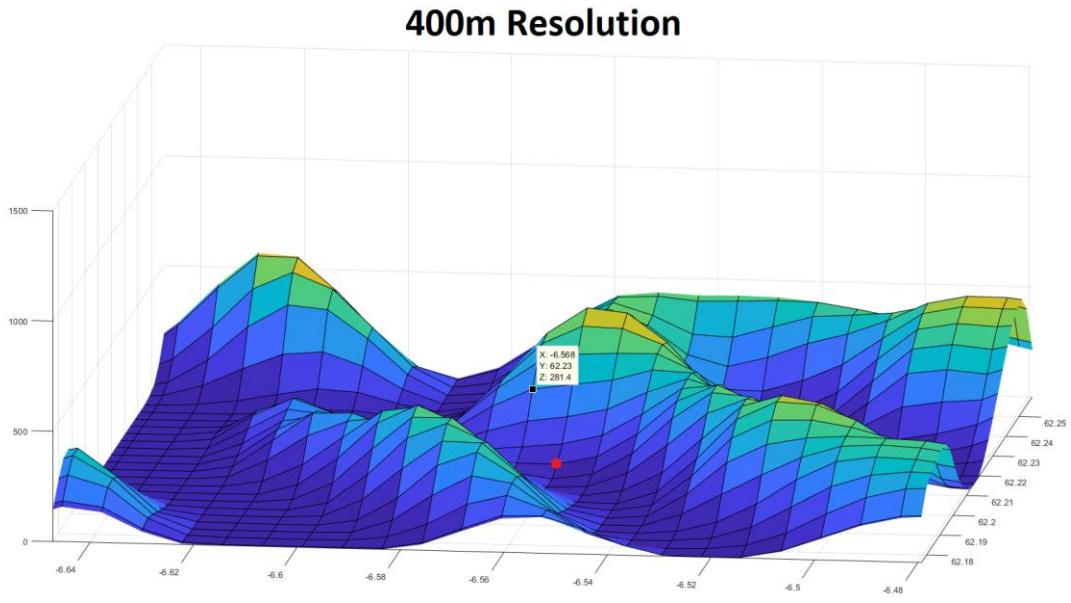

Figure 46 Klaksvík as interpreted on the 400m grid. The black dot denotes the gridcell chosen to represent the simulated values, while the red dot denotes the relocation of the measurement site for this study

4.4.4 Some crucial differences between the topography of the 1km and 400m run

The impact of simulating weather in a topography as complex as the Faroe Islands at a high resolution can be crucial to the result when comparing with measurements. Figure 47 shows a mountain pass leading to the village of Oyndarfjørður as shown by Google Earth in a south to north perspective with the measurement site placed on the mountainside. The village of Oyndarfjørður lies just on the other side of the mountain pass while a valley crosses the complex landscape just south of the pass.

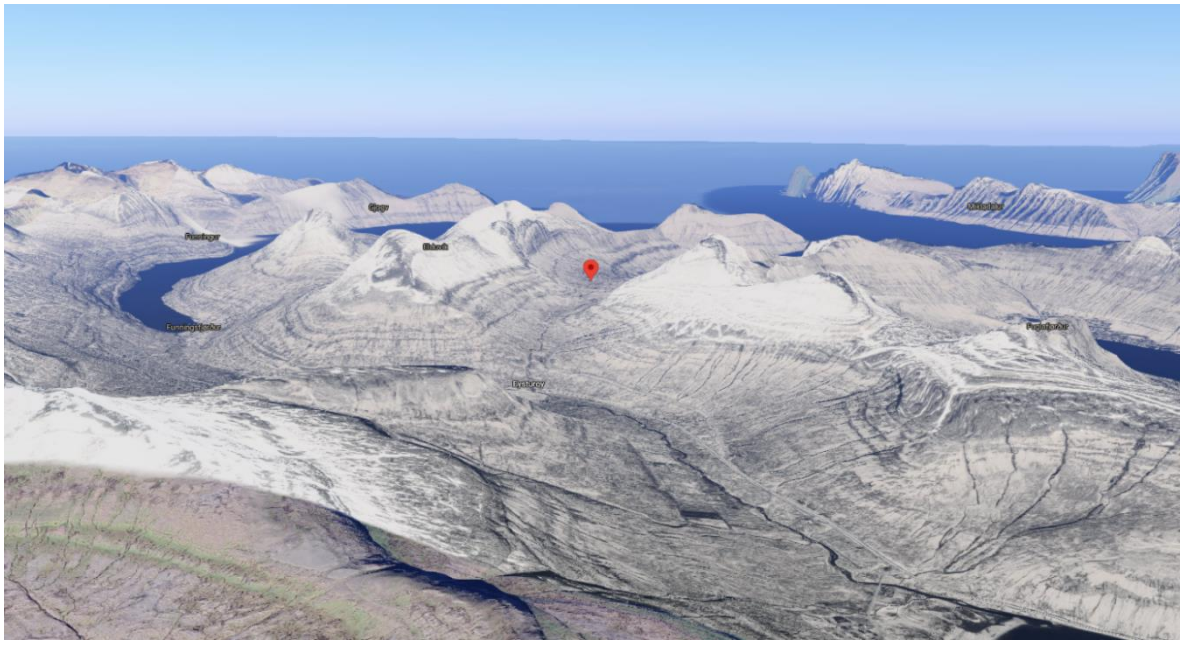

Figure 47 Heltnin, Oyndarfjørður as shown by Google Earth. The red dot denotes the coordinate of the measurement station

Figure 48 shows an example where the 1km model topography is barely able to define most of the topographic features shown Figure 47. Meanwhile, the 400m model topography in Figure 49 shows all of the topographic features to a much greater detail. The impact of this along with the site being misplaced northwards is that the 1km simulation was not able to define the mountain pass leading to Oyndarfjørður. As a result, the measurement site is placed on the lee-side of a mountain during the simulation. In this case, the comparison site in the 1km run was moved southwards to a grid point resembling the mountaintop of this topographic feature. This is because the wind magnitudes on a mountain pass would most likely be more similar to the magnitudes on a mountaintop

compared to the lee side of a mountain, unless downslope winds are present. An analysis of this measurement site can be found in Appendix C.

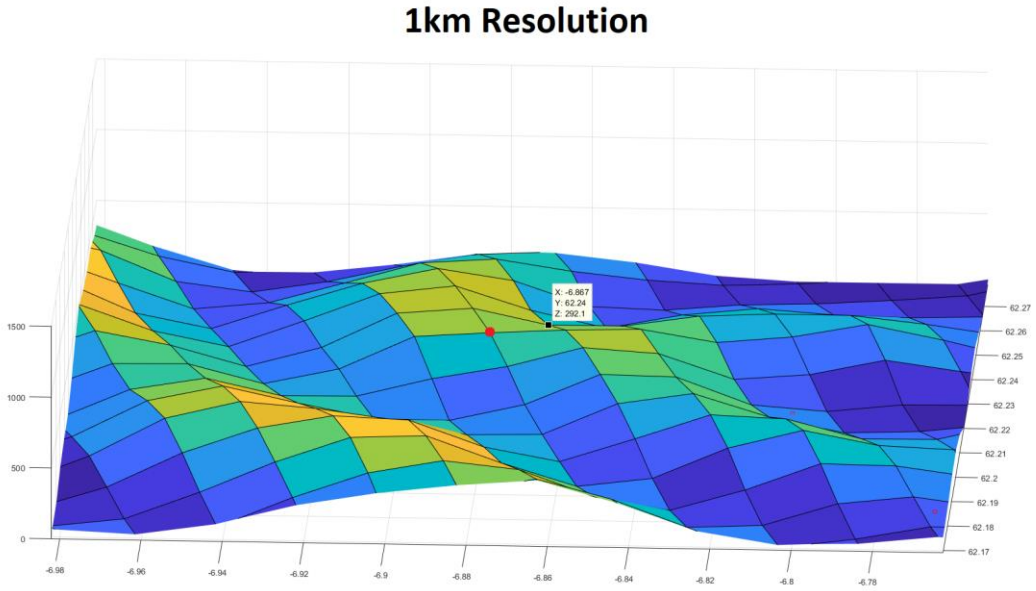

Figure 48 Heltnin, Oyndarfjørður as interpreted on the 1km grid. The black dot denotes the gridcell chosen to represent the simulated values, while the red dot denotes the relocation of the measurement site for this study

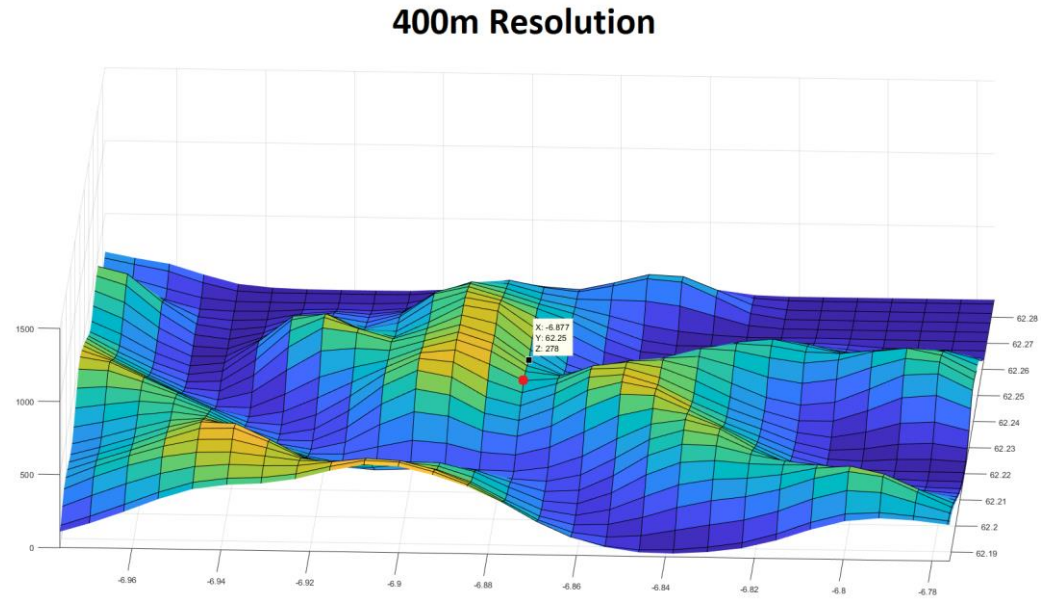

Figure 49 Heltnin, Oyndarfjørður as interpreted on the 400m grid. The black dot denotes the gridcell chosen to represent the simulated values, while the red dot denotes the relocation of the measurement site for this study

4.5 Local Analysis of Selected Measurement Sites

Different types of complex terrain can have different local effects on the weather conditions. Therefore, after having examined the topographic model data, we now move on to analyse three selected measurement sites surrounded by different types of topography. One site is placed in the mountain pass of Norðadalsskarð, one is placed on the mountainside of Høgareyn and one is placed in Klaksvík between two mountain barriers that are perpendicular to the wind direction during the passage of Urd. The impact of simulating at different resolutions with the WRF model as well as relocating the measurement sites is now analysed. An analysis of three additional measurement sites has to a lesser extent been made and is shown in Appendix C.

4.5.1 Norðadalsskarð

Figure 50 shows the 10 meter surface wind magnitudes at the mountain pass of Norðadalsskarð simulated by the 1km and 400m run during the peak of the storm on December 25th 15:00.

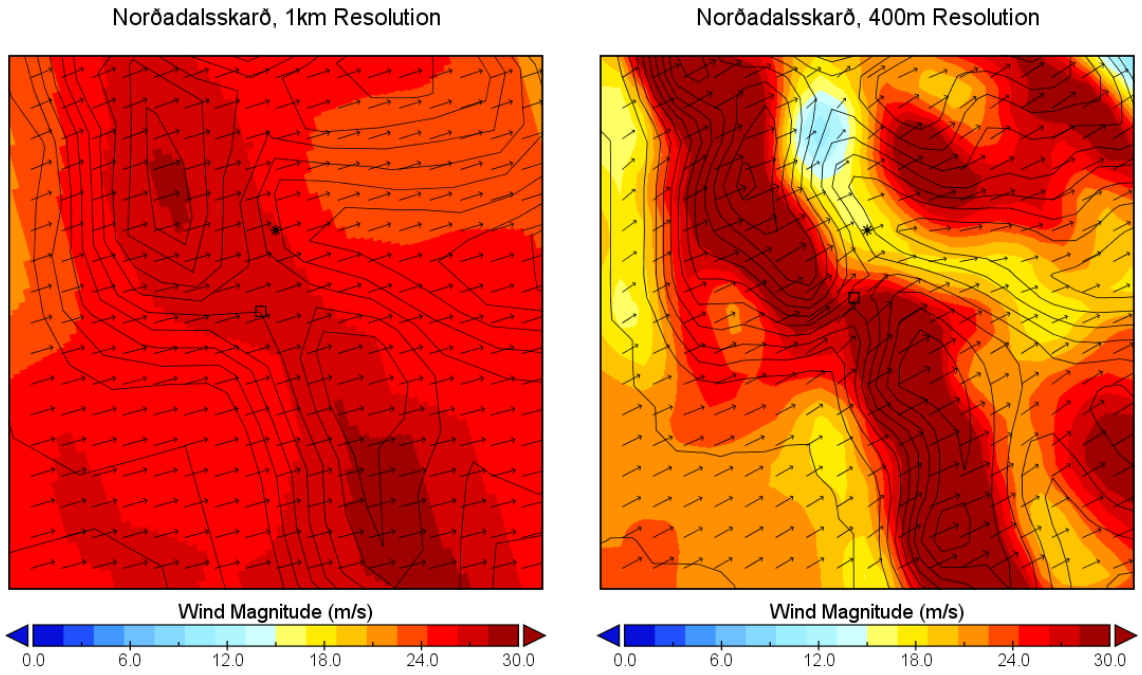

Figure 50 Simulated wind magnitudes with 1km (left) and 400m (right) horizontal resolution at Norðadalsskarð, 15:00 P.M. on December 25th 2016. The star (*) denotes the geographical coordinates of the weather station, while the square denotes the centre of the grid cell, that is the best geographical representation of the placement of the station.

In the 1km simulation, the wind magnitudes appears quite uniform with small increases in wind magnitudes near mountaintops. The simulation appears not to be able to capture

local channelling effects nor altering of the wind direction near the mountain pass of Norðadalsskarð.

Both the 1km and 400m run capture extreme wind magnitudes near the mountaintops. However, the 400m run shows much more localized surface wind extremes near the mountaintops and the mountain pass of Norðadalsskarð. The 400m run also appears to simulate sheltering effects on the lee side of Sornfelli north-west of the measurement site.

Figure 51 shows a time series of the 10 minute average wind magnitudes and direction observed at Norðadalsskarð during the passage of Urd. As the cold front passes, the wind magnitudes at Norðadalsskarð increase further surpassing 50 m/s, which is considerably higher compared to what was simulated, before slowing down to 30 m/s. It is however interesting to see in Figure 52 that the 400m run is able to predict the slow-down of the wind magnitudes during the morning of December 26, albeit with a one-hour lead compared to what was observed.

The wind direction during the passage of Urd at Norðadalsskarð is shown in Figure 53. It is measured to have a south-south-western direction directed along the mountain pass during the passage of Urd. This means, that the wind is most likely affected by the pass, which is also somewhat simulated in the 400m run, but not in the 1km run.

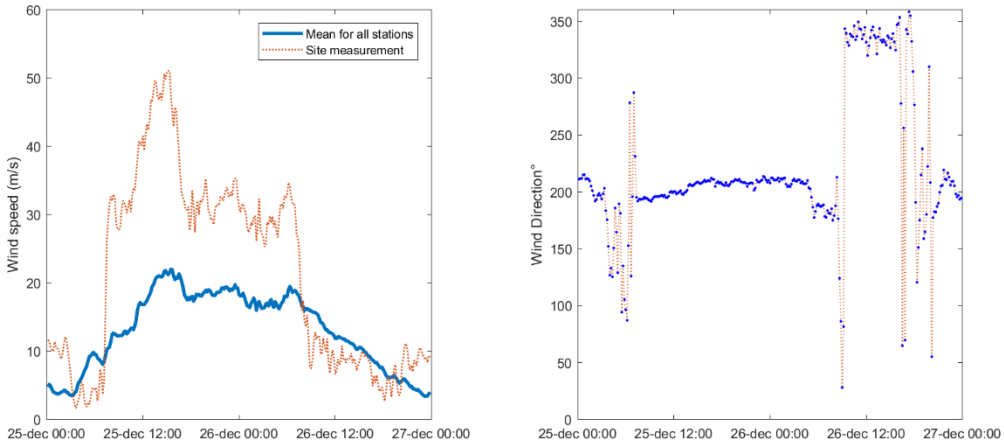

Figure 51 Time series of measured wind speed and direction at Norðadalsskarð during Urd

It is interesting to note when comparing Figure 52 and Figure 53 that as the observed wind magnitudes slow down dramatically at 08:00 on December 26th followed by a drastic anticlockwise turn northwards. In contrast, the 1km and 400m run appear to take a clockwise turn northwards.

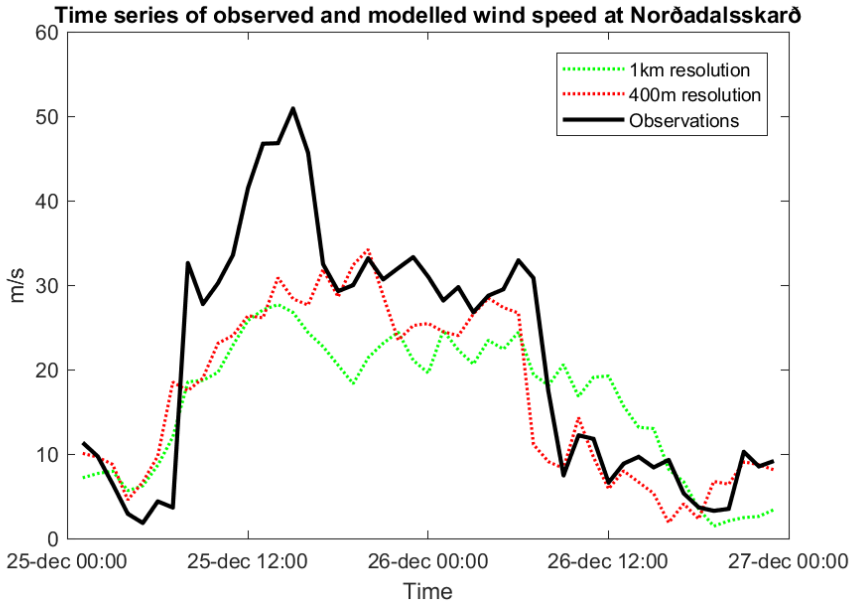

Figure 52 Time series of the measured and modelled wind speeds at Norðadalsskarð after relocating the site

The drastic slow-down in wind speeds and turn in wind direction at Norðadalsskarð from south-south-west to north may be the result of a blocking effect by the adjacent mountain Núgvan north-west of the mountain pass. The faster slow-down in wind magnitude and turning of wind direction simulated in the 400m run indicates that this configuration is to a greater extent able to simulate this local effect than the 1km simulation.

One reason for the extreme wind speeds measured at Norðadalsskarð could be the temperature difference between the southern and northern side of the mountain barrier strengthening the gap wind that causes these extreme winds.

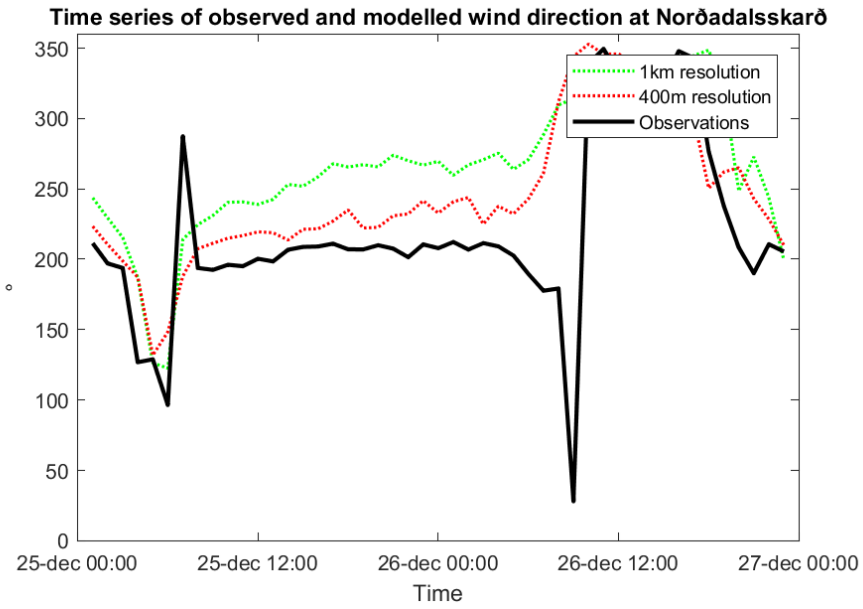

Figure 53 Time series of wind direction measured and modelled at Norðadalsskarð after the relocating the site

Figure 54 compares temperatures measured at the two measurement sites displayed in Figure 55. The measured decrease in temperatures as the cold front passes are lagging at Sund compared to Norðadalsskarð. If this is the case for the entire fjord, there may be warmer air north of the mountain pass compared to south of the mountain pass, which makes a horizontal temperature gradient between the northern and southern side of the mountain pass. This could make the mountain pass an outlet for cold air northwards which could lead to stronger gap winds as the cold front passes. This would explain some of the wind extremes observed at Norðadalsskarð between 12:00 and 18:00. As the temperatures stopped decreasing in Norðadalsskarð and Sund, wind magnitudes measured at Norðadalsskarð dropped relatively quickly back to 30 m/s.

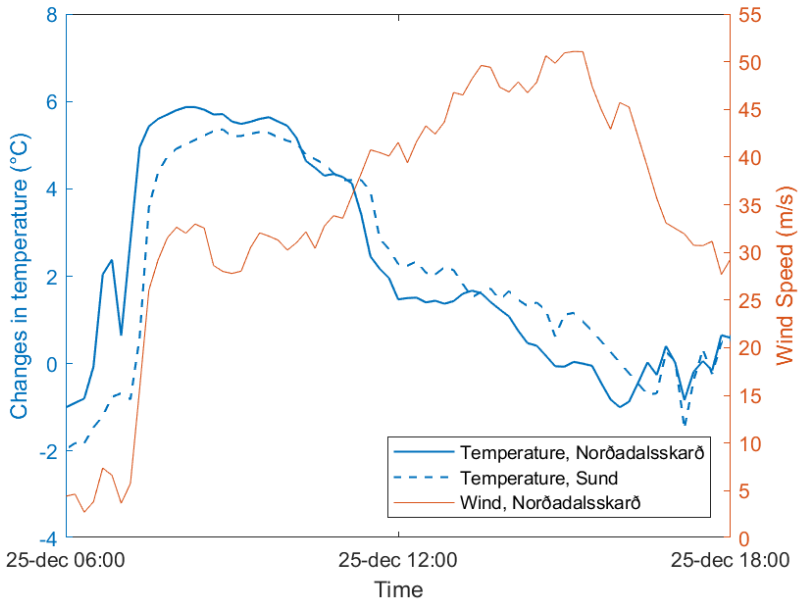

Figure 54 Comparison between measured changes in temperature at Norðadalsskarð and Sund with wind speeds at Norðadalsskarð. Temperatures are shown as deviations from December 25th 00:00

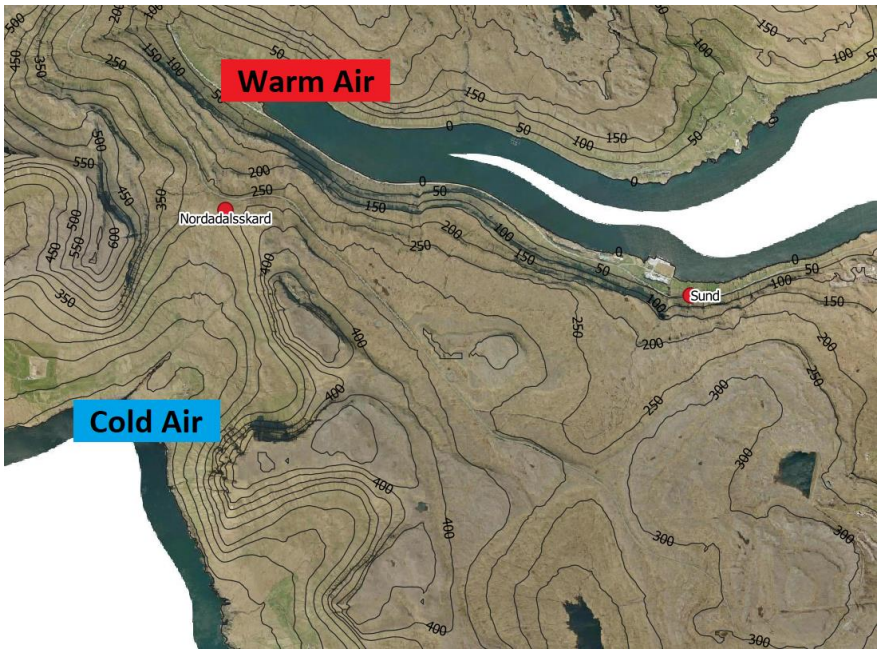

Figure 55 Norðadalsskarð placed atop of a mountain pass, and Sund placed down in the adjacent fjord

The scatter plots in Figure 56 show vast underestimations in peak wind speeds by the WRF model especially in the 400m run during the passage of Urd, before the relocation of the measurement site. In addition, some of the lower observed wind magnitudes are severely overestimated in the 1km run at 20 m/s modelled over 7 m/s measured.

It should be noted in Figure 56 that the measurement site appeared to be placed in a fjord downstream of the mountain pass as shown in section 4.4.1. Better results are obtained by adjusting the location of the measurement site in the model data to a more physically representative site. Comparing Figure 56 with Figure 57, the 400m run predicts significantly higher extremes of wind magnitudes, and predicts some of the extreme wind speeds observed. Meanwhile, the new location of the site does not seem to have affected the results obtained in the 1km run as much.

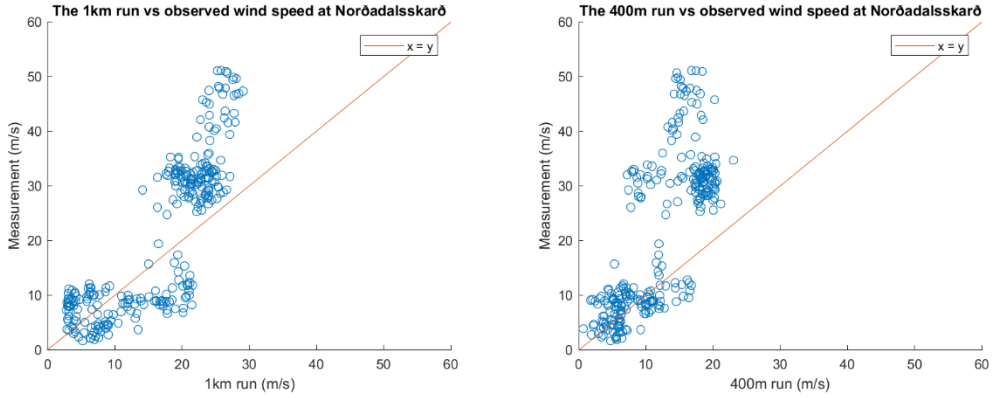

Figure 56 Scatter plots of simulated and measured wind magnitudes at Norðadalsskarð during Urd, before the relocation of each measurement site

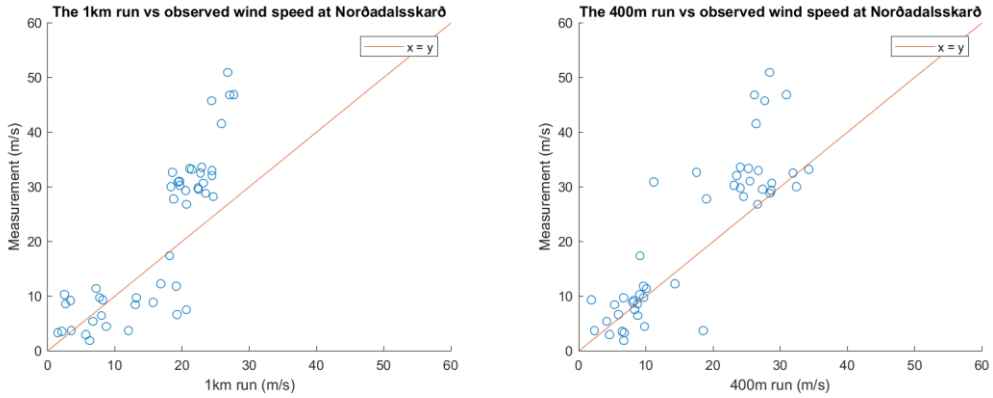

Figure 57 Scatter plots of simulated and measured wind magnitudes at Norðadalsskarð during Urd, after the relocation of each measurement site

Overall considering the four scatter plots in Figure 56 and Figure 57, the model data from the 400m run after the relocation of the measurement site appears to fit the measured data best. It should once again be noted that there is significantly less model data available from the new site locations compared to the original sites, since only hourly instantaneous model data was available at the new locations compared to 10-minute averages at the old locations.

4.5.2 Høgareyn

Figure 58 shows the surface wind magnitudes at Høgareyn simulated by the two WRF simulations during the passage of Urd. Compared to the localized wind directions observed in the 400m run, the 1km run shows a more uniform wind direction from the south-west. Both the 1km and 400m run show slower wind magnitudes at the channel of Vestmannasund and speed-ups of wind magnitudes near the mountaintops west of the channel. However, the 400m run simulates much more localized speed-ups and slow-downs compared to the 1km model.

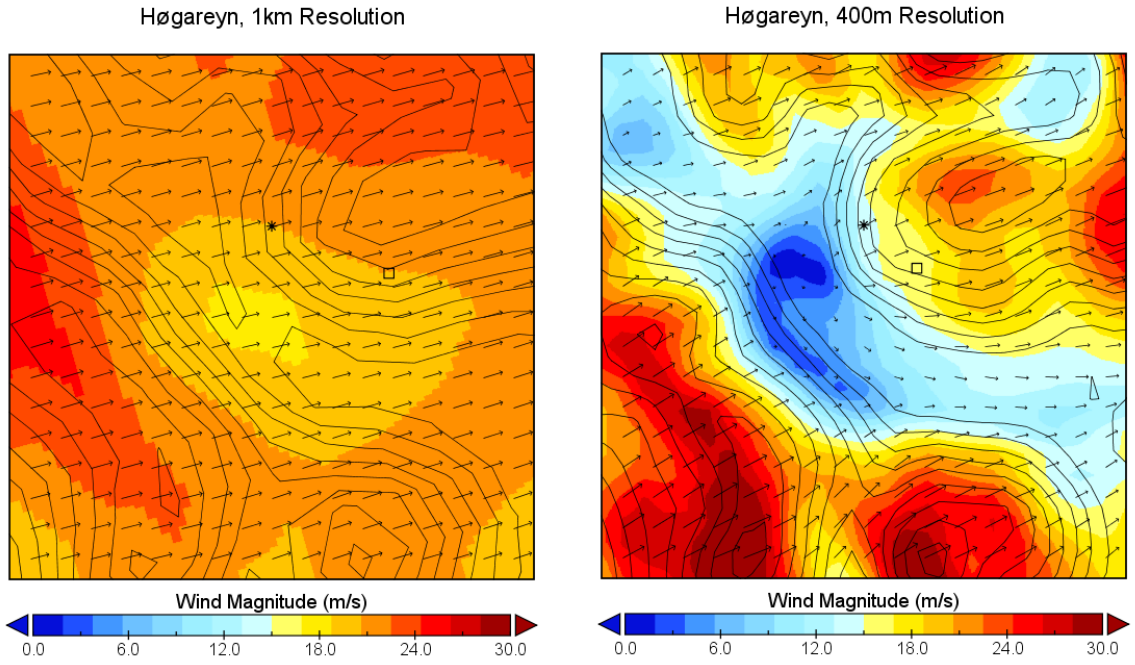

Figure 58 Simulated wind magnitudes with 1km (left) and 400m (right) horizontal resolution at Høgareyn, 15:00 P.M. on December 25th 2016. The star (*) denotes the geographical coordinates of the weather station, while the square denotes the centre of the grid cell, that is the best geographical representation of the placement of the station.

Figure 59 shows a time series of the 10 minute average wind magnitudes and direction observed at Høgareyn between December 25th and December 26th. One may notice that the 10-minute average wind speeds suddenly increase in magnitudes on two occasions. Firstly from 20 m/s to 40 m/s between 13:00 and 15:00 before settling at 25 m/s at 17:00, secondly from 25 m/s to 35 m/s on December 26th between 07:00 and 10:00. While the weather stations on average measured increases in wind magnitudes at this time, the sudden increases measured at Høgareyn are more severe than elsewhere. Considering the measured wind direction in Figure 59, winds are blowing from south-west during the first spike and from west during the second spike.

As was described in section 2.3, the non-dimensional mountain height can determine the fate of a flow. As the non-dimensional mountain height depends on the wind speed and stability, a reduction in stability or increase in wind magnitudes reduces the non-dimensional mountain height, which can cause wave breaking (Smith, 1989). One reason for the spikes in wind magnitudes could be that the wind flow beneath the measurement site was mostly split traveling around the mountain barrier. If the non-dimensional mountain height decreases either due to the strength of the flow, a change in stability or a combination of both, the flow starts to travel upwards the mountain. This would add extra pressure to the existing flow near the mountaintop, which would cause an increase in wind magnitudes where the measurement site is placed.

Figure 60 shows a time series of the hourly observed and modelled wind speeds at Høgareyn during the passage of Urd. Both the 1km and 400m runs are able to simulate the trend in increasing wind speeds during the passage of Urd, but are not able to simulate the sudden jumps in wind magnitudes that were observed between 13:00 and 17:00.

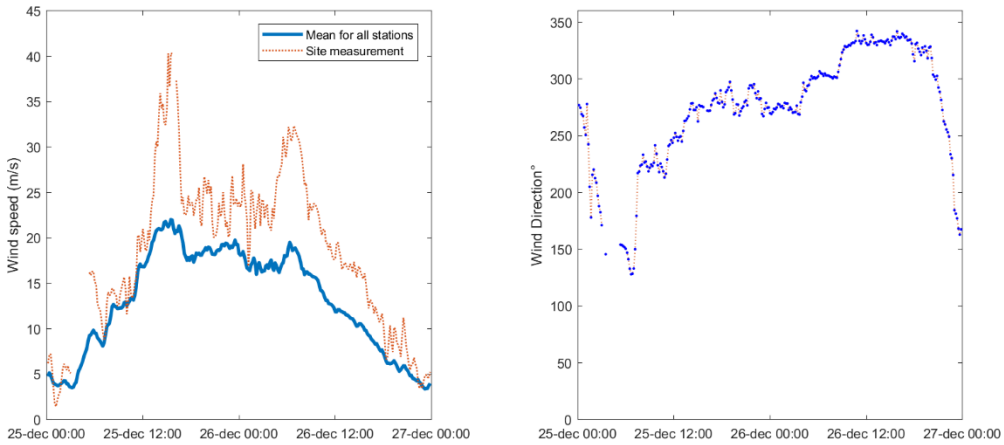

Figure 59 Time series of measured wind speed and direction at Høgareyn during Urd

Looking at the time series in Figure 60 the WRF model generally captures wind speeds well except for the spikes at noon in both the 1km and 400m run.

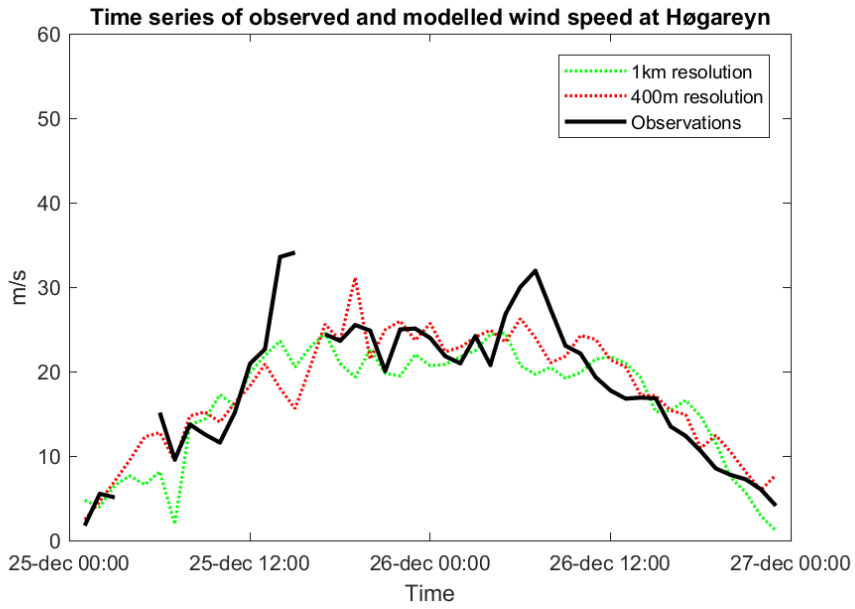

Figure 60 Time series of the measured and modelled wind speeds at Høgareyn after relocating the site

Considering Figure 61, the WRF model is able to capture wind direction at Høgareyn both in the 1km and 400m run during the passage of Urd. As the wind direction appears rather uniform in the 1km run and follows the synoptic pattern in Figure 18, this could indicate that the wind direction measured at Høgareyn is not heavily affected by the local topography during the passage of Urd.

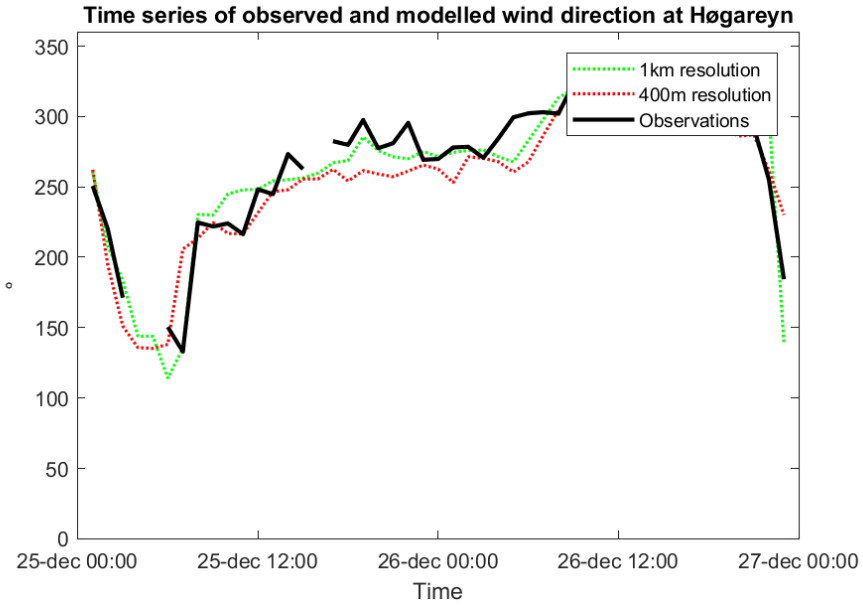

Figure 61 Time series of the measured and modelled wind direction at Høgareyn after relocating the site

The scatter plots of measured versus modelled wind magnitudes in Figure 62 show, that the WRF model underestimates the peak wind magnitudes at Høgareyn during the passage of Urd in both the 1km and 400m run, as was shown in the time series of Figure 60.

The scatter plots in Figure 63 give an indication that the 400m run may be able to simulate some of the wind extreme better by moving the measurement sites. The same cannot be said in the 1km run, and it should once again be noted that there is significantly less model data available from the new site compared to the original site.

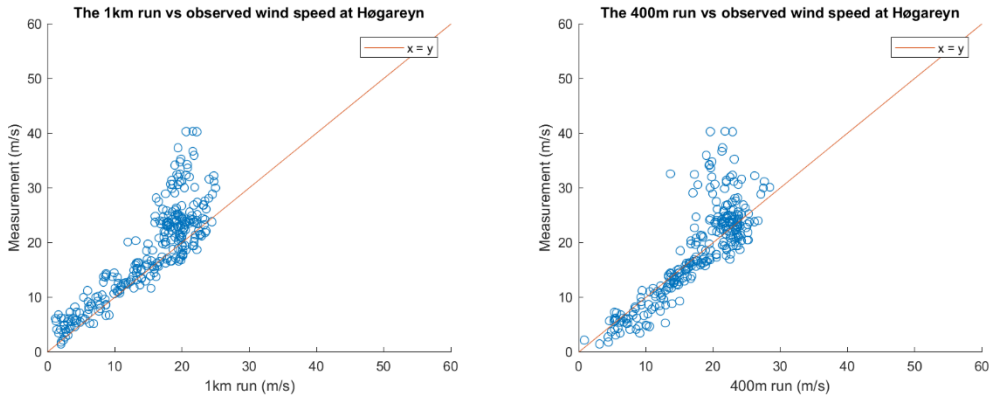

Figure 62 Scatter plots of simulated and measured wind magnitudes at Høgareyn during Urd, before the relocation of each measurement site

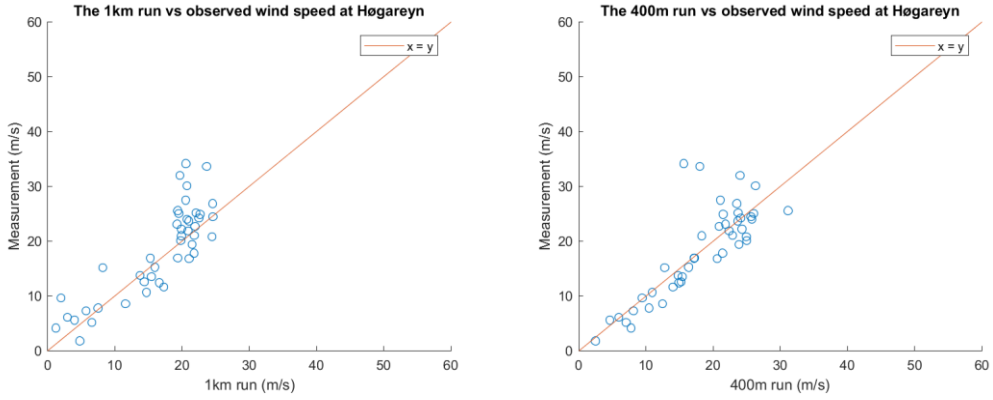

Figure 63 Scatter plots of simulated and measured wind magnitudes at Høgareyn during Urd, after the relocation of each measurement site

4.5.3 Klaksvík

Figure 64 shows the surface wind magnitudes at Klaksvík simulated by the two WRF model runs on December 25th 15:00. The 400m run is able to simulate strong localized wind magnitudes near the tops of the two mountain barriers between Klaksvík as well as localized wind shelters between them. The same is observed in Árnarfjørður east of the eastern mountain barrier. The 1km run is only able to simulate speed-ups of wind magnitudes near the eastern mountaintops of Gásafelli and Hæddin, but no sheltering effects from the western mountaintops. These findings correspond well with the coarser resolution of the 1km topography compared to the interpolated 400m topography also discussed in section 4.4.

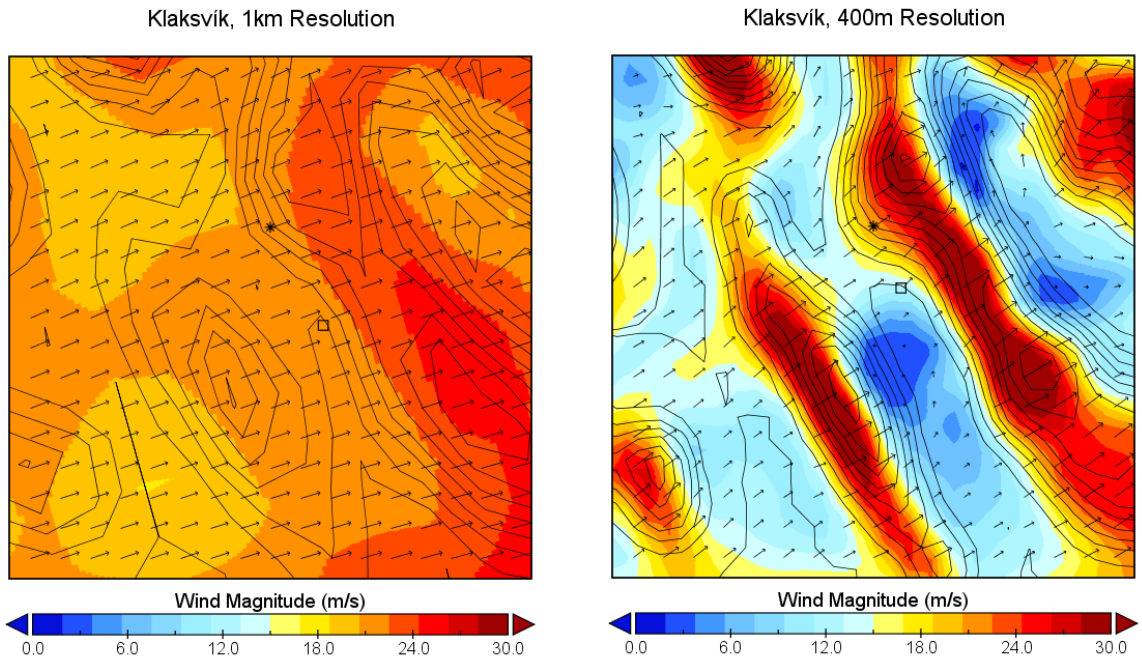

Figure 64 Simulated wind magnitudes with 1km (left) and 400m (right) horizontal resolution at Klaksvík, 15:00 P.M. on December 25th 2016. The star (*) denotes the geographical coordinates of the weather station, while the square denotes the centre of the grid cell, that is the best geographical representation of the placement of the station.

Figure 65 shows a time series of the 10 minute average wind magnitudes and direction observed in Klaksvík during the passage of Urd. In comparison to the mean wind magnitudes observed for all weather stations, the wind magnitudes in Klaksvík are slightly lower.

It appears as if the measured wind speed takes drastic turns between north-east and south as the warm front passes and winds slowly start to increase in magnitude. This may be a

result of local effects due to the surrounding terrain, which may be more prominent during lower wind speeds directed towards the western mountain barrier.

The wind direction at 15:00 during the peak of the storm appeared to take a turn from 150° clockwise from north, which is in the south-eastern direction, to 300°, which is to the north-west. This direction corresponds to strong channelling effects by alignment of the mountain barriers between Klaksvík. This effect may also be the reason for the wind magnitudes being slightly lower than the 10-minute average wind speed measured in general on the Faroe Islands.

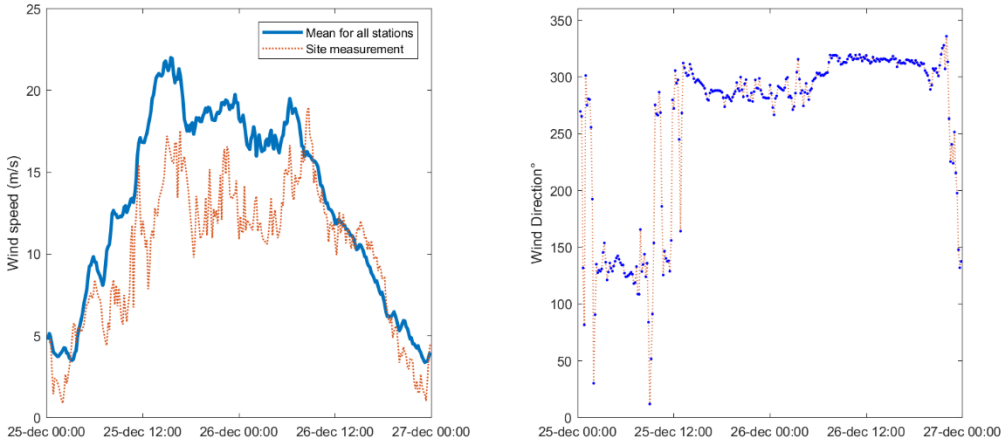

Figure 65 Time series of measured wind speed and direction in Klaksvík during Urd

The time series in Figure 66 shows that the WRF model is able to simulate the trend in increasing wind speeds during the passage of Urd in both the 1km and 400m run. However, wind speeds tend to be overestimated in the 1km run, which is also evident in the scatterplot of Figure 69. The reason for this may be the lack of sheltering effects from the western mountain barrier during the passage of Urd, which is much more prominent in the 400m interpolated topography.

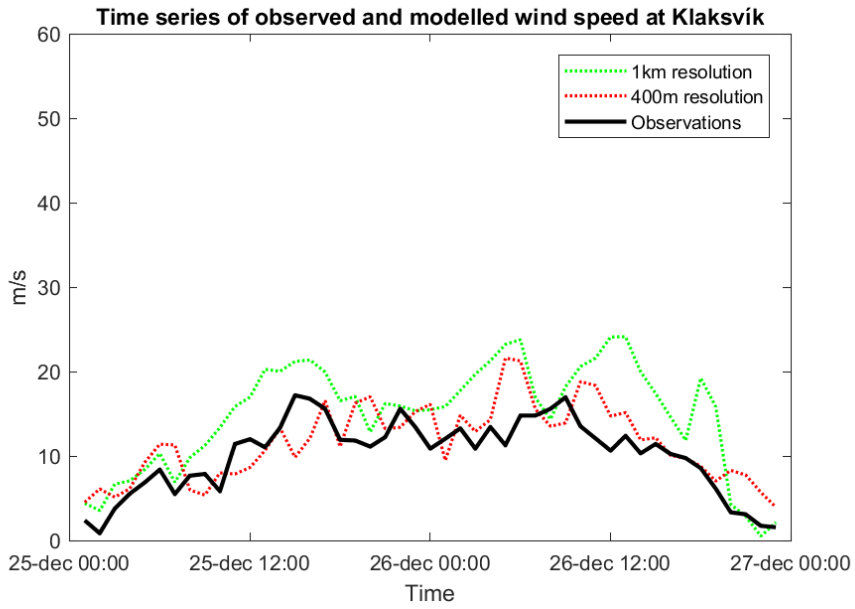

Figure 66 Time series of the measured and modelled wind speeds in Klaksvík after relocating the site

Looking at the time series of the wind direction in Figure 67, the large jumps in wind direction were not captured by the WRF model in either case. Both the 1km and 400m run predict a steady change from south during the frontal passage slowly turning westwards as the storm passes, just as expected by the synoptic pattern of the wind direction in Figure 18 (compared to the off-shore point).

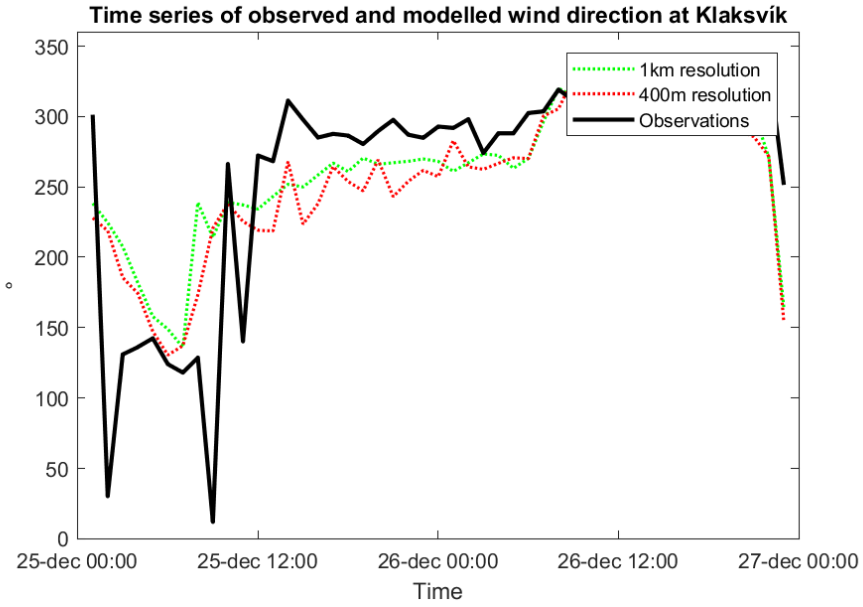

Figure 67 Time series of the measured and modelled wind direction in Klaksvík after relocating the site

Figure 68 shows a scatterplot of the simulated wind speeds in Klaksvík by the 1km run and the 400m run in comparison to measurements during the passage of Urd, before the relocation of each measurement site. Recalling from section 4.4.3, the measurement site appeared to be placed atop of a mountain in the model topography. One may also observe from Figure 68 that the WRF model overestimates wind magnitudes in both the 1km and 400m run.

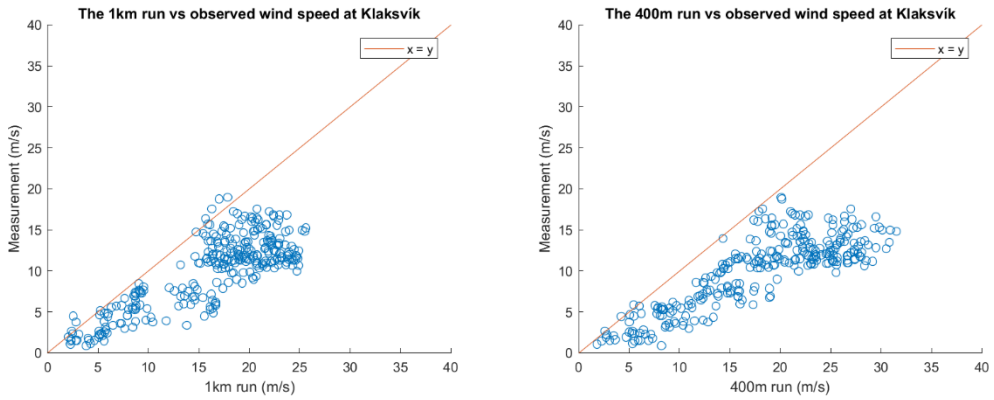

Figure 68 Scatter plots of simulated and measured wind magnitudes in Klaksvík during Urd, before the relocation of each measurement site

Figure 69 shows that after relocating the measurement sites to a more physically representative position, the 400m run appears to predict wind magnitudes much closer to the observed values. The same cannot be said in the 1km run, which may be due to the coarser topography not being able to shelter the wind magnitudes during the passage of Urd. It should once again be noted that there is significantly less model data available from the new site compared to the original site.

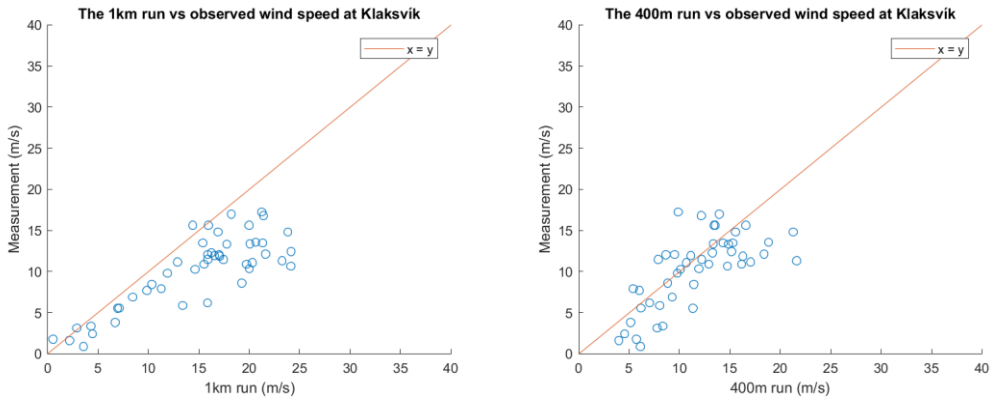

Figure 69 Scatter plots of simulated and measured wind magnitudes in Klaksvík during Urd, after the relocation of each measurement site

4.6 Model Verification Analysis

After having compared the measured and modelled weather data during the passage of Urd, verification metrics and skill scores are calculated and discussed in this section. The skill score in this analysis is calculated by comparing the verification metrics of the 400m run with the verification metrics of the 1km run. It should be noted that the verification metrics and skill scores in this study are only calculated from 23 measurement stations over two days. Furthermore, it should be noted that due to the relocation of each measurement site, instantaneous model data is compared to 10-minute averaged measurements. Therefore, these metrics do not necessarily reflect the overall skill of the model when predicting weather conditions. Appendix D shows all the verification metrics for both the 1km run and the 400m run obtained at all 23 measurement sites used in this study.

4.6.1 Temperature

The verification metrics presented in Table 4 show that the 1km run generally predicted more accurate temperatures during the passage of Urd compared to the 400m run. Considering the mean absolute error (MAE), a skill score of the 400m run shows a 4% decrease in skill when compared to the 1km run.

Table 4 Accuracy measures for the simulated temperatures during Urd after the relocation of each measurement site. The model data and mdeasurements are adiabatically adjusted to the 0m elevation.

	1km run (°C)	400m run (°C)	Skill Score
Mean Absolute Error	1.16	1.21	-0.04
Mean Squared Error	2.06	2.18	-0.06
Bias	-0.15	-0.24	

4.6.2 Wind Speed

Table 5 shows that the 400m run generally predicted more accurate wind speeds compared to the 1km run during the passage of Urd, before the relocation of each measurement site. The same is true in Table 6 after the relocation of each measurement site. When comparing Table 5 with Table 6, it is interesting to observe that the mean absolute error

and bias for the 1km run slightly increases after relocating the measurement site. In contrast the 400m run shows a significant improvement in the mean absolute error (MAE) and mean squared error (MSE), albeit with a higher bias. The reason for this could be the more localized wind magnitudes that were shown in the 400m run in which a misplacement of the measurement site can have a major impact. Therefore, the same impact may not be expected with the 1km run as the wind magnitudes appeared to be more uniform. Considering the mean absolute error, a skill score of the 400m run shows a 28% increase in skill when compared to the 1km run.

Table 5 Accuracy measures for the simulated wind magnitudes during Urd

	1km run (m/s)	400m run (m/s)	Skill Score
Mean Absolute Error	5.78	4.84	0.16
Mean Squared Error	53.50	42.74	0.20
Bias	3.59	0.95	

Table 6 Accuracy measures for the simulated wind magnitudes during Urd after the relocation of each measurement site

	1km run (m/s)	400m run (m/s)	Skill Score
Mean Absolute Error	5.80	4.15	0.28
Mean Squared Error	55.30	30.98	0.44
Bias	3.84	1.26	

4.6.3 Pressure

The verification metrics presented in Table 7 show that the 400m run generally predicted more accurate surface pressure during the passage of Urd compared to the 400m run. Considering the mean absolute error (MAE), a skill score of the 400m run shows a 36% increase in skill when compared to the 1km run. However, it should be noted that the 400m run was less successful at predicting the magnitude of decline in pressure values than the 1km run as was shown in Figure 28. This should also be taken into account for when predicting storms of these magnitudes.

Table 7 Accuracy measures for the simulated pressure during Urd after the relocation of each measurement site. Pressure is adiabatically adjusted to the 0m elevation.

	1km run (hPa)	400m run (hPa)	Skill Score
Mean Absolute Error	3.75	2.39	0.36
Mean Squared Error	23.16	12.00	0.48
Bias	-2.49	-0.13	

4.6.4 Selected Measurement Sites

Norðadalsskarð

The verification metrics for wind speeds simulated by the WRF model at Norðadalsskarð in Table 8 show, that the 400m run had better results than the 1km run, as was observed in the scatterplots of Figure 57. In comparison to the verification metrics for all 23 sites in Table 6, the WRF model was not able to predict wind speeds as accurately at Norðadasskarð. The reason for this is the underestimation of wind magnitudes during the warm front passage of Urd which was also shown in the time series in Figure 52.

Table 8 Accuracy measures for the simulated wind magnitudes at Norðadalsskarð during Urd after the relocation of each measurement site.

	1km model (m/s)	400m model (m/s)	Skill Score
Mean Absolute Error	8.10	5.74	0.29
Mean Squared Error	96.33	70.37	0.27
Bias	-4.86	-3.95	

Høgareyn

The verification metrics for wind speeds simulated by the WRF model at Høgareyn in Table 9 show, that the 400m run had better results than the 1km run, as was observed in the scatterplots of Figure 63. Comparing with Table 6, both the 1km and 400m run have significantly lower errors and biases compared to the overall verification metrics for all 23 stations. This indicates that it was easier for the WRF model to simulate wind speeds at this site compared to the average of all 23 sites.

The skill scores show an improvement in prediction of wind speeds by 17% in MAE when simulating with a 400m resolution compared to a 1km resolution. This improvement is slightly lower than the overall improvement of 23% when comparing all 23 measurement sites.

Table 9 Accuracy measures for the simulated wind magnitudes at Høgareyn during Urd after the relocation of each measurement site.

	1km model (m/s)	400m model (m/s)	Skill Score
Mean Absolute Error	3.57	2.98	0.17
Mean Squared Error	22.39	21.47	0.04
Bias	-1.60	-0.18	

Klaksvík

The verification metrics for wind speeds simulated by the WRF model in Klaksvík in Table 10 show, that the 400m run had better results than the 1km run, as was observed in the scatterplots of Figure 69. Comparing with Table 6, both the 1km and 400m run have significantly lower errors and biases compared to the overall verification metrics for all 23 stations.

The 400m run shows an improvement of 40% in MAE compared to the 1km run when simulating wind speeds in Klaksvík during the passage of Urd. This is a major improvement, also when compared to the overall skill score of 28% obtained when considering all 23 measurement sites. As mentioned earlier, one of the reasons for this improvement may be the result of better resolved topography, which was discussed in section 4.4.

Table 10 Accuracy measures for the simulated wind magnitudes in Klaksvík during Urd after the relocation of each measurement site.

	1km model (m/s)	400m model (m/s)	Skill Score
Mean Absolute Error	4.80	2.90	0.40
Mean Squared Error	35.20	13.38	0.62
Bias	4.68	1.44	

4.7 Comments on results and future work

The results show that while both the 1km run and the 400m run predicted the warm front and cold front to hit the Faroe Islands on time, both simulations underestimated the rapid changes in temperature and pressure during the frontal passage. This indicates that the WRF model may have underestimated the severity of Urd as it passed the Faroe Islands. For future work, it would be interesting to see, how the WRF model performs when using different background data such as data from the ECMWF model.

The issues that were faced when simulating with WRF's integrated 30 arc-second topography needs to be addressed. One needs to be careful if working with this topographic dataset on the Faroe Islands in the future for operational forecasts, as the results may not be representative due to the geographical placements of the terrain. Since most measurement sites in this study were shifted less than one kilometre southwards, the simulations with the highest resolution will suffer the most from this shift in the terrain. Consequently, simulations with resolutions of several kilometres may not experience the complications that were faced in this study, as the coarse resolution of their model terrain will probably not capture a shift in the terrain at such small scales.

An analysis of the 30 arc-second model topography used for the Faroe Islands in this study would be interesting. Such analysis may also help future studies of weather simulations in the Faroe Islands greatly.

The difference between simulating weather conditions on the Faroe Islands at a 1km resolution compared to a 400m resolution can be significant, since some crucial details in the terrain may not be captured by the coarser model terrain, as was the case in section 4.4.4. This should also be noted as a future reference when starting operational forecasts at a high resolution for the Faroe Islands. The improvement of relocating each measurement site can be quite prominent as was the case for the 400m simulation in Klaksvík, where the site was placed atop of a mountain prior relocating the site.

When starting an operational forecast in the Faroe Islands, it may be important to examine the model terrain beforehand due to the complex terrain of the islands. This is to see, if the most relevant places in the Faroe Islands to forecast are well defined geographically.

It is quite clear that the 400m run to a greater extent simulates localized wind conditions throughout Faroe Islands during a storm compared to the 1km run. While the 400m showed peak wind speeds near mountaintops and smaller wind magnitudes on lee sides of a mountain, the 1km run in general showed more uniform wind magnitudes throughout the Faroe Islands. In addition, the wind direction was heavily affected in various places in the 400m run, while the wind direction tends to follow the synoptic flow in the 1km run. The skill score analysis shows that the verification metrics in the 400m run are significantly better in terms of wind magnitudes compared to the 1km run.

The reason for the 400m run performing better than the 1km run during the passage of Urd can be due to a higher horizontal resolution, a higher vertical resolution or a combination of both. For future work, it would be interesting to analyse to what extent the number of vertical layers improve the performance when simulating Urd. Analysing a simulation with a horizontal resolution of one kilometre performs with 60 vertical layers or a simulation with a horizontal resolution of 400 meters and 40 vertical layers would therefore be relevant in future studies. It would also be relevant to analyse the performance of such simulations with different microphysics schemes and boundary layer schemes or no boundary layer schemes in the case of a 400m run.

None of the weather stations operated by Landsverk had measurements of the gust direction during the passage of Urd. For future work, it would be interesting to analyse the direction of gusts hitting weather stations on the Faroe Islands during a storm to see, if there are some local effects that need to be addressed at these locations during such an event.

5. Conclusion

Due to the frequent passage of cyclones in the North Atlantic causing extreme weather conditions on the Faroe Islands, the quality of weather prediction is of high importance to the islands, their people and industry. Due to the complex terrain in the Faroe Islands, one of the key points in providing accurate weather forecasts, especially on a local scale, is to provide high resolution operational forecasts for the islands.

This thesis examined the performance of the Weather Research and Forecast (WRF) model with horizontal resolutions of 1km and 400m during the passage of a storm named Urd that hit the Faroe Islands on December 25th 2016.

One goal of this study was to obtain results that can be applied in the work of setting up and running operational high resolution forecasts for the Faroe Islands in the future.

The aim of this thesis was to study the accuracy of the two simulations mainly in terms of wind speed, but also in terms of pressure levels and temperatures.

The accuracy of the two simulations in predicting wind speed, pressure levels and temperatures during this storm is examined by comparing them with on-ground measurements from 23 weather stations operated by Landsverk. In addition, the two simulations are compared to each other in terms of wind conditions at selected measurement sites during the peak of the storm.

The WRF model simulated the 1km run using one-way offline nesting and the 400m run using one-way inline nesting. The 1km run was simulated by running three coarser domains with resolutions of 27km, 9km and 3km for the 1km run, while the 400m run was simulated by running two coarser domains with resolutions of 10km and 2km. The simulations ran between December 25th and 26th 2016 during the passage of the low pressure system that hit the Faroe Islands with extreme wind speeds.

Some complications arose while analysing the model data since it appeared as if the Faroese terrain was misplaced southwards in both WRF simulations. Since geographic locations of the measurement sites were selected prior to the simulations being run, time series of the model data were in most cases saved from points in the WRF model that were

physically unrepresentative to the actual measurement sites. Consequently, new points were manually selected to form time series that represented each measurement site during the passage of Urd. The result of this was that the study mostly had time series of hourly instantaneous model data to compare with 10-minute average measurements between December 25th and 26th. Prior, the study had time series sampled for each time step, that were interpolated to 10-minute averages which could be compared to the 10-minute average data throughout the passage of Urd.

The results showed that both the 1km run and the 400m run predicted the warm front to hit the Faroe Islands at 06:00 A.M. and the cold front to hit the Faroe Islands at noon. However, the WRF underestimated the rapid changes in temperature and pressure levels during the frontal passage in either simulations indicating that the WRF model may have underestimated the severity of Urd as it passed the Faroe Islands.

When comparing the simulated wind speeds with on ground measurements, it was clear that relocating the 23 measurement sites generally improved the prediction of wind speeds in the 400m run, but not the 1km run. One explanation for the improvement in the 400m run that was not seen in the 1km run is the spatially uniform wind magnitudes simulated in the 1km run not showing localized wind speeds to the same degree as the 400m run. The improvement of relocating each measurement site was especially prominent in Klaksvík, where the site was placed atop of a mountain prior to the relocation.

When comparing the verification metrics of the two WRF simulations, the 400m run did not improve the prediction of temperature, but did improve the prediction of pressure levels and wind speeds compared to the 1km run. A skill score analysis of the two WRF simulations showed a 4% increase in Mean Absolute Error (MAE) of temperatures and a 36% decrease in the MAE of pressure during the passage of Urd by the 400m run compared to the 1km run. The skill score analysis of the relocated measurement sites showed a 28% decrease of MAE in prediction of wind speeds by the 400m run compared to the 1km run.

Despite the improvements that the verification metrics showed when comparing the 400m run to the 1km run, the small time window and lack of model data available in this study should be noted. In addition, more model data of the relocated measurement sites over a

larger time frame will be required in order to study the overall viability of simulating weather conditions on the Faroe Islands at a 400m horizontal resolution.

When analysing the WRF simulations at selected measurement sites during the peak of the storm, the 400m run showed localized wind magnitudes with stronger winds near the mountaintops and weaker winds near the shelters. In comparison, the 1km run simulated more uniform wind magnitudes during the peak of the storm. One reason for this may be the higher resolution of the 400m run and the model terrain, which makes it possible to capture the local effects of a complex terrain to a larger extent.

Regarding the underestimation of the rapid changes in temperature and pressure levels during the passage of Urd, it would be interesting to see, how the WRF model performs when using different background data such as data from the ECMWF model.

For future reference, due to the challenges that were faced with the topography in this study, the issues that were faced when simulating with WRF's integrated 30 arc-second topography needs to be addressed. One needs to be careful if working with this topographic dataset on the Faroe Islands in the future for operational forecasts, as the results may not be representative due to the geographical placements of the terrain.

An analysis of the 30 arc-second model topography used for the Faroe Islands in this study would be interesting. Such analysis may also help future studies of weather simulations in the Faroe Islands greatly.

The direction of gusts was not measured at the 23 weather stations operated by Landsverk. For future work, it would be interesting to analyse the direction of gusts hitting weather stations on the Faroe Islands during a storm to see, if there are some local effects that need to be addressed at these locations during such an event.

6. References

Articles

Ágústsson, H. and Ólafsson, H., 2010: The bimodal downslope windstorms at Kvísker. Meteorology and Atmospheric Physics, 116, 27– 42.

Durran, D.R., 1990: Mountain Waves and Downslope Winds. In: Atmospheric Processes over Complex Terrain. Meteorological Monographs Vol. 23 No. 45. American Meteorological Society, pp. 59– 83.

Eliassen, A. and E. Palm, 1960: On the transfer of energy in stationary mountain waves. Geofys. Publ., 22, 1-23.

Gaberšek, S. and Durran, D.R., 2004: Gap flows through idealized topography. Part I: Forcing by large-scale winds in the nonrotating limit. Journal of the Atmospheric Sciences, 61, 2846– 2862.

Gaberšek, S. and Durran, D.R., 2006: Gap flows through idealized topography. Part II: Effects of rotation and surface friction. Journal of the Atmospheric Sciences, 63, 2720–2739.

Laprise R., 1992: The Euler Equations of motion with hydrostatic pressure as as independent variable, Mon. Wea. Rev., 120, 197–207.

Liu, H and Grant, L. D., 1989: Wind effect on Measured Atmospheric Pressure, J. Atmos. Oceanic Technol. Vol. 6 (1): 5–12.

Long, R.R., 1953: A laboratory model resembling the "Bishop-wave" phenomenon. Bull. Amer. Meteor. Sco., 34, 205-211.

Monin, A.S. and A.M. Obukhov, 1954: Basic laws of turbulent mixing in the surface layer of the atmosphere. Contrib. Geophys. Inst. Acad. Sci., USSR, (151), 163–187.

Rögnvaldsson, Ó., Bao, J.W., Ágústsson, H. and Ólafsson, H., 2011: Downslope windstorm in Iceland – WRF/MM5 model comparison. Atmospheric Chemistry and Physics, 11, 103–120.

Rogers, R. R. , Yau, M. K. 'A Short Course in Cloud Physics', 3rd edition, Elsevier, 1989

Smith, R. B. , 1989: Hydrostatic Airflow over Mountains, Advances in Geophysics, Volume 31, 1989, Pages 1-41, Academic Press.

Books

Stull, R. B. 'An Introduction to Boundary Layer Meteorology, 1st edition, Kluwer Academic Publishers", 1988.

Holton, J. R. 'An Introduction ot Dynamic Meteorology, 5th edition, Elsevier, 2013.

Wallace, J. M. and Hobbs, P. V. 'Atmospheric Science, An Introductory Survey', Elsevier, 2006.

Whiteman, C. D. 'Mountain Meteorology: Fundamentals and Applications', Oxford University Press. Inc., 2000.

Warner, T. T. 'Numerical Weather and Climate Prediction, Cambridge University Press, 2011.

Reports

Cappelen, J. and Laursen, E.V., TR-98-14: "The Climate of The Faroe Islands - with Climatological Standard Normals, 1961-1990 ", DMI, 1998

Olsen, A. and Granerød, M. "Ekstremværrapport, Hendelse: Urd 26. Desember 2016", Norwegian Meteorological Institute, no. 18/2017, Bergen

Gregoriussen, A. K.: "Weather data in the Faroe Islands: Jan 2009, Oct 2016", University of the Faroe Islands, 2019

Skamarock, W.; Klemp, JJ.; Dudhia ,J.; Gill, D.; Barker, D.; Duda, M.; Huang, X.; Wang, W.; Powers, J.; "A Description of the Advanced Research WRF Version 3, June 2008, NCAR Technical Note, NCAR/TN-475+STR".

Rasmussen, R. A.; Kjølbro, H.; Niclasen, B. A.; Poulsen, A. M.; Heimustovu, J.; "Frágreiðing og tilmæli um dagførda, nøktandi og útbygda veðurtænastu í Føroyum – Menning av veðurtænastuni", April 26th, 2019,

Websites

http://vedur.is

http://www.kvf.fo

http://www.us.fo

http://foroyakort.fo

http://qgis.com

http://sev.fo

http://dmi.dk

http://lv.fo

http://weather.uwyo.edu

Appendix A

This appendix covers the radiosonde data that was studied in this thesis. The radiosonde measurements were taken at the local weather station in Tórshavn are provided by the University of Wyoming[6]. The radiosonde data is presented as Skew-t diagrams in this appendix.

Radiosonde data

Figure 70 shows the radiosonde data in a Skew-T graph measured at the initial time on December 25th 00:00 while Figure 71 shows the modelled Skew-T data by the 1km run.

Considering Figure 70 and Figure 71, no CAPE is measured nor simulated at this point. The "dip" in dew point temperature at 700 mb and incline at 200-100 mb is measured to be considerably larger than what is modelled.

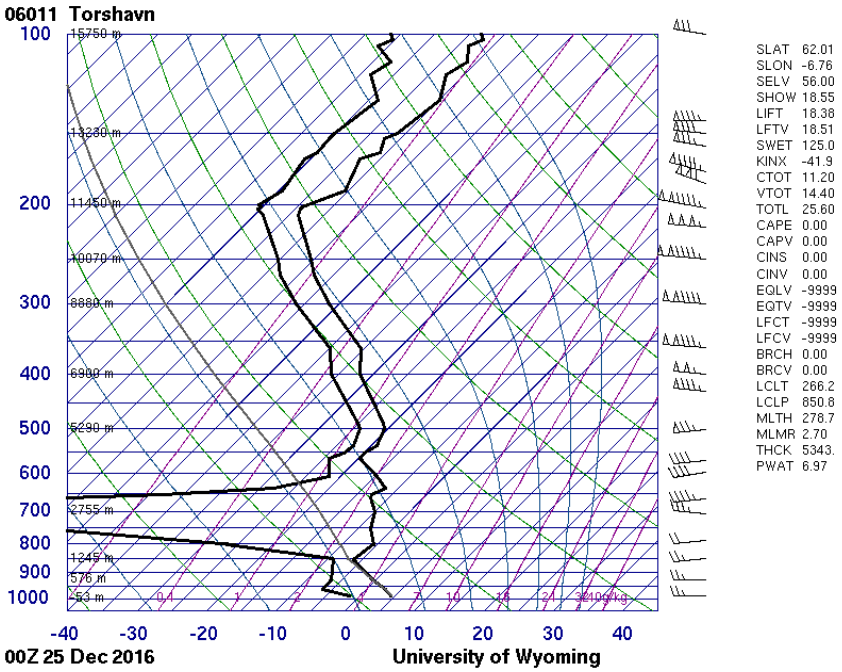

Figure 70 Radiosonde data measured on December 25th 2016 at 00:00

[6] http://weather.uwyo.edu/upperair/sounding.html

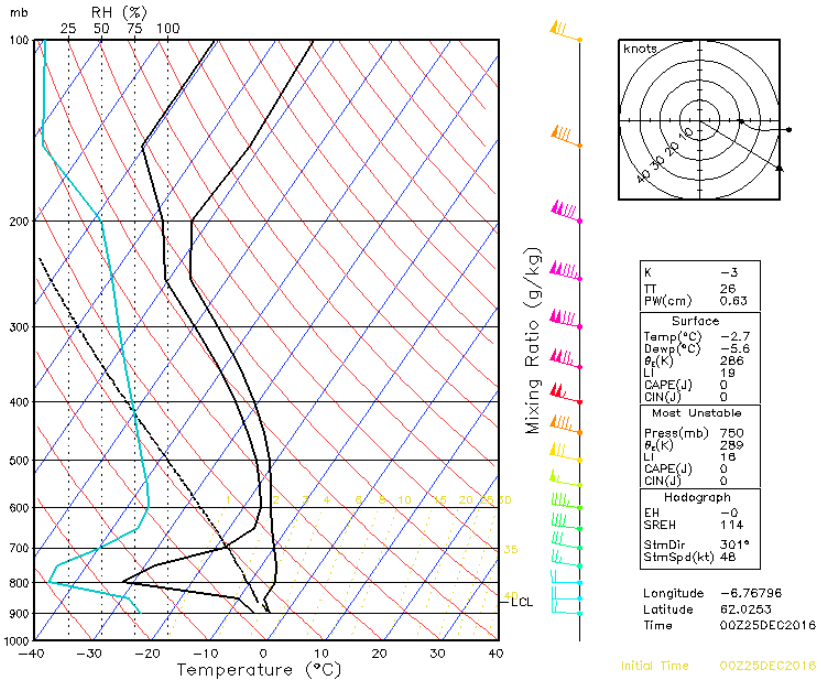

Figure 71 Radiosonde data modelled with a 1km horizontal resolution on December 25th 2016 at 00:00

Figure 72 and Figure 73 show the measured and modelled Skew-T graph of the radiosonde data at noon, just before the cold front passes. The wind measured at this time is slightly more to the south than what the WRF model predicts. Meanwhile, the modelled radiosonde data has an LCL close to 900 hPa, while the measured radiosonde data on Figure 72 has the LCL as high as 750 hPa. The measured temperature appears to correspond well with what was simulated by the WRF model.

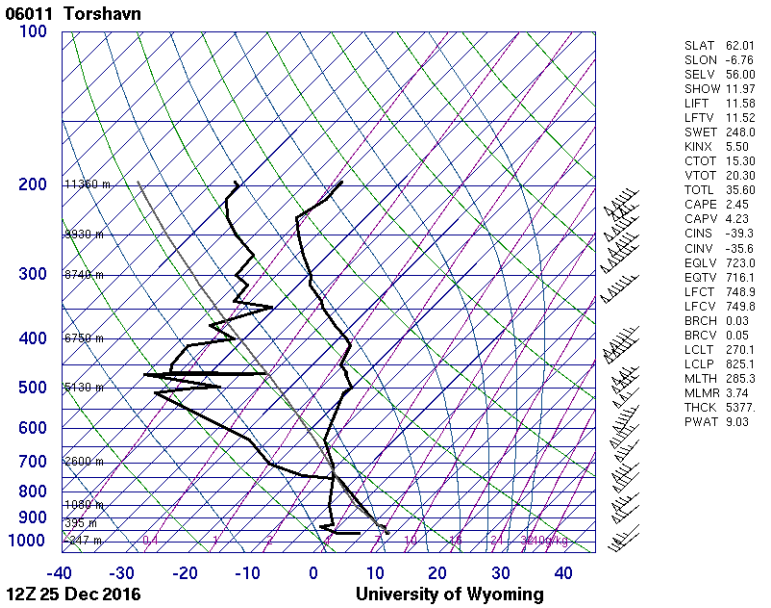

Figure 72 Radiosonde data measured on December 25th at 12:00

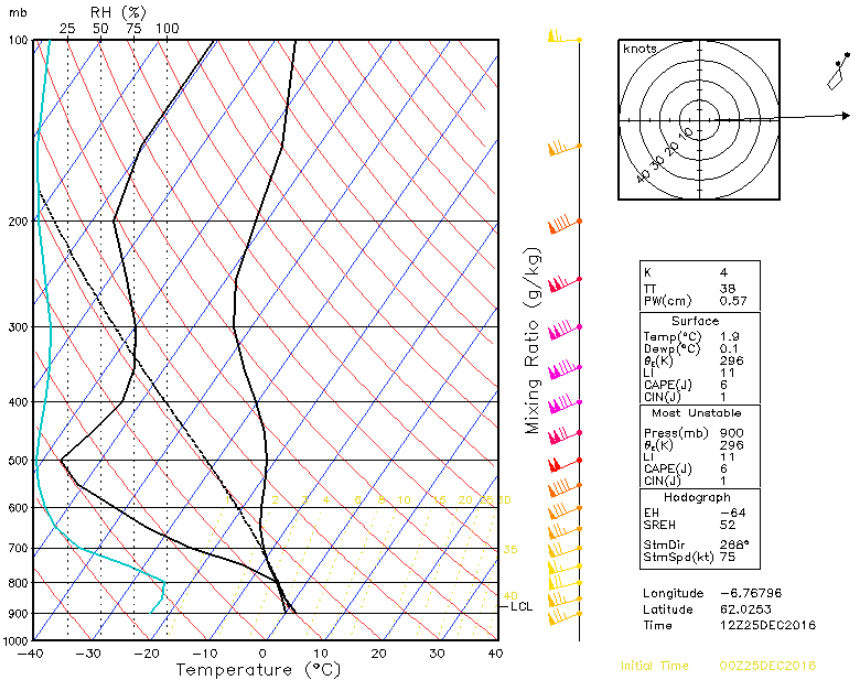

Figure 73 Radiosonde data modelled with a 1km horizontal resolution on December 25th at 12:00

Figure 74 shows a slight change in the modelled radiosonde data compared to Figure 73, as the wind direction across the vertical profile changes from south-west to west and north-west near the surface. No measured radiosonde data in Tórshavn could be found for December 26th at 00:00.

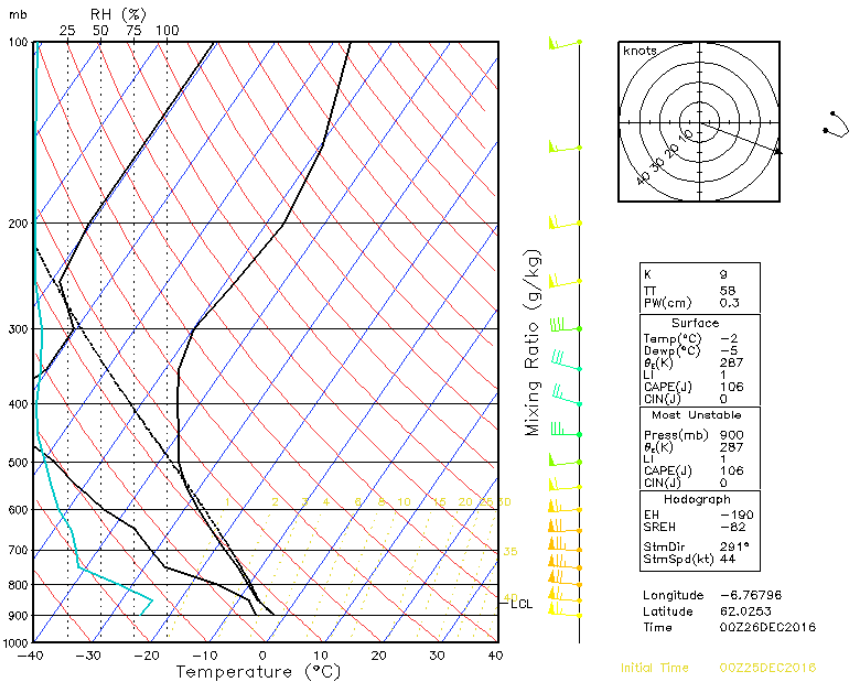

Figure 74 Radiosonde data modelled with a 1km horizontal resolution on December 26th at 00:00

Figure 75 shows the measured Skew-T radiosonde data at 12:00 on December 26th at the local weather station, while Figure 76 shows the modelled skew-T graph for this location by the 1km run.

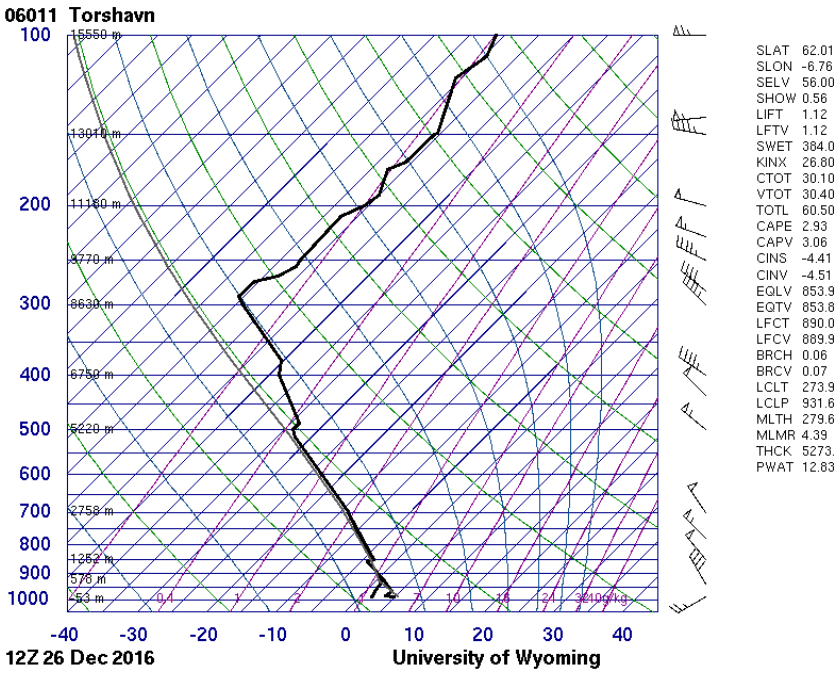

Figure 75 Radiosonde data measured on December 26th at 12:00

The measured radiosonde data shows a sharp temperature increase from 300mb to 100mb, which was partly captured by the WRF model. The WRF model predicts a north-eastern wind direction throughout the vertical profile, while the radiosonde measures a slightly more western direction, especially from 300mb and upwards.

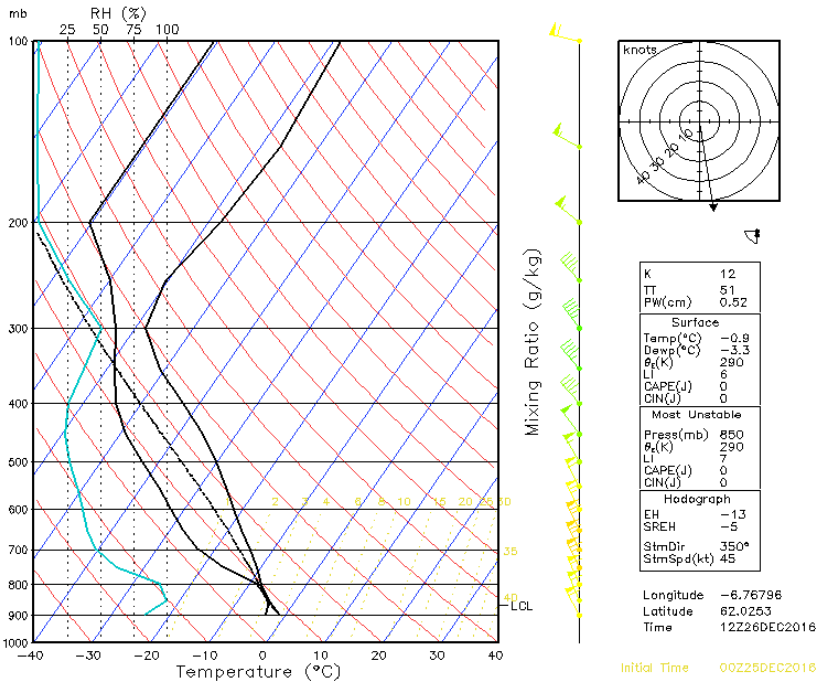

Figure 76 Radiosonde data modelled with a 1km horizontal resolution on December 26th at 12:00

Figure 77 shows the measured Skew-T radiosonde data at 00:00 on December 27th at the local weather station, while Figure 78 shows the modelled skew-T graph for this location by the 1km run.

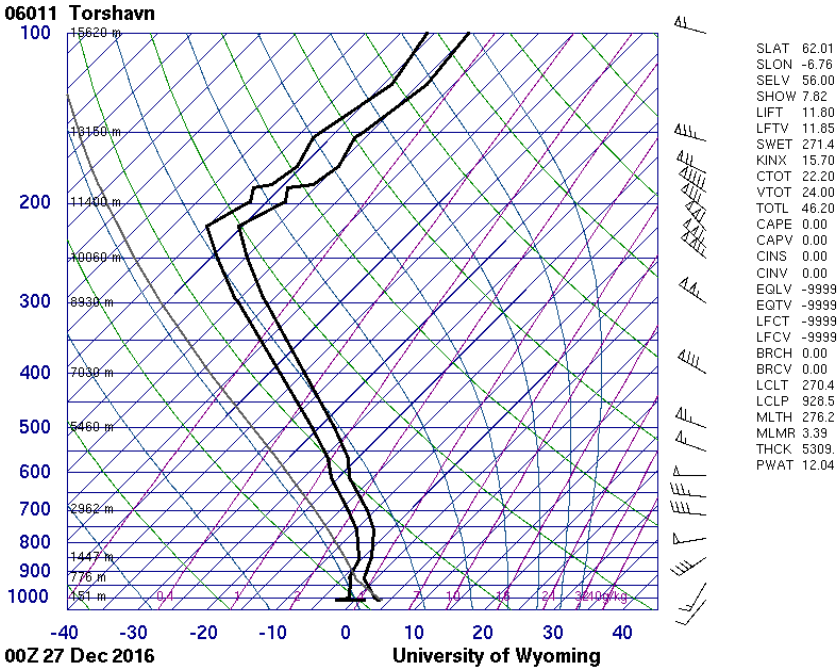

Figure 77 Radiosonde data measured on December 27th at 00:00

The WRF model seems to follow the same trend in temperature and wind direction as the observed radiosonde data, although the incline in temperature from 200mb and upwards is measured to be sharper than what was simulated.

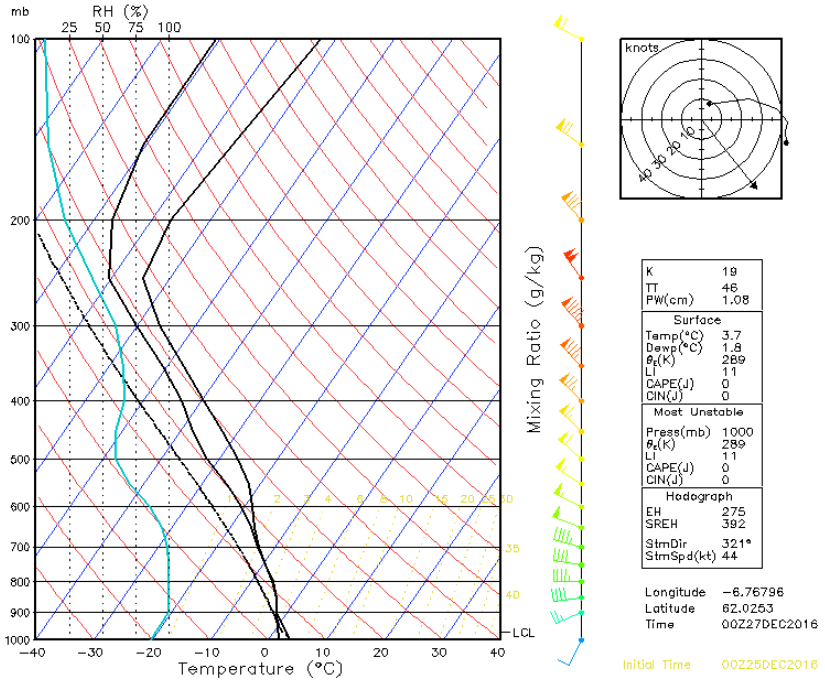

Figure 78 Radiosonde data modelled with a 1km horizontal resolution on December 27th at 00:00

Appendix B

This appendix contains the WRF and WPS namelists that were used for the simulation of Urd

WPS-Namelists

1km Run

```
&share
 wrf_core = 'ARW',
 max_dom = 4,
 start_date = '2011-11-24_00:00:00','2011-11-24_00:00:00','2011-11-24_00:00:00','2011-11-
24_00:00:00'
 end_date   = '2011-11-26_00:00:00','2011-11-26_00:00:00','2011-11-26_00:00:00','2011-11-
26_00:00:00'
 interval_seconds = 10800
 io_form_geogrid = 2,
/

&geogrid
 parent_id       =   1,   1, 2,   3
 parent_grid_ratio =   1,   3,       3,   3
 i_parent_start    =   1,  55,       74,  65
 j_parent_start    =   1,  60,       42,  54
 e_we          =  150, 160, 160, 160
 e_sn          =  150, 160,          160, 160
 !
 !!!!!!!!!!!!!!!!!!!!!!!!!!! IMPORTANT NOTE !!!!!!!!!!!!!!!!!!!!!!!!!!!
 ! The default datasets used to produce the HGT_M, GREENFRAC,
 ! and LU_INDEX/LANDUSEF fields have changed in WPS v3.8. The HGT_M field
 ! is now interpolated from 30-arc-second USGS GMTED2010, the GREENFRAC
 ! field is interpolated from MODIS FPAR, and the LU_INDEX/LANDUSEF fields
 ! are interpolated from 21-class MODIS.
 !
 ! To match the output given by the default namelist.wps in WPS v3.7.1,
 ! the following setting for geog_data_res may be used:
 !
 ! geog_data_res =
'gtopo_10m+usgs_10m+nesdis_greenfrac+10m','gtopo_2m+usgs_2m+nesdis_greenfrac+2m',
 !
 !!!!!!!!!!!!!!!!!!!!!!!!!!! IMPORTANT NOTE !!!!!!!!!!!!!!!!!!!!!!!!!!!
 !
 geog_data_res = 'usgs_30s+default','usgs_30s+default','usgs_30s+default','usgs_30s+default'
 dx = 27000,
 dy = 27000,
 map_proj = 'lambert',
 ref_lat   =  59.25,
 ref_lon   = -12.50,
 truelat1  =  30.0,
 truelat2  =  60.0,
 stand_lon =  15.0,
 geog_data_path = '/Build_WRF/WPS_GEOG/'
/
```

```
&ungrib
 out_format = 'WPS',
 prefix = 'FILE',
/

&metgrid
 fg_name = 'FILE'
 io_form_metgrid = 2,
/
```

400m Run

```
&share
 wrf_core = 'ARW',
 max_dom = 3,
 start_date = '2016-12-24_18:00:00','2016-12-24_18:00:00','2016-12-24_18:00:00',
 end_date   = '2016-12-27_06:00:00','2016-12-27_06:00:00','2016-12-27_06:00:00',
 interval_seconds = 21600
 io_form_geogrid = 2,
 OPT_OUTPUT_FROM_GEOGRID_PATH = './GEOfiles/foroyar-10-2-04'
/

&geogrid
  dx                    = 10000,
  dy                    = 10000,
  e_sn                   = 151, 201, 481, 255,
  e_we                    = 151, 201, 481, 323,
  geog_data_res             = 'usgs_lakes+30s','usgs_lakes+30s','usgs_lakes+30s',
  i_parent_start            = 1, 73, 52,
  j_parent_start            = 1, 66, 52,
  map_proj                 = 'lambert',
  opt_geogrid_tbl_path        = './',
  parent_grid_ratio          = 1, 5, 5,
  parent_id                = 1, 1, 2,
  ref_lat                 = 61.,
  ref_lon                  = -10.0,
  stand_lon                 = -7.0,
  truelat1                 = 64.,
  truelat2                 = 58.,
  geog_data_path             = './geog',
/

&ungrib
 out_format = 'WPS',
 prefix = './FILE',
/

&metgrid
 fg_name = './FILE',
! constants_name  = './TAVGSFC'
```

```
 io_form_metgrid = 2,
 opt_metgrid_tbl_path = '/sleggjan/shared/wrf/V3.9.1/WPS',
 OPT_OUTPUT_FROM_METGRID_PATH = './METfiles/foroyar-10-2-04'
/
```

Input files

1km Run

```
&time_control
 run_days                  = 2,
 run_hours                 = 0,
 run_minutes               = 0,
 run_seconds               = 0,
 start_year                = 2016, 2016, 2016,  2016,
 start_month               = 12,   12,   12,    12,
 start_day                 = 25,   25,   25,    25,
 start_hour                = 00,   00,   00,    00,
 start_minute              = 00,   00,   00,    00,
 start_second              = 00,   00,   00,    00,
 end_year                  = 2016, 2016, 2016,  2016,
 end_month                 = 12,   12,   12,    12,
 end_day                   = 27,   27,   27,    27,
 end_hour                  = 00,   00,   00,    00,
 end_minute                = 00,   00,   00,    00,
 end_second                = 00,   00,   00,    00,
 interval_seconds          = 10800
 input_from_file           = .true.,.true.,.true.,.true.,
 history_interval          = 180,  60,   60,   60,
 frames_per_outfile        = 1000, 1000, 1000,  1000,
 restart                   = .true.,
 restart_interval          = 1440,
 io_form_history           = 2
 io_form_restart           = 2
 io_form_input             = 2
 io_form_boundary          = 2
 debug_level               = 0
/

 &domains
 time_step                 = 135,
 time_step_fract_num       = 0,
 time_step_fract_den       = 1,
 max_dom                   = 4,
 e_we                      = 150,    160,    160,    160,
 e_sn                      = 150,    160,    160,    160,
 e_vert                    = 40,    40,    40,     40,
 p_top_requested           = 5000,
 num_metgrid_levels        = 32,
 num_metgrid_soil_levels   = 4,
 dx                        = 27000, 9000,  3000,    1000,
```

```
dy                          = 27000, 9000,  3000,    1000,
grid_id                      = 1,     2,     3,     4,
parent_id                    = 0,     1,     2,     3,
i_parent_start               = 1,     55,    74,    65,
j_parent_start               = 1,     60,    42,    54,
parent_grid_ratio            = 1,     3,     3,     3,
parent_time_step_ratio       = 1,     3,     3,     3,
feedback                     = 1,
smooth_option                = 0
max_ts_locs                  = 30
/

&physics
mp_physics                   = 10,    10,    10,   10,
ra_lw_physics                = 4,     4,     4,    4,
ra_sw_physics                = 4,     4,     4,    4,
radt                         = 15,    10,    10,   10,
sf_sfclay_physics            = 2,     2,     2,    2,
sf_surface_physics           = 2,     2,     2,    2,
bl_pbl_physics               = 2,     2,     2,    2,
bldt                         = 0,     0,     0,    0,
cu_physics                   = 3,     0,     0,    0,
cudt                         = 0,     5,     5,    5,
isfflx                       = 1,
ifsnow                       = 1,
icloud                       = 1,
surface_input_source         = 3,
num_soil_layers              = 4,
num_land_cat                 = 24,
sf_urban_physics             = 0,     0,     0,    0,
/

&fdda
/

&dynamics
w_damping                    = 0,
diff_opt                     = 1,     1,     1,    1,
km_opt                       = 4,     4,     4,    4,
diff_6th_opt                 = 0,     0,     0,    0,
diff_6th_factor              = 0.12,  0.12,  0.12, 0.12,
base_temp                    = 290.
damp_opt                     = 0,
zdamp                        = 5000.,  5000.,  5000., 5000.,
dampcoef                     = 0.2,    0.2,    0.2,   0.2
khdif                        = 0,     0,     0,    0,
kvdif                        = 0,     0,     0,    0,
non_hydrostatic              = .false., .true., .true.,.true.,
moist_adv_opt                = 1,     1,     1,    1,
scalar_adv_opt               = 1,     1,     1,    1,
/
```

```
&bdy_control
spec_bdy_width                = 5,
spec_zone                     = 1,
relax_zone                    = 4,
specified                     = .true., .false.,.false.,.false.,
nested                        = .false., .true., .true.,.true.,
/

&grib2
/

&namelist_quilt
nio_tasks_per_group = 0,
nio_groups = 1,
/
```

400m Run

```
!! Template to build namelist.input for both real.exe and wrf.exe modeling steps

&time_control
   start_year   = 2016, 2016,  2016,
   start_month  = 12, 12,12,
   start_day    = 25, 25,25,
   start_hour   = 0, 0, 0,
   start_minute = 0, 0, 0,
   start_second = 0, 0, 0,

   end_year   = 2016, 2016, 2016,
   end_month  = 12, 12, 12,
   end_day    = 27, 27, 27,
   end_hour   = 0, 0,0,
   end_minute = 0, 0,0,
   end_second = 0, 0,0,

   input_from_file = .true., .true., .true.,
   fine_input_stream = 2, 2,2,
   frames_per_outfile = 12000,12000, 12000,
   auxinput4_inname = "wrflowinp_d<domain>",
   auxinput4_interval = 360, 360,360,
   debug_level = 0,
   history_interval = 60, 60,60,
   interval_seconds = 21600,
!   iofields_filename = "iofields.txt", "iofields.txt","iofields.txt",
!   ignore_iofields_warning = .true.,

   io_form_auxinput2 = 2,
   io_form_auxinput4 = 2,
   io_form_auxinput8 = 2,
   io_form_auxinput12 = 2,
```

```
 io_form_auxinput13 = 2,

 io_form_boundary = 2,
 io_form_history = 2,
 io_form_input = 2,
 io_form_restart = 2,

 reset_simulation_start = .true.,
 restart = .false.,
 restart_interval = 273600,
/

&domains
 max_dom = 3,
 grid_id = 1, 2,3,
 parent_id = 0, 1, 2,

 parent_grid_ratio = 1, 5, 5,
 dx = 10000, 2000, 400,
 dy = 10000, 2000, 400,
 s_sn = 1, 1,1,
 s_we = 1, 1,1,
 e_sn = 151, 201, 481,
 e_we = 151, 201, 481,
 i_parent_start = 1, 73, 52,
 j_parent_start = 1, 66, 52,

 s_vert = 1, 1, 1,
 e_vert = 65, 65, 65,
 eta_levels = 1.00000, 0.99452, 0.99113, 0.98873, 0.98594, 0.98305,
        0.98026, 0.97737, 0.97458, 0.97178, 0.96899, 0.96620,
        0.96341, 0.95783, 0.95095, 0.93923, 0.92752, 0.91581,
        0.90409, 0.87836, 0.85334, 0.82901, 0.80538, 0.77677,
        0.74915, 0.72253, 0.69681, 0.67208, 0.64816, 0.62054,
        0.59412, 0.56052, 0.52124, 0.48455, 0.45045, 0.41874,
        0.38913, 0.36171, 0.31216, 0.29003, 0.26929, 0.25005,
        0.23210, 0.21545, 0.19990, 0.18544, 0.16560, 0.14776,
        0.13170, 0.11735, 0.10439, 0.09272, 0.07906, 0.06720,
        0.05693, 0.04806, 0.04028, 0.03061, 0.02283, 0.01645,
        0.01137, 0.00728, 0.00399, 0.00130, 0.000,

 time_step = 40,
 time_step_fract_num = 0,
 time_step_fract_den = 1,
 parent_time_step_ratio = 1, 5, 5,

 use_adaptive_time_step = .true.,
 target_cfl = 1.2, 1.2,
 target_hcfl = 0.84, 0.84,
 max_step_increase_pct = 5, 51,
 step_to_output_time = .true.,
```

```
 starting_time_step = 10,2,1,
 max_time_step = 180,20,5,
 min_time_step = -1, -1, -1,
 feedback = 0,
 !!adaptation_domain = 2,

 num_metgrid_levels = 27,
 num_metgrid_soil_levels = 4,
 p_top_requested = 5000,
 smooth_option = 2,

 max_ts_locs = 27,
 max_ts_level = 1,

 !!nproc_x = 1,
 !!nproc_y = 16,
/

&physics
 mp_physics = 10, 10, 10,
 ra_sw_physics = 4, 4,4,
 ra_lw_physics = 4, 4,4,
 radt = 10, 10,10,
 sf_sfclay_physics = 2, 2,2,
 sf_surface_physics = 2, 2,2,
 bl_pbl_physics = 2, 2,2,
 cu_physics = 3, 0,0,
 cu_diag = 1, 0, 0,
 cu_rad_feedback = .true.,.false.,.false.,
 num_land_cat = 28,
 bldt = 0,
 cudt = 0,
 icloud = 1,
 ifsnow = 1,
 isfflx = 1,
 num_soil_layers = 4,
 sf_urban_physics = 0,
 sst_update = 1,
 slope_rad = 1, 1, 1,
 topo_shading = 1, 1,1,
 shadlen = 25000.,
 surface_input_source = 1,
/

&dynamics
 hybrid_opt = 2,
 moist_adv_opt = 1,1, 1,
 scalar_adv_opt = 1,1, 1,
 base_temp = 290.,
 damp_opt = 3,
 dampcoef = 0.2, 0.2,0.2,
```

```
   diff_6th_factor = 0.12,0.12,0.12,
   diff_6th_opt = 0,0,0,
   diff_opt = 2,2, 2,
   km_opt = 4,4,4,
   non_hydrostatic = .true.,
   rk_ord = 3,
   w_damping = 1,
   zdamp = 5000.,
   epssm = 0.3, 0.6,1.2,
/

&bdy_control
   specified = .true., .false.,.false.,
   nested = .false., .true.,.true.,
   relax_zone = 4,
   spec_bdy_width = 5,
   spec_zone = 1,
/

&namelist_quilt
   nio_tasks_per_group = 2,
   nio_groups = 16,
/

!! Disable wrf-chem if that is compiled in
&chem
   chem_opt = 0,
/
```

Appendix C

This appendix contains a short analysis of 3 additional selected measurement sites.

Heltnin, Oyndarfjørður

Figure 79 shows the 10 meter surface wind magnitudes at the mountain mass of leading to Oyndarfjørður simulated by the 1 km and 400m run during the peak of the storm on December 25th 15:00. It is clear that the lack of a mountain pass in the 1km run also discussed in section 4.4.4 has a significant impact on the wind speeds simulated at this location. The 400m run shows larger wind magnitudes near the mountaintops compared to the mountain passes and even smaller wind magnitudes near the bottom of the valley of Millum Fjarða just south of the mountain pass. The 400m run also captures a shelter just north of the mountain pass leading to Oyndarfjørður. In contrast, the 1km run simulates slightly more uniform wind magnitudes with the highest magnitudes being at the mountaintops, which in this case also includes the mountain pass leading to Oyndarfjørður, as it is not defined in this grid. One reason for the smaller wind magnitudes near the mountaintops can be the simulated wind direction, which is not pointed directly south at the mountain pass at this point in time, but rather in a south-western direction.

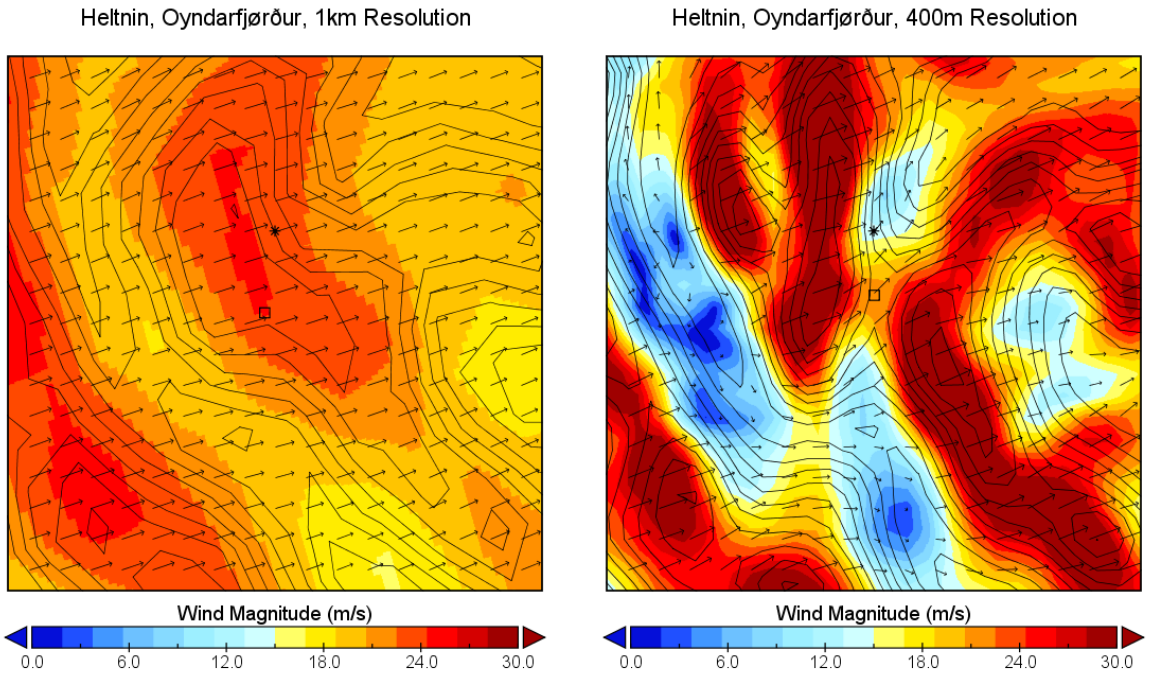

Figure 79 Simulated wind magnitudes with 1km (left) and 400m (right) horizontal resolution at Oyndarfjarðarvegurin, 15:00 P.M. The star (*) denotes the geographical coordinates of the weather station, while the square denotes the centre of the grid cell, that is the best geographical representation of the placement of the station.

Figure 80 shows a time series of the 10 minute average wind magnitudes and direction observed at the mountain pass leading to Oyndarfjørður during the passage of Urd. Likewise to the event in Norðadalsskarð the weather station at this mountain pass measures a rapid increase in wind magnitudes as the cold front passes, albeit these magnitudes are significantly smaller than what was measured at Norðadalsskarð.

The wind direction is measured to be south to southeast along the mountain pass during the peak of this storm, which corresponds well with what the 400m run simulates. However, the wind direction turns anticlockwise afterwards followed by a rapid decrease in wind speeds measured.

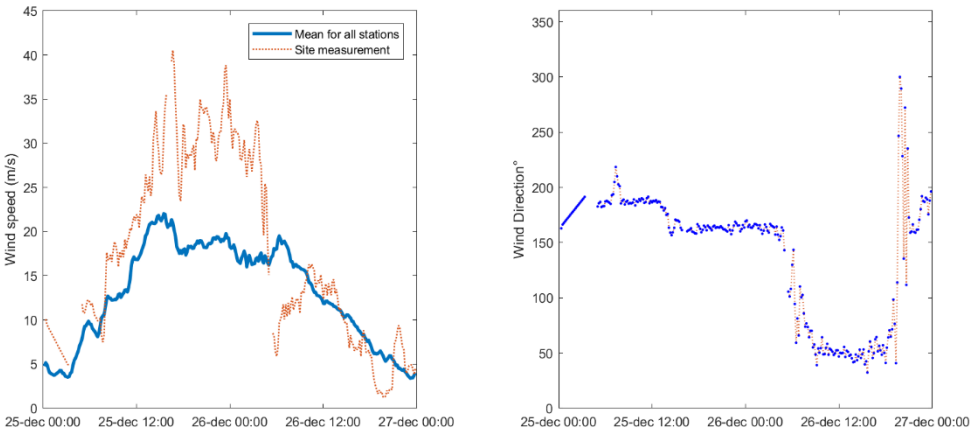

Figure 80 Time series of measured wind speed and direction at Heltnin, Oyndarfjørður during the passage of Urd

The time series in Figure 81 and Figure 82 show that both the 1km and 400m do not capture the peak of the wind magnitudes measured during the passage of Urd, the 400m model captures the slow-down in wind speeds once the wind direction turns. In addition, the 400m run simulates a more accurate wind direction in comparison to the 1km run, which is probably related to the lack of a mountain pass in the 1km grid. However, neither simulations capture the anticlockwise turn in direction.

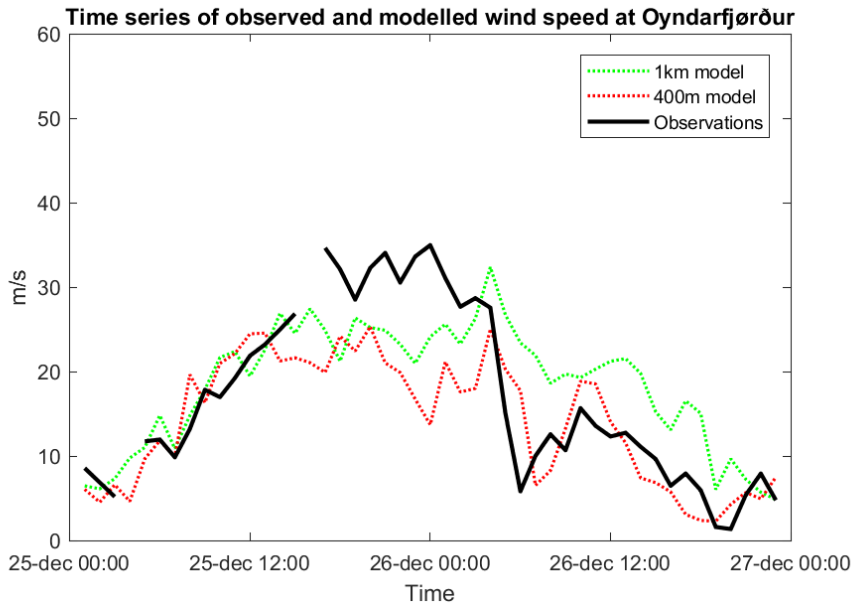

Figure 81 Time series of the measured and modelled wind speeds at Oyndarfjørður after relocating the site

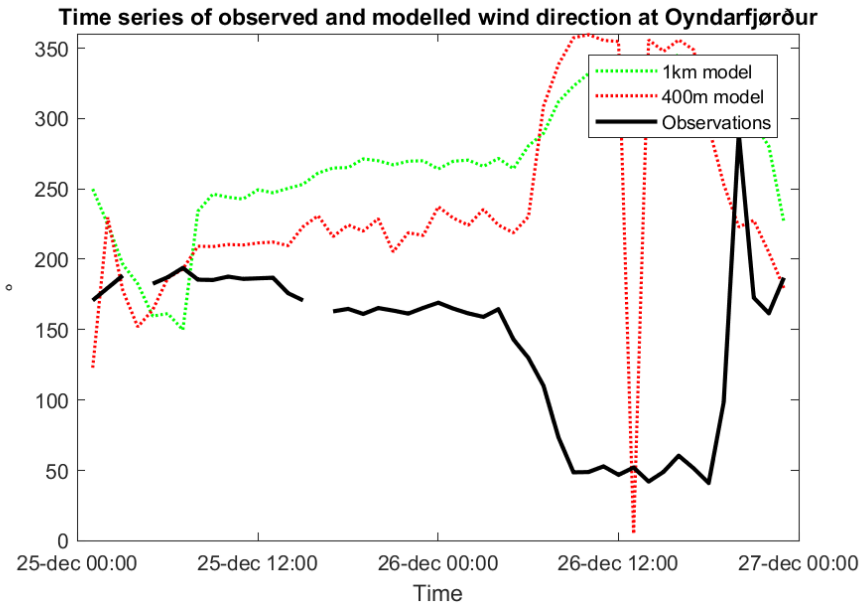

Figure 82 Time series of wind speed measured and modelled at Oyndarfjørður after relocating the site

Tjørnuvík

Figure 83 shows the 10 meter surface wind magnitudes at the road to Tjørnuvík simulated by the 1 km and 400m run during the peak of the storm on December 25th 15:00. The 1km run simulates to a small extent speed-ups of wind magnitudes near the mountaintops west of Tjørnuvík, while slower magnitudes are simulated at the channel most likely due to sheltering effects. In contrast, the 400m run simulates to a much greater detail the sheltering effects as well as the wind speed-ups localized near the mountaintops.

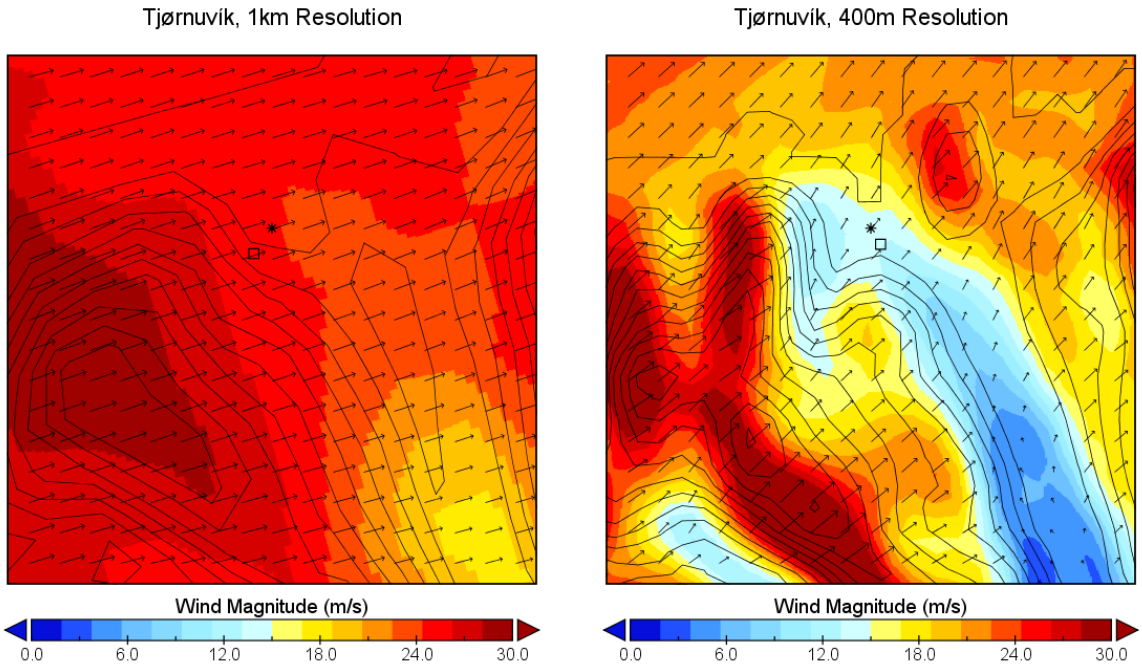

Figure 83 Simulated wind magnitudes with 1km (left) and 400m (rigth) horizontal resolution at Tjørnuvík, 15:00 P.M. on December 25th 2016. The star (*) denotes the geographical coordinates of the weather station, while the square denotes the centre of the grid cell, that is the best geographical representation of the placement of the station.

Figure 84 shows a time series of the 10 minute average wind magnitudes and direction observed on the road to Tjørnuvík. In comparison to the mean wind magnitudes observed for all weather stations, the wind magnitudes at 15:00 are significantly lower ranging between 8 and 12 m/s in this period. The reason for this may be due to the station being placed on the lee side of a mountain at this point in time. During the frontal passage, the measured wind direction is south to south-east indicating that the wind flow is moving along the mountainside westwards. After the cold front passage, the wind direction turns westwards as the wind speeds increase. Wind magnitudes suddenly make a jump peaking in the morning of December 26th 2016, while the wind direction only turns slightly northwards.

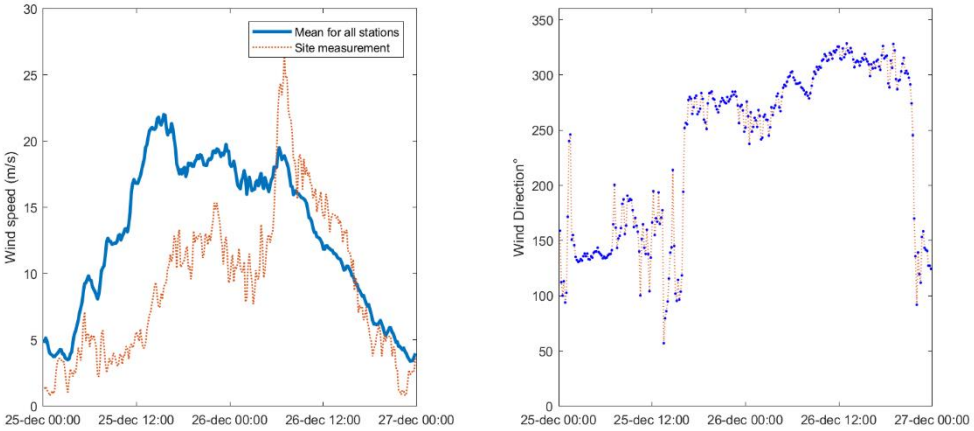

Figure 84 Time series of measured wind speed and direction on the road to Tjørnuvík during the passage of Urd

Comparing with Figure 85, both the 1km and 400m run overestimate the wind speeds prior to the turning in wind direction. However, the 400m run predicts smaller wind magnitudes at this location compared to the 1km run possibly due to the more localized wind shelter also observed in Figure 83. Both the 1km run and the 400m run capture the measured peak in wind magnitudes, as well as the following slow-down in wind speeds.

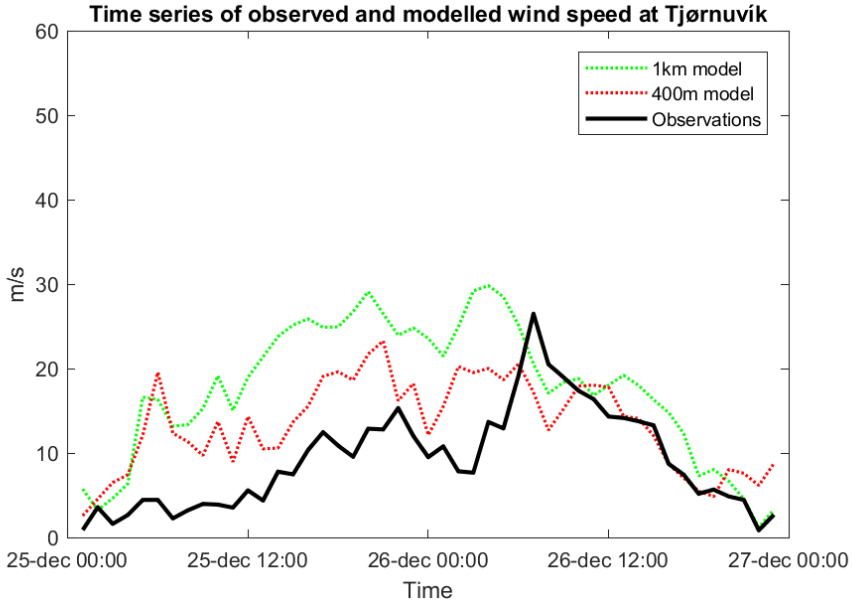

Figure 85 Time series of the measured and modelled wind speeds at Tjørnuvík after relocating the site

Figure 86 shows that while the measured south-eastern wind direction was neither captured by the 1km run nor the 400m run, both simulations generally capture the wind direction well during the passage of Urd.

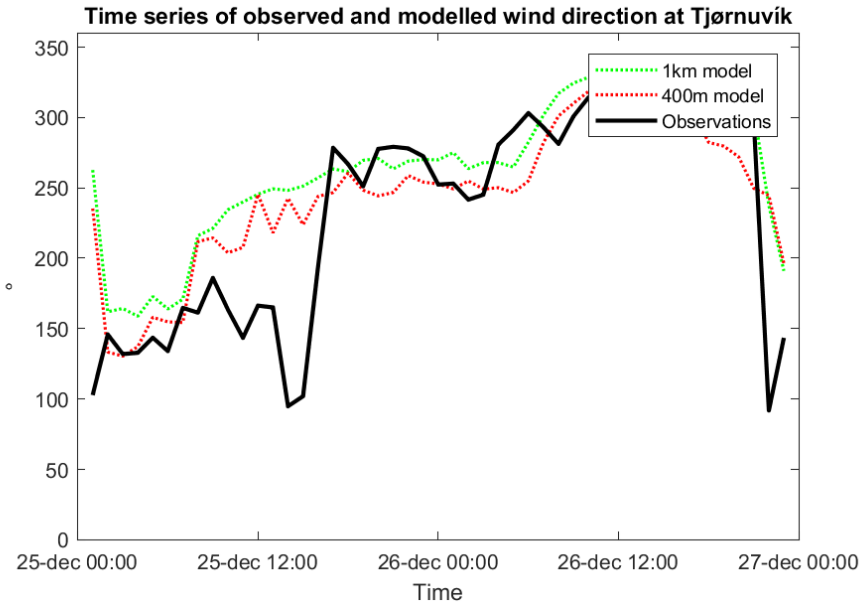

Figure 86 Time series of measured and modelled wind direction at Tjørnuvík after relocating the site

Viðareiði

Figure 87 shows the 10 meter surface wind magnitudes at the road to Viðareiði simulated by the 1 km and 400m run during the peak of the storm on December 25th 15:00. The 1km run simulates speed-ups of wind magnitudes near the mountain barriers between the weather station. In contrast, these speed-ups are mostly prominent on the windward side of the mountain barriers in the 400m simulation, where the wind magnitudes in the fjord between these two barriers are significantly smaller during the peak of the storm.

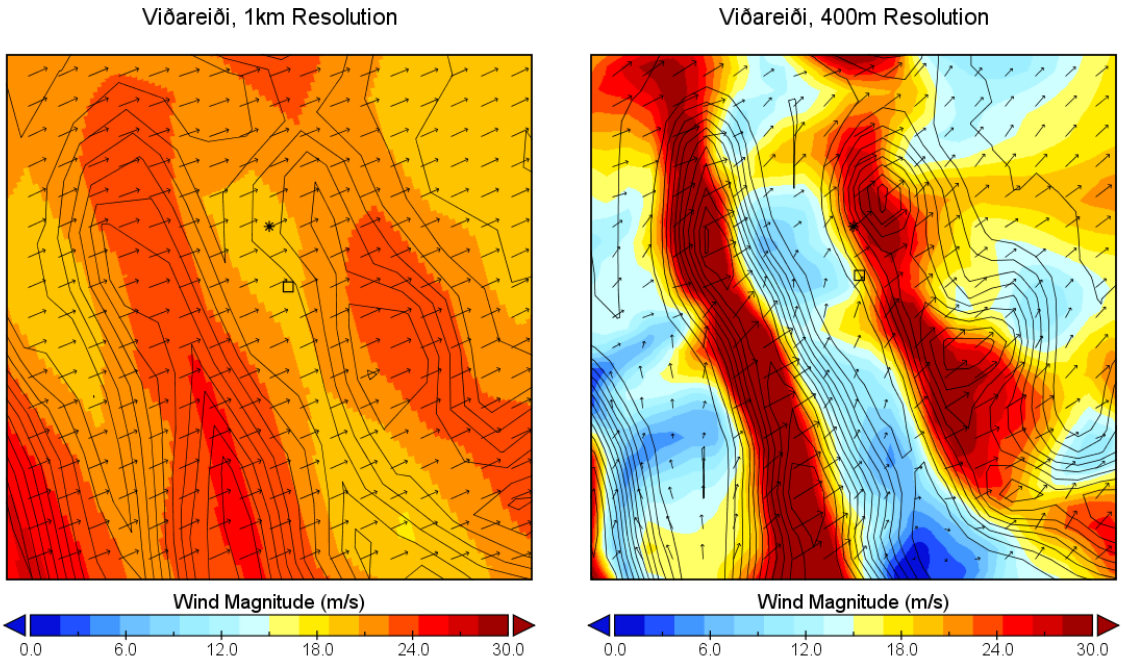

Figure 87 Simulated wind magnitudes with 1km (left) and 400m (rigth) horizontal resolution at Viðareiði, 15:00 P.M. on December 25th 2016. The star (*) denotes the geographical coordinates of the weather station, while the square denotes the centre of the grid cell, that is the best geographical representation of the placement of the station.

Figure 88 shows a time series of the 10 minute average wind magnitudes and direction observed on the road to Viðareiði. In comparison to the mean wind magnitudes observed for all weather stations, the wind magnitudes at 15:00 are significantly lower ranging between 12 and 15 m/s in this period. Considering Figure 89, this corresponds well with the wind magnitudes simulated by the 400m run, however not as much with the 1km run.

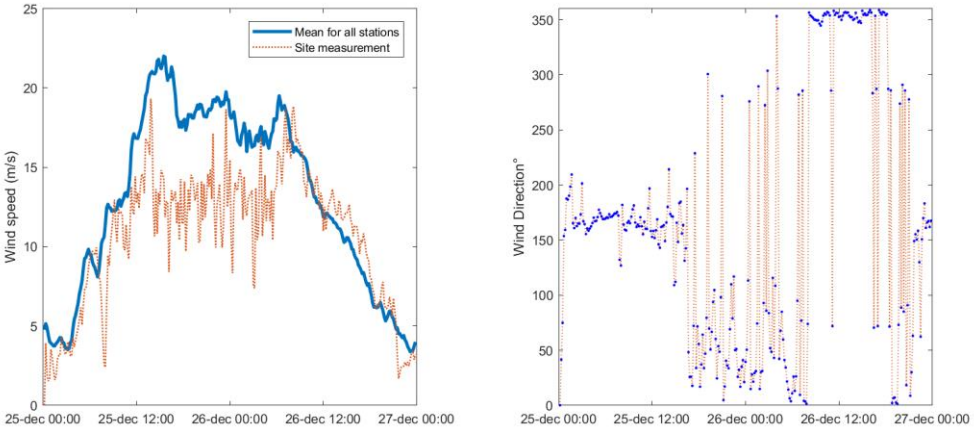

Figure 88 Time series of measured wind speed and direction near Viðareiði during hurricane Urd

The measured wind direction was initially south, but changed to north-east after the frontal passage and later to north. It is quite noticeable that there are rapid fluctuations in the wind direction measured at this location during the passage of Urd. Considering Figure 90, these rapid fluctuations in wind direction were not captured by either of the two WRF simulations. Instead, both the 1km run and the 400m run predict a graduate clockwise turning in the wind direction from south to west as Urd passes the Faroe Islands.

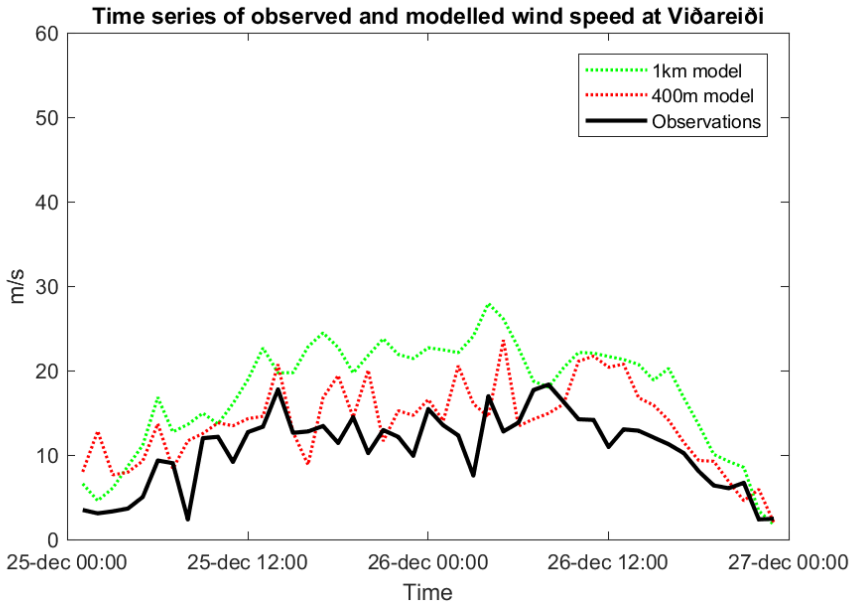

Figure 89 Time series of the measured and modelled wind speeds at Viðareiði after relocating the site

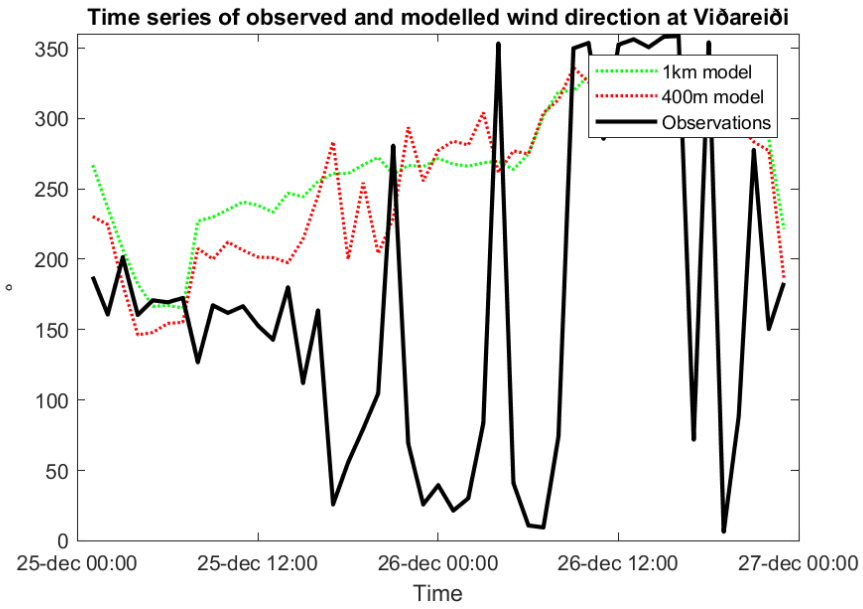

Figure 90 Time series of wind direction measured and modelled at Viðareiði after relocating the site

Appendix D

This appendix contains verification metrics obtained for all measurement sites for both WRF simulations during the passage of Urd

Verification metrics for wind speed (m/s)

Mean Absolute Error (MAE)

Location	1km run	400m run
Gjáarskarð	9.52	4.82
Glyvursnes	2.98	3.30
Høgareyn	3.34	2.79
Hvalba	8.64	5.78
Kambsdalur	6.34	4.47
Klaksvík	4.80	2.90
Kollafjørður	4.14	2.71
Krambatangi	7.85	2.91
Norðadalsskarð	8.10	5.74
Norðskálatunnilin	5.55	4.88
Oyndarfjørður	5.38	4.91
Porkeri	3.82	3.59
Runavík	7.38	7.82
Sandavágur	5.11	4.29
Sandoy	2.82	2.35
Skopun	6.49	5.58
Streymnes	3.57	2.78
Sund	6.42	3.59
Syðradalur	5.71	2.84
Tjørnuvík	8.87	5.25
Vatnsoyrar	5.49	3.92
við Velbastaðháls	2.35	2.96
Viðareiði	6.81	3.87

Mean Squared Error (MSE)

Location	1km run	400m run
Gjáarskarð	142.88	35.53
Glyvursnes	15.87	19.09
Høgareyn	20.96	20.10
Hvalba	97.00	49.51
Kambsdalur	55.91	31.02
Klaksvík	35.20	13.38
Kollafjørður	27.74	11.95
Krambatangi	87.54	15.38
Norðadalsskarð	96.33	70.37
Norðskálatunnilin	46.63	40.23
Oyndarfjørður	45.84	46.22
Porkeri	24.13	20.61
Runavík	82.73	92.30
Sandavágur	44.44	29.12
Sandoy	12.44	10.56
Skopun	57.92	47.23
Streymnes	20.45	12.67
Sund	61.32	20.12
Syðradalur	43.99	13.50
Tjørnuvík	116.26	41.38
Vatnsoyrar	48.08	21.87
við Velbastaðháls	8.34	15.63
Viðareiði	61.00	24.29

Bias

Location	1km run	400m run
Gjáarskarð	8.95	3.48
Glyvursnes	0.95	-0.89
Høgareyn	-1.87	-0.43
Hvalba	8.64	5.74
Kambsdalur	4.90	2.82
Klaksvík	4.68	1.44
Kollafjørður	3.75	-1.87
Krambatangi	7.27	2.30
Norðadalsskarð	-4.86	-3.95
Norðskálatunnilin	5.51	-2.70
Oyndarfjørður	1.48	-2.75
Porkeri	-2.76	-2.83
Runavík	7.03	7.48
Sandavágur	2.87	-0.57
Sandoy	-0.68	-1.23
Skopun	6.36	5.54
Streymnes	2.39	-0.24
Sund	5.91	3.38
Syðradalur	5.39	-0.11
Tjørnuvík	8.43	4.26
Vatnsoyrar	5.66	4.00
við Velbastaðháls	0.50	2.25
Viðareiði	6.77	3.08

Verification metrics for temperature (°C)

Note: Measured data of temperature was not available at Oyndarfjarðarvegurin during the passage of Urd.

Mean Absolute Error (MAE)

Location	1km run	400m run
Gjáarskarð	0.93	1.26
Glyvursnes	1.23	1.32
Høgareyn	0.87	1.51
Hvalba	1.03	0.89
Kambsdalur	1.32	1.35
Klaksvík	1.20	1.17
Kollafjørður	1.25	1.15
Krambatangi	1.25	1.41
Norðadalsskarð	0.73	0.75
Norðskálatunnilin	1.15	1.35
Oyndarfjørður	NaN	NaN
Porkeri	1.00	1.10
Runavík	1.33	1.07
Sandavágur	0.98	1.04
Sandoy	1.02	1.02
Skopun	1.25	1.30
Streymnes	1.56	1.16
Sund	1.39	1.47
Syðradalur	1.22	0.86
Tjørnuvík	1.17	1.32
Vatnsoyrar	0.99	1.12
við Velbastaðháls	1.00	1.09
Viðareiði	1.24	1.32

Mean Squared Error (MSE)

Location	1km run	400m run
Gjáarskarð	1.43	2.08
Glyvursnes	2.22	2.53
Høgareyn	1.14	2.99
Hvalba	1.45	1.42
Kambsdalur	2.93	2.76
Klaksvík	2.00	1.95
Kollafjørður	2.18	2.08
Krambatangi	2.14	2.80
Norðadalsskarð	1.51	1.85
Norðskálatunnilin	2.11	2.59
Oyndarfjørður	NaN	NaN
Porkeri	1.45	1.86
Runavík	2.57	1.65
Sandavágur	1.64	1.61
Sandoy	1.68	1.50
Skopun	2.01	2.36
Streymnes	3.19	2.03
Sund	3.06	2.79
Syðradalur	1.99	1.43
Tjørnuvík	2.12	2.47
Vatnsoyrar	1.54	1.92
við Velbastaðháls	1.67	1.66
Viðareiði	2.33	2.78

Bias

Location	1km run	400m run
Gjáarskarð	-0.39	0.98
Glyvursnes	-0.45	-0.96
Høgareyn	-0.03	1.36
Hvalba	0.13	-0.14
Kambsdalur	0.89	-1.17
Klaksvík	-0.86	0.71
Kollafjørður	-0.43	0.48
Krambatangi	-0.21	-1.04
Norðadalsskarð	0.05	0.07
Norðskálatunnilin	-0.27	-0.86
Oyndarfjørður	NaN	NaN
Porkeri	-0.20	0.34
Runavík	-0.77	-0.78
Sandavágur	0.00	-0.46
Sandoy	-0.07	-0.48
Skopun	-0.61	-1.01
Streymnes	1.23	-0.82
Sund	-0.57	-0.98
Syðradalur	0.85	0.23
Tjørnuvík	-0.40	-0.93
Vatnsoyrar	-0.39	0.85
við Velbastaðháls	-0.22	0.53
Viðareiði	-0.60	-1.06

Verification metrics for pressure levels (hPa)

Observed pressure was not available at Glyvursnes, Oyndarfjørður and Velbastaðháls during the passage of Urd.

Mean Absolute Error (MAE)

Location	1km run	400m run
Gjáarskarð	5.34	3.32
Glyvursnes	NaN	NaN
Høgareyn	3.21	1.63
Hvalba	3.45	3.12
Kambsdalur	3.58	2.41
Klaksvík	3.58	2.11
Kollafjørður	3.95	2.18
Krambatangi	3.04	1.46
Norðadalsskarð	3.25	4.00
Norðskálatunnilin	4.28	2.62
Oyndarfjørður	NaN	NaN
Porkeri	3.64	2.30
Runavík	3.64	2.14
Sandavágur	4.55	2.74
Sandoy	2.36	2.32
Skopun	3.61	1.79
Streymnes	3.08	1.84
Sund	4.03	2.34
Syðradalur	3.42	1.96
Tjørnuvík	3.74	2.00
Vatnsoyrar	4.39	2.82
við Velbastaðháls	NaN	NaN
Viðareiði	3.38	1.79

Mean Squared Error (MSE)

Location	1km run	400m run
Gjáarskarð	42.47	17.00
Glyvursnes	NaN	NaN
Høgareyn	16.17	4.45
Hvalba	20.15	20.57
Kambsdalur	19.97	10.40
Klaksvík	19.14	7.57
Kollafjørður	22.54	7.68
Krambatangi	15.03	3.84
Norðadalsskarð	41.32	57.95
Norðskálatunnilin	27.26	11.96
Oyndarfjørður	NaN	NaN
Porkeri	20.54	9.76
Runavík	20.13	7.12
Sandavágur	31.36	11.53
Sandoy	8.94	8.52
Skopun	20.52	5.28
Streymnes	15.94	6.72
Sund	24.22	8.43
Syðradalur	17.68	9.30
Tjørnuvík	21.36	6.73
Vatnsoyrar	30.94	13.47
við Velbastaðháls	NaN	NaN
Viðareiði	18.06	6.87

Bias

Location	1km run	400m run
Gjáarskarð	-4.34	-1.33
Glyvursnes	NaN	NaN
Høgareyn	-2.57	-0.40
Hvalba	-0.25	2.34
Kambsdalur	-1.41	-0.14
Klaksvík	-2.54	-0.23
Kollafjørður	-3.28	-0.75
Krambatangi	-2.75	-0.27
Norðadalsskarð	12.42	15.04
Norðskálatunnilin	-3.37	-0.71
Oyndarfjørður	NaN	NaN
Porkeri	-2.55	-0.13
Runavík	-3.38	-1.12
Sandavágur	-4.07	-1.60
Sandoy	-0.24	2.09
Skopun	-3.37	-0.90
Streymnes	-2.30	-0.11
Sund	-3.68	-1.20
Syðradalur	-2.02	0.80
Tjørnuvík	-3.13	-0.60
Vatnsoyrar	-4.06	-1.96
við Velbastaðháls	NaN	NaN
Viðareiði	-2.03	0.12

Appendix E

Several simulations of the storm Urd have been made for this study, while the thesis only focuses on two simulations. This appendix contains tables of verification metrics for wind speed simulated during the passage of Urd. It should be noted that these verification tables were produced before the discovery that the Faroese topography was misplaced. Consequently, these verification metrics compare measurements with model data that has not been relocated, which may impact the result.

Average verification results for all stations

Table 0.1 shows the Mean Absolute Error of the WRF simulations of Urd. It should be noted that three different domains setups were used. One for the Eta microphysics scheme, one for the Morrison microphysics scheme and one for the 400m run. All simulations except for the 400m run had a horizontal resolution of one kilometre at their innermost domain. The table shows that the 400m run had the best prediction of wind speeds in terms of the Mean Absolute Error during the passage of Urd. The simulations that used the Morrison scheme had a lower error when they were run with two-way nesting compared to one-way nesting.

Mean Absolute Error

Type of simulation	Domain 1	Domain 2	Domain 3	Domain 4
Eta Microphysics Scheme, two-way, 40 layers	5.85	5.98	5.27	
Eta Microphysics scheme, one-way, 40 layers	6.02	5.59	4.98	
Morrison Scheme, two-way, 40 layers	5.72	5.65	5.97	5.44
Morrison Scheme, one-way, 40 layers	6.36	5.94	5.81	5.82
Morrison Scheme + new Landuse data, two-way, 40 layers	5.71	5.64	5.97	5.45
Morrison Scheme + new Landuse data, one-way, 40 layers	6.35	5.92	5.78	5.78
Morrison Scheme + new Landuse data, two-way, 60 layers	5.79	5.74	6.07	5.54
400m resolution, 60 layers	5.97	5.45	4.83	

Table 0.1 Mean Absolute Error of all simulations during the passage of Urd

Mean Squared Error

Table 0.2 shows the Mean Squared Error of the WRF simulations of Urd. The table shows that the one-way nested run with 40 vertical layers using the Eta microphysics scheme had the lowest Mean Squared Error during the passage of Urd. Like with Table 0.1, the simulations that used the Morrison scheme had a lower error when they were run with two-way nesting compared to one-way nesting.

Type of simulation	Domain1	Domain2	Domain3	Domain4
Eta Microphysics Scheme, two-way, 40 layers	53.78	59.36	46.08	
Eta Microphysics scheme, one-way, 40 layers	56.92	49.77	42.18	
Morrison Scheme, two-way, 40 layers	50.88	50.01	55.74	47.38
Morrison Scheme, one-way, 40 layers	60.16	54.78	52.93	53.93
Morrison Scheme + new Landuse data, two-way, 40 layers	50.68	49.87	55.71	47.47
Morrison Scheme + new Landuse data, one-way, 40 layers	59.95	54.64	52.94	53.65
Morrison Scheme + new Landuse data, two-way, 60 layers	52.04	51.49	57.35	48.88
400m resolution, 60 layers	54.74	47.97	42.65	

Table 0.2 Mean Squared Error of all simulations during the passage of Urd

Bias

Table 0.3 shows the Bias of the WRF simulations of Urd. The table shows that the 400m simulation had the by far lowest bias of 0.94 m/s during the passage of Urd. The simulations that used the Morrison scheme had lower bias when they were run with two-way nesting compared to one-way nesting. It is interesting to note that all simulations had a positive bias meaning that the WRF simulations generally overpredicted the wind speeds measured during the passage of Urd.

Models	Domain1	Domain2	Domain3	Domain4
Eta Microphysics Scheme, two-way, 40 layers	3.95	4.41	2.72	
Eta Microphysics scheme, one-way, 40 layers	4.46	3.42	1.36	
Morrison Scheme, two-way, 40 layers	3.86	3.45	3.94	2.89
Morrison Scheme, one-way, 40 layers	4.76	3.89	3.73	3.58
Morrison Scheme + new Landuse data, two-way, 40 layers	3.82	3.41	3.91	2.85
Morrison Scheme + new Landuse data, one-way, 40 layers	4.75	3.88	3.74	3.58
Morrison Scheme + new Landuse data, two-way, 60 layers	3.86	3.48	3.98	2.93
400m resolution, 60 layers	4.4	3.48	0.94	

Table 0.3 Bias of all simulations during the passage of Urd